

# Coherent transfer of spin and entanglement in optoelectronics

INAUGURALDISSERTATION

zur

Erlangung der Würde eines Doktors der Philosophie

vorgelegt der

Philosophisch-Naturwissenschaftlichen Fakultät

der Universität Basel

von

Verónica Cerletti

aus Argentinien

Basel, 2005

Genehmigt von der Philosophisch-Naturwissenschaftlichen Fakultät auf Antrag von

Prof. Dr. Daniel Loss

Prof. Dr. Christoph Bruder

Basel, den 11. April 2005

Prof. Dr. Hans-Jakob Wirz  
Dekan

# Summary

In the last few years there has been a growing interest in the possible applications of quantum properties of different physical systems in well established technologies. This was motivated by the miniaturization of electronic devices. For very small systems, the laws of quantum mechanics start to govern their behavior and it is then to expect that for instance electronic components reach their “quantum limit”. A good example of the introduction of quantum properties into conventional technologies is the case of the electron spin, which offers an alternative to electron-charge for the storage and transport of information in electronics. The idea of using electron spins in electronics gave rise to the new and exciting field of *spintronics* and was encouraged by experiments that showed coherent spin transport over long distances (over hundred micrometers) in semiconductors and long electron spin dephasing times. In addition to its applications in conventional technologies, the use of the electron spin as information-carrier has been suggested for the new field of quantum information processing. An important advantage of the electron spin with respect to other quantum information-carriers proposed is that it can profit from the well developed semiconductor industry and its related technologies. For the long-range transport of information, however, the highly interacting environment in solid-state devices represents a difficulty to the use of electron spins. In contrast, photons are very weakly coupled to their environment, and therefore more suitable for the transfer of information over long distances (on the order of kilometers), required, for instance, in quantum communication. Furthermore, the technology needed for the transport of photons over such long distances is well developed. Thus, an efficient transfer of quantum information between electron spins and photons is highly desirable.

In this dissertation, we show that the transfer of entanglement, a quantum correlation, from electron spins to the polarization of photons is not only theoretically possible, but also feasible under realistic experimental conditions. We study the transport of an entangled pair of electron spins through Fermi leads which split them spatially until they reach spin-LEDs, semiconductor structures containing quantum dots. In these structures, the electrons optically recombine with holes, producing then photons. We analyze the polarization state of the out-coming photons and give the conditions for which the entanglement of the electron spins is fully recovered in the photon-polarizations. We further show that it is possible to produce four-photon entanglement.

We also include in this work the study of coherent spin-transfer between quantum dots layers bridged by molecules. This study was motivated by an experiment showing that the

molecules act not only as binders to construct the multilayer structures, but also as “wires” for the information through electron spins in the quantum dots. We show that a two-site Hamiltonian captures some of the essential features of the experiment. We calculate the dependence of the experimentally observed Faraday rotation (FR) signal as a function of probe energy on microscopic parameters such as spin transfer probabilities. The Faraday angle is related to the difference in the dielectric response for different polarizations of the light. We calculate the dielectric response functions of coupled quantum dots and derive an analytical expression for the FR angle in terms of electron transfer probabilities and Heisenberg exchange splittings.

# Contents

<b>Summary</b>	<b>i</b>
<b>1 Introduction</b>	<b>1</b>
1.1 Entanglement . . . . .	1
1.1.1 Basic description . . . . .	2
1.1.2 Non-locality of entanglement . . . . .	3
Simple model and derivation of a Bell-type inequality . . . . .	4
Bell's original inequality . . . . .	6
Generalization of Bell's inequality (CHSH) . . . . .	6
1.1.3 Production of entanglement . . . . .	8
Andreev entangler with quantum dots . . . . .	8
Triple-quantum dot entangler . . . . .	9
Coulomb scattering entangler . . . . .	9
1.1.4 Characterization of entanglement . . . . .	10
1.2 The electron spin in quantum dots . . . . .	11
1.2.1 Spin control . . . . .	11
1.2.2 Spin relaxation and decoherence . . . . .	11
1.2.3 Spin initialization . . . . .	12
1.2.4 Single-spin detection . . . . .	12
1.2.5 Optical interaction, initialization and readout of spins . . . . .	13
<b>2 Entanglement transfer from electron spins to photons.</b>	<b>19</b>
2.1 Introduction . . . . .	19
2.2 Electrons injection and recombination . . . . .	20
2.2.1 Two-spin dynamics . . . . .	22
2.3 Recombination process and optical output . . . . .	25
2.4 Conclusions . . . . .	30
<b>3 Coherent spin transfer in coupled quantum dots</b>	<b>31</b>
3.1 Introduction . . . . .	31
3.1.1 Experimental motivation . . . . .	32
3.2 The theoretical model . . . . .	33

3.3	Time resolved Faraday rotation for coupled Quantum Dots . . . . .	34
3.4	Optical spin injection . . . . .	36
3.5	Doping of coupled Quantum Dots . . . . .	41
3.6	Comparison with experiment . . . . .	44
3.7	Conclusions . . . . .	47
<b>A</b>	<b>Two-spin density matrix</b>	<b>57</b>
<b>B</b>	<b>Two-exciton eigenstates of coupled quantum dots</b>	<b>59</b>
<b>C</b>	<b>Eigenstates of doped coupled quantum dots</b>	<b>61</b>
	<b>Bibliography</b>	<b>65</b>
	<b>Curriculum Vitae</b>	<b>71</b>

# Chapter 1

## Introduction

The fields of semiconductor physics and electronics have been successfully combined for many years. The invention of the transistor meant a revolution for electronics and has led to significant development of semiconductor physics and its industry. More recently, the use of the spin degree of freedom of electrons, as well as the charge, has attracted great interest [1–3]. In addition to applications for spin electronics (spintronics) in conventional devices, for instance based on the giant magneto-resistance effect [4] and spin-polarized field-effect transistors [5], there are applications that exploit the quantum coherence of the spin. This was encouraged by ground-breaking experiments that showed coherent spin transport over long distances in semiconductors and long electron-spin dephasing times, on the order of 100 nanoseconds [6, 7]. In addition, spin-polarized carrier injection from magnetic to non-magnetic semiconductors has been demonstrated [8,9]. Since the electron spin is a two-level system, it is a natural candidate for the realization of a quantum bit (qubit) [10], the basic unit of information in quantum computation and communication. In this chapter we will give an introduction and overview to some of the most important issues related to the use of electron spins in semiconductors for quantum information and spintronics. In Sec. 1.1 we introduce one of the main resources for quantum information processing, *entanglement*. A summary of the experimental achievements in spin-related issues in semiconductors is given in Sec. 1.2.

### 1.1 Entanglement

Entanglement is one of the most interesting features of Quantum Mechanics. At first, the interest in entanglement was related to its non-local character, in the frame of foundations of Quantum Mechanics. More recently, the growing field of Quantum Information Theory has renewed the interest for entanglement, since it is one of its main resources. There had been many proposals describing *entangler*s [11–18], setups which work as sources of entangled particles. In particular, the use of the spin of the electron as a degree of freedom for quantum computation and the growing field of spintronics [1] make entanglement of electron spins an important object of study.

### 1.1.1 Basic description

Entanglement is a quantum correlation. It is defined with respect to some given properties of a composite system. Some physical properties of several parts of a composite system are said to be *entangled* if the state of each *individual* part referred to these particular physical properties *cannot be defined*, while the state of the composite system as a whole is clearly defined. This implies that a full description of the state of the system in terms of the individual components is not possible. Formally, we can formulate this statement as follows <sup>1</sup>:

*Two or more parties are said to be entangled if and only if the state of the composite system cannot be decomposed into the direct product <sup>2</sup> of the individual states of the parties.*

To illustrate this idea, let's take as an example two spins  $\frac{1}{2}$  in the singlet state  $|\Psi^-\rangle$ . The Hilbert space of each spin can be spanned on the basis  $\{|\uparrow\rangle_i, |\downarrow\rangle_i\}$  with  $i = 1, 2$ . The Hilbert space for the two electrons as a system can be then spanned on the basis  $\{|\uparrow\uparrow\rangle, |\uparrow\downarrow\rangle, |\downarrow\uparrow\rangle, |\downarrow\downarrow\rangle\}$ , where

$$\begin{aligned} |\uparrow\uparrow\rangle &= |\uparrow\rangle_1 \otimes |\uparrow\rangle_2 \\ |\uparrow\downarrow\rangle &= |\uparrow\rangle_1 \otimes |\downarrow\rangle_2 \\ |\downarrow\uparrow\rangle &= |\downarrow\rangle_1 \otimes |\uparrow\rangle_2 \\ |\downarrow\downarrow\rangle &= |\downarrow\rangle_1 \otimes |\downarrow\rangle_2 \end{aligned}$$

The singlet can be written in this basis as  $(0, \frac{1}{\sqrt{2}}, -\frac{1}{\sqrt{2}}, 0)$ . This state is an entangled state, because we can show that it cannot be decomposed in the direct product of states of the individual spins. In general, the state of a single spin  $i = 1, 2$  can be written as  $(\alpha_i|\uparrow\rangle + \beta_i|\downarrow\rangle)/N_i$  with  $N_i = \sqrt{|\alpha_i|^2 + |\beta_i|^2}$  and  $\alpha_i, \beta_i$  arbitrary complex numbers. Therefore, given two arbitrary states of the single spins, the most general two-spin state obtained from the direct product of the individual single-spin states takes the form  $|\phi\rangle = \frac{1}{N_1} (\alpha_1|\uparrow\rangle_1 + \beta_1|\downarrow\rangle_1) \otimes \frac{1}{N_2} (\alpha_2|\uparrow\rangle_2 + \beta_2|\downarrow\rangle_2)$ . Now we will prove that there are no  $\alpha_i, \beta_i$  such that  $|\Psi^-\rangle = |\phi\rangle$ .

---

<sup>1</sup>Here we restrict ourselves to pure states. For mixed states, we need to look at the density matrix  $\rho$  corresponding to a state. A mixed state is then entangled if and only if  $\rho$  cannot be written as the statistical mixture of unentangled pure states.

<sup>2</sup>Between the Hilbert spaces of each part of the system.



$$\begin{aligned}
|\phi\rangle &= \frac{1}{N_1} (\alpha_1|\uparrow\rangle_1 + \beta_1|\downarrow\rangle_1) \otimes \frac{1}{N_2} (\alpha_2|\uparrow\rangle_2 + \beta_2|\downarrow\rangle_2) \\
&= \frac{1}{N_1 N_2} [\alpha_1 \alpha_2 |\uparrow\uparrow\rangle + \alpha_1 \beta_2 |\uparrow\downarrow\rangle + \beta_1 \alpha_2 |\downarrow\uparrow\rangle + \beta_1 \beta_2 |\downarrow\downarrow\rangle] \\
&\stackrel{?}{=} |\Psi^-\rangle = \frac{1}{\sqrt{2}} |\uparrow\downarrow\rangle - \frac{1}{\sqrt{2}} |\downarrow\uparrow\rangle \iff \begin{cases} \alpha_1 \alpha_2 = 0 \\ \alpha_1 \beta_2 = \frac{N_1 N_2}{\sqrt{2}} \\ \alpha_2 \beta_1 = -\frac{N_1 N_2}{\sqrt{2}} \\ \beta_1 \beta_2 = 0 \end{cases}
\end{aligned}$$

Clearly,  $\alpha_1 \alpha_2 = 0$  implies that at least one of the  $\alpha_i$  is zero, and therefore it is impossible to fulfill  $\alpha_1 \beta_2 = \frac{N_1 N_2}{\sqrt{2}}$  and  $\alpha_2 \beta_1 = -\frac{N_1 N_2}{\sqrt{2}}$  at the same time. Thus, no set of  $\alpha_i, \beta_i$  can be found such that  $|\Psi^-\rangle = |\phi\rangle$ , that is,  $|\Psi^-\rangle$  cannot be written as the direct product of individual states of the spins.

### 1.1.2 Non-locality of entanglement

One of the most striking features of entanglement is its non-local nature. The fact that an entangled state cannot be factorized into individual states of the parts of a system, even if these parts are far apart from each other, leads to the non-locality of entanglement. We can illustrate this idea coming back to the example of the spin-singlet from Subsection 1.1.1. Once that the two spins are prepared in the singlet spin-state, as long as the spin is preserved, they will stay in this entangled state, independently of what happens with the other properties of the electrons. For instance, position and orbital state of one spin can be completely independent of these properties for the other electron. Therefore, the two electrons can be located at any distance from each other, as far as to not be able to interact anymore, and still have an entangled spin-state. Since entanglement is a correlation, to observe the spin of one of the electrons gives information about the spin of the other, although information exchange between the electrons is not possible. For the singlet, the spins are *anticorrelated*, which means that the outcomes for each spin after a measurement along a given axis are always opposite. If the electrons are separated enough so that they cannot interact anymore, and a measurement of the spin along an axis  $\hat{a}$  is performed on one of them, from the output one can immediately know with certainty the outcome of a spin measurement along  $\hat{a}$  performed on the other electron, although information between them could not be exchanged. This means that the first electron could not “inform” the second about the outcome of the measurement, as to “set” the second spin to the opposite state. Still, this correlation is present. This motivated discussion among scientists, including Einstein [19] and Bohr [20], since the early days of Quantum Theory. In 1935 Einstein, Podolsky and Rosen [19] pointed out that a physical theory should obey a locality principle, their seminal paper being the starting point of hidden

variable theories. According to Einstein, the probabilistic behavior of the outcomes of measurements in quantum mechanics is a result of our ignorance of some parameters of the system (“hidden variables”). This idea applies for instance to the measurement of a spin along orthogonal axis. Let us take as an example the measurements of spin components (e.g. along  $\hat{z}$  OR  $\hat{x}$ ) of a pair of spins  $\frac{1}{2}$  in the singlet state. The singlet is seen in this model as two particles, the  $z$  and  $x$  spin components of which have opposite sign. In an experiment where two observers measure one of the two components of the spin (chosen at random) of one of the members of the singlet each one, and repeat this with many singlets, the outcome predicted is the same that quantum mechanics would predict: measurements performed along different axes would have no correlation, and perfect anticorrelations would be observed for measurements along the same axis, without need for any non-local correlation. But not all type of measurements show agreement between the quantum mechanical predictions and those expected from local hidden variables theories. Thirty years passed until Bell showed that hidden variable theories obeying Einstein’s locality principle predict experimental results contradicting Quantum Mechanics [21]. In his work, Bell presents a testable inequality in which quantum mechanics and local hidden variables models disagree. We will show the ideas underlying Bell’s work with a concrete example to gain insight and later derive Bell’s original inequality.

### Simple model and derivation of a Bell-type inequality

We will consider:

- *Three axes non mutually orthogonal  $\hat{a}, \hat{b}, \hat{c}$*
- *Eight possible pairs of particles of opposite type with different populations ( $N_i$ )*

All possible pairs are shown in Table 1.1.

Table 1.1: Possible combinations of properties for a pair particles and their corresponding populations (“natural abundance”).

Population	Particle 1	Particle2
$N_1$	$(\hat{a}+, \hat{b}+, \hat{c}+)$	$(\hat{a}-, \hat{b}-, \hat{c}-)$
$N_2$	$(\hat{a}+, \hat{b}+, \hat{c}-)$	$(\hat{a}-, \hat{b}-, \hat{c}+)$
$N_3$	$(\hat{a}+, \hat{b}-, \hat{c}+)$	$(\hat{a}-, \hat{b}+, \hat{c}-)$
$N_4$	$(\hat{a}+, \hat{b}-, \hat{c}-)$	$(\hat{a}-, \hat{b}+, \hat{c}+)$
$N_5$	$(\hat{a}-, \hat{b}+, \hat{c}+)$	$(\hat{a}+, \hat{b}-, \hat{c}-)$
$N_6$	$(\hat{a}-, \hat{b}+, \hat{c}-)$	$(\hat{a}+, \hat{b}-, \hat{c}+)$
$N_7$	$(\hat{a}-, \hat{b}-, \hat{c}+)$	$(\hat{a}+, \hat{b}+, \hat{c}-)$
$N_8$	$(\hat{a}-, \hat{b}-, \hat{c}-)$	$(\hat{a}+, \hat{b}+, \hat{c}+)$

In this picture two observers measure the spin  $\mathbf{S}$  along one of the three axes, chosen at random. They could measure, say, along  $\hat{a}$  and  $\hat{b}$  and both obtain  $+$ . The number of pairs for which this happens is

$$N_3 + N_4$$

Since  $N_i \geq 0$  the following holds

$$N_3 + N_4 \leq (N_2 + N_4) + (N_3 + N_7) \quad (1.1)$$

Let's define  $P(\hat{a}+; \hat{b}+)$  as the *probability* of both observers obtaining  $+$  along  $\hat{a}$  and  $\hat{b}$  in a random selection. This probability is

$$P(\hat{a}+; \hat{b}+) = \frac{N_3 + N_4}{\sum_{i=1}^8 N_i} \quad (1.2)$$

Then, from Eq. (1.1), dividing every term by  $\sum_{i=1}^8 N_i$  and comparing with Table 1.1, we obtain Bell's inequality:

$$P(\hat{a}+; \hat{b}+) \leq P(\hat{a}+; \hat{c}+) + P(\hat{c}+; \hat{b}+) \quad (1.3)$$

For pairs of particles of spin  $\frac{1}{2}$  in the singlet state, quantum mechanics predicts

$$P(\hat{a}+; \hat{b}+) = \frac{1}{2} \sin^2\left(\frac{\theta_{ab}}{2}\right) \quad (1.4)$$

where  $\theta_{ab}$  is the angle between the axes  $\hat{a}$  and  $\hat{b}$ . The factor  $\frac{1}{2}$  comes from the probability of  $(\hat{a}+)$  and **given this result**, then  $\sin^2(\frac{\theta_{ab}}{2})$  is the probability of  $(\hat{b}+)$ . As an example, we choose the three axes in the same plane and in such a way that

$$\theta_{ab} = 2\theta \quad \text{and} \quad \theta_{ac} = \theta_{cb} = \theta \quad (1.5)$$

Thus, Bell's inequality is violated for  $0 < \theta < \frac{\pi}{2}$ . To illustrate it we take a particular value for  $\theta$

$$\theta = \frac{\pi}{3} \Rightarrow \begin{cases} \sin^2\left(\frac{\theta_{ab}}{2}\right) = \frac{3}{4} \\ \sin^2\left(\frac{\theta_{ac}}{2}\right) = \frac{1}{4} \\ \sin^2\left(\frac{\theta_{cb}}{2}\right) = \frac{1}{4} \end{cases} \quad (1.6)$$

Then Bell's inequality leads to

$$\frac{3}{4} \stackrel{??}{\leq} \frac{1}{4} + \frac{1}{4} = \frac{1}{2}$$

### Bell's original inequality

Now we derive the original form of Bell's inequality. For this, we consider the following starting points:

**i)** Spin measurements for singlets (or analogous)

**ii)** Two observers obtain results  $A_\lambda(\hat{n}_1)$  and  $B_\lambda(\hat{n}_2)$  the possible values of which are  $\pm 1$ .  $\lambda$  is the set of local hidden variables (LHV) and  $\hat{n}_{1,2}$  are the directions chosen for the measurement.

**iii)** Correlation of the results:

$$E^\rho(\hat{n}_1, \hat{n}_2) = \int_{\Gamma} A_\lambda(\hat{n}_1) B_\lambda(\hat{n}_2) \rho(\lambda) d\lambda$$

where  $\Gamma$  is the total  $\lambda$  space.

As a consequence of **i)**  $\rightarrow E^\rho(\hat{n}_i, \hat{n}_i) = -1$ . Then,

$$\begin{aligned} & E^\rho(\hat{n}_1, \hat{n}_2) - E^\rho(\hat{n}_1, \hat{n}_3) = \\ &= - \int_{\Gamma} [A_\lambda(\hat{n}_1) A_\lambda(\hat{n}_2) - A_\lambda(\hat{n}_1) A_\lambda(\hat{n}_3)] \rho(\lambda) d\lambda = \\ &= - \int_{\Gamma} A_\lambda(\hat{n}_1) A_\lambda(\hat{n}_2) (1 - A_\lambda(\hat{n}_2) A_\lambda(\hat{n}_3)) \rho(\lambda) d\lambda \end{aligned}$$

And therefore, using **ii)**

$$\begin{aligned} |E^\rho(\hat{n}_1, \hat{n}_2) - E^\rho(\hat{n}_1, \hat{n}_3)| &\leq 1 - E^\rho(\hat{n}_2, \hat{n}_3) \\ &\Rightarrow \end{aligned}$$

$$|E^\rho(\hat{n}_1, \hat{n}_2) - E^\rho(\hat{n}_1, \hat{n}_3)| + E^\rho(\hat{n}_2, \hat{n}_3) \leq 1$$

which is the original Bell's inequality.

### Generalization of Bell's inequality (CHSH)

In 1969 J. Clauser *et al.* [22] presented an adaptation of Bell's inequality to realizable experiments. In the following we present their inequality, known as CHSH Bell's inequality.

We will refer to the values measured in two different apparatus as  $A(a)$  and  $B(b)$  where  $a$  and  $b$  are the parameters related to the setting of each apparatus and  $A(a)$  and  $B(b)$  can take one of two possible values  $\pm 1$ . The correlation between  $A(a)$  and  $B(b)$  is due to information shared in the past for the particles of the pair, which now

carry this information with them. In the frame of LHV the results are deterministic  $\{A(a, \lambda), B(b, \lambda)\}$  due to the information shared in  $\lambda$  (set of hidden variables) and by virtue of locality  $A(a, \lambda)$  ( $B(b, \lambda)$ ) is independent of  $b$  ( $a$ ). Also  $\rho(\lambda)$  (probability distribution of the ensemble) is independent of both  $a$  and  $b$ . The correlation function  $P(a, b)$  is defined as follows,

$$P(a, b) = \int_{\Gamma} A(a, \lambda)B(b, \lambda)\rho(\lambda)d\lambda \quad (1.7)$$

where again  $\Gamma$  is the total  $\lambda$  space. We then have

$$\begin{aligned} |P(a, b) - P(a, c)| &\leq \int_{\Gamma} |A(a, \lambda)B(b, \lambda) - A(a, \lambda)B(c, \lambda)| \rho(\lambda)d\lambda \quad (1.8) \\ &= \int_{\Gamma} |A(a, \lambda)B(b, \lambda)| [1 - B(b, \lambda)B(c, \lambda)] \rho(\lambda)d\lambda = \int_{\Gamma} [1 - B(b, \lambda)B(c, \lambda)] \rho(\lambda)d\lambda \\ &= 1 - \int_{\Gamma} B(b, \lambda)B(c, \lambda)\rho(\lambda)d\lambda. \end{aligned}$$

Suppose that for some  $b$  and  $b'$   $P(b', b) = 1 - \delta$  with  $0 \leq \delta \leq 1$ , where experimental interesting cases are those for which  $\delta$  is close but not equal to 0. This allows for non-perfect correlations, in contrast to Bell's original inequality, and is more realistic from the experimental point of view. We now divide  $\Gamma$  in two regions  $\Gamma_+$  and  $\Gamma_-$  such that  $\Gamma_{\pm} = \{\lambda | A(b', \lambda) = \pm B(b, \lambda)\}$ . Then  $\int_{\Gamma_-} \rho(\lambda)d\lambda = \frac{1}{2}\delta$ , therefore

$$\begin{aligned} \int_{\Gamma} B(b, \lambda)B(c, \lambda)\rho(\lambda)d\lambda &= \int_{\Gamma} A(b', \lambda)B(b, \lambda)\rho(\lambda)d\lambda - 2 \int_{\Gamma_-} A(b', \lambda)B(b, \lambda)\rho(\lambda)d\lambda \quad (1.9) \\ &\geq P(b', c) - 2 \int_{\Gamma_-} |A(b', \lambda)B(b, \lambda)| \rho(\lambda)d\lambda = P(b', c) - \delta. \end{aligned}$$

Using the result of Eq. (1.9) combined with Eq. (1.8) we obtain

$$\begin{aligned} P(a, b) - P(a, c) &\leq |P(a, b) - P(a, c)| \leq 2 - P(b', b) - P(b', c) \\ \implies &\boxed{P(a, b) - P(a, c) + P(b', b) + P(b', c) \leq 2} \quad (1.10) \end{aligned}$$

In quantum mechanics and for measurements performed on two 1/2-spin particles, the correlation is

$$P(a, b) = \langle \phi | \vec{\sigma} \cdot \hat{a} \vec{\sigma} \cdot \hat{b} | \phi \rangle \quad (1.11)$$

where  $\hat{a}$  and  $\hat{b}$  are the unit vectors corresponding to the directions along which each spin is measured,  $\phi$  is the two-spin state of the particles and  $\vec{\sigma} = (\sigma_1, \sigma_2, \sigma_3)$  with  $\sigma_i$  the Pauli matrices.

Bell's results motivated many experiments [23–25] which showed agreement with the predictions of Quantum Mechanics. Nevertheless, these experiments suffer from so-called “loopholes”, which means that not all the conditions for the test of Bell's inequalities are strictly met in the experiments. In some experiments, the locality loophole is present, in the others the detection loophole. In the detection loophole the problem is that not all the particles under test can be detected. Therefore, the test is performed only on a sample of the total particles; if the sample is not representative, the test is not strictly valid. This is the case in the experiments performed on photons. In the case of the locality loophole, the problem is that particles cannot be put apart from each other at a distance long enough, while preserving entanglement, so as to rule out the possibility of information exchange. This is the case for experiments performed on massive particles.

### 1.1.3 Production of entanglement

Here we give a brief overview of some of the schemes proposed for the production of entangled electron spins (entanglers). Entanglement of electron spins is quite often present in nature; for instance, the ground state of a Helium atom is a singlet. The Cooper pairs in a superconductor are also in a singlet state. However, for quantum communication, entangled spins need to be individually controlled and separated in space. Therefore, a crucial prerequisite for an entangler is to produce spatially separated entangled electrons. One approach to obtain entangled and spatially separated electrons is to take advantage of the entanglement present in nature, extract the electrons from where they are present and use interactions or energy conservation to separate them. Another approach is to use interaction between the electrons to create entanglement between them and then try to separate them while preserving entanglement. In the following, as example, we shortly describe the underlying ideas in three different proposals for entanglers [11, 16, 18]. In the first two the entanglement present in nature is extracted and in the third one, entanglement is created via interaction of the electrons.

#### Andreev entangler with quantum dots

The Andreev entangler [11] is schematically shown in Fig. 1.1. A superconducting contact with chemical potential  $\mu_S$  is weakly coupled to two quantum dots in the Coulomb blockade regime. The dots are also weakly coupled to Fermi liquid leads at the same chemical potential  $\mu_L$ . The tunneling amplitudes between superconductor and dots, and

dots and leads, are denoted by  $T_{SD}$  and  $T_{DL}$  respectively. A bias voltage  $\Delta\mu = \mu_S - \mu_L$  is applied between the superconductor and the leads. The chemical potential of the dots ( $\epsilon_1$  and  $\epsilon_2$ ) are tuned by external gate voltages, so that  $\epsilon_1 + \epsilon_2 = 2\mu_S$ . This condition makes the tunneling of the two electrons via different dots into different leads resonant. The resonance for electrons tunneling into the same dots is suppressed by the on-site Coulomb repulsion  $U$  of the dots and/or the superconducting gap  $\Delta$ . The regime under which the entanglement of the Cooper pairs in the superconductor is successfully transported to the leads is

$$\Delta, U, \delta\epsilon > \Delta\mu > \gamma_l, k_B T \quad \text{and} \quad \gamma_l > \gamma_S$$

where  $\delta\epsilon$  is the mean level separation of the dots,  $\gamma_l = 2\pi\nu_l |T_{DL}|^2$  and  $\gamma_S = 2\pi\nu_S |T_{SD}|^2$  are the tunneling rates from the dots to the leads and from the superconductor to the dots respectively, with  $\nu_l$  and  $\nu_S$  being the corresponding electron densities of states per spin at the Fermi level. Under this regime processes are excluded in which electrons already present in the dots are transported, single electron tunneling and tunneling via the same dot. Also, the asymmetry of the tunneling barriers ( $\gamma_l > \gamma_S$ ) excludes correlations between subsequent Cooper pairs. The time delay between electrons from the same Cooper pair is given by  $1/\Delta$  and the time separation between pairs is given approximately by  $\gamma_l/\gamma_S^2$ .

### Triple-quantum dot entangler

The setup for this proposal [16] is shown in Fig. 1.2. Electrons are injected into the quantum dot  $D_C$  from a source via tunneling. This dot accepts at most two electrons. The idea is to get an entangled pair from  $D_C$  since its ground state is a singlet. Similarly to the Andreev entangler, to get the entangled pair out of the dot and suppress non-entangled currents, the idea is to have a resonance for the joint transport of the two electrons from  $D_C$  to secondary dots ( $D_L$  and  $D_R$ ), from where the electrons tunnel to the output leads. The non-entangled currents come from the tunneling of single electrons or tunneling of a pair into the same lead. To get the desired resonance the condition  $\epsilon_L + \epsilon_R = 2\epsilon_C$  must hold, where  $\epsilon_L$  and  $\epsilon_R$  are the energy levels available in  $D_L$  and  $D_R$  respectively, and  $2\epsilon_C$  is the total energy of the two electrons in the dot  $D_C$ . The transport of a single electron is suppressed by the energy mismatch  $\epsilon_C \pm U \neq \epsilon_L, \epsilon_R$ , where  $\epsilon_C \pm U$  is the energy of the other electron in the dot  $D_C$ . The time delay between electrons of an entangled pair is approximately  $1/U$ , and the time separation between entangled pairs is approximately  $2/\alpha$ , with  $\alpha$  the tunneling rate from the electron source to the dot  $D_C$ .

### Coulomb scattering entangler

In this case, a setup is proposed [18] as shown in Fig. 1.3. Entangled electron-spin pairs are generated by collision of pairs of electrons in a 2-DEG interacting electron gas. Electrons are coming from two reservoirs and their momenta are filtered by two quantum point contacts, so that  $\vec{p}_1 \simeq -\vec{p}_2$ . The electrons collide and scatter, and later are collected

by two detectors, which are placed such that only electrons that collide at a scattering angle around  $\pi/2$  are collected. At this angle there is constructive two-particle interference in the spin-singlet channel and the scattering amplitude vanishes for the spin-triplet states. Therefore, collecting at  $\pi/2$  allows to get the spin-singlets, each electron of the pair in a different detector. Because of the condition  $\vec{p}_1 \simeq -\vec{p}_2$ , the energies are individually conserved ( $p_1 \simeq p_2 \simeq p'_1 \simeq p'_2$ ,  $p_i = |\vec{p}_i|$  and  $\vec{p}'_i$  the momenta after the scattering). This ensures that the outgoing scattering states are unoccupied ( $p'_{1,2} > k_F$ ). The electrons are further assumed to be injected with small excitation energies  $\xi_i = \hbar^2 p_i^2 / 2m - E_F \ll E_F$  with  $E_F = \hbar^2 k_F^2 / 2m$  the Fermi energy and  $m$  the effective mass in order to have well-defined quasiparticle states with long lifetimes. It is important to prevent in the counting of uncorrelated electrons which accidentally enter the detectors (e.g., due to impurities). For this purpose, coincidence measurements could be carried out or an AC modulation could be applied to each reservoir with different frequencies  $\omega_1$  and  $\omega_2$ . This way electrons which have actually interacted could be selected, since they would be modulated by the frequency  $\omega_1 \pm \omega_2$ .

#### 1.1.4 Characterization of entanglement

In order to characterize entanglement, there are two important aspects, the quantitative and the qualitative. With respect to the former, it is of practical interest to quantify the amount of entanglement of a given system, and for that purpose there have been several ideas on how to measure entanglement. One of these entanglement measures is the von Neumann entropy, which we will use later on in Chap. 2. For a pure bipartite system described by a density matrix  $\rho$  it is defined as follows:

$$E(\rho) = -\text{tr}_A (\rho_A \log_2 \rho_A) = -\text{tr}_B (\rho_B \log_2 \rho_B)$$

where  $\rho_{A,B} = \text{tr}_{B,A} \rho$  are the partial density matrices obtained by tracing out one of the subsystems. The value of  $E(\rho)$  lies between  $E = 0$  (no entanglement) and  $E = 1$  (maximal entanglement). Among maximally entangled states, there are some of particular relevance. This is the case for the so-called ‘‘Bell states’’. These are two-particle states, where the entangled properties of the particles are  $\frac{1}{2}$ -spins<sup>3</sup>. The Bell states form a basis called ‘‘Bell’s basis’’. These states are

$$\begin{aligned} |\phi^\pm\rangle &= \frac{1}{\sqrt{2}} (|00\rangle \pm |11\rangle) \\ |\psi^\pm\rangle &= \frac{1}{\sqrt{2}} (|01\rangle \pm |10\rangle) \end{aligned} \tag{1.12}$$

where  $|ij\rangle = |i\rangle \otimes |j\rangle$  and  $\{|0\rangle, |1\rangle\}$  represents the basis for the  $\frac{1}{2}$ -spin-like property of each particle. For multipartite entanglement, where more than two particles are involved, there

---

<sup>3</sup>It can also be defined for other properties with the same formal properties as the  $\frac{1}{2}$ -spin.



are also maximally entangled states of practical relevance, since Greenberger, Horne and Zeilinger [26] have shown quantum predictions for these states which cannot be reproduced by any local hidden variables theory. These are known as GHZ states and for three particles take the general form

$$|\Psi_{GHZ}\rangle = \frac{1}{\sqrt{2}} (|000\rangle + e^{i\phi} |111\rangle) \quad (1.13)$$

We will be interested in the following four-photon states

$$|\Psi^\pm\rangle \rightarrow |\sigma_+\sigma_-\sigma_-\sigma_+\rangle \pm |\sigma_-\sigma_+\sigma_+\sigma_-\rangle, \quad (1.14)$$

$$|\Phi^\pm\rangle \rightarrow |\sigma_-\sigma_-\sigma_+\sigma_+\rangle \pm |\sigma_+\sigma_+\sigma_-\sigma_-\rangle, \quad (1.15)$$

where  $\sigma_\pm$  denotes the two orthogonal states in the circularly polarized photon-state basis. These states are equivalent to the four-particle generalization of GHZ states, since (1.14) and (1.15) can be obtained from the GHZ state by redefining + and - for two of the photons. We come back to these photon-polarization entangled states in Chap. 2.

## 1.2 The electron spin in quantum dots

In this section we will focus on spins in solid-state systems. More specifically, we will discuss different issues related to the electron spin in quantum dots, since these systems are a central part of this work. We will give an overview over the main points to take into account and their current state on the experimental side.

### 1.2.1 Spin control

It has been shown that the single-electron states in the low-energy range of quantum dots agree with a shell model. In lateral quantum dots, the confinement is stronger in one dimension, therefore the dot potential is effectively two dimensional and can be approximated by a two-dimension harmonic oscillator potential. If a magnetic field is applied, the degeneracy between the spin states  $|\uparrow\rangle$  and  $|\downarrow\rangle$  is lifted due to the Zeeman interaction and makes them distinguishable. The precise control over the number of confined electrons has been demonstrated in InGaAs self-assembled quantum dots [27], in gated vertical quantum dots [28], in quantum rings [29], and also in electrostatically defined single [30] and double [31–33] dots in GaAs.

### 1.2.2 Spin relaxation and decoherence

One of the conditions for the use of the spin degree of freedom of electrons is a long spin lifetime. There are two important processes that contribute to a shortening of the spin

lifetime: spin relaxation and spin decoherence. Their time scales are characterized by the relaxation ( $T_1$ ) and decoherence ( $T_2$ ) times respectively. The relaxation time  $T_1$  is the time required for the relaxation of a single spin in an external magnetic field from an excited state into the thermal equilibrium. The decoherence time  $T_2$  is the time in which a relative phase in a superposition state between spin-up and spin-down of a single spin is preserved. Usually  $T_2 \leq T_1$ , so the limiting time scale for applications based on the electron spin is  $T_2$ . The relevance of this scale has motivated a lot of work both on the theoretical and experimental sides, which intends to find the value of  $T_1$  and  $T_2$  under different conditions and in several systems. For the electron-spin relaxation in quantum dots, Fujisawa *et al.* [34] reported a triplet-to-singlet relaxation time of  $\tau_{S-T} = 200 \mu\text{s}$  in vertical quantum dots. More recently, a lower bound on the singlet-triplet relaxation time has been measured in lateral dots, giving  $\tau_{S-T} \geq 70 \mu\text{s}$  [35]. Later, a much longer relaxation time ( $\tau_{S-T} = (2.58 \pm 0.09) \text{ ms}$ ) was measured independently [36]. Several groups have measured  $T_1$  for *single* electron spins, reporting values of e.g.  $T_1 \gtrsim 50 \mu\text{s}$  at a magnetic field of  $B = 7.5 \text{ T}$  in gated GaAs dots [37] and later [38]  $T_1 \approx (0.85 \pm 0.11) \text{ ms}$  at  $B = 8 \text{ T}$ . For In(Ga)As self-assembled dots there has been recently established [39] a lower bound  $T_1 \gtrsim 20 \text{ ms}$  at  $T = 1 \text{ K}$  and  $B = 4 \text{ T}$ . In this experiment, the larger level spacing of self-assembled dots (compared to gated GaAs dots) is responsible for the longer  $T_1$ -time.

### 1.2.3 Spin initialization

There are two possibilities to initialize the spins. First, a strong magnetic field can be applied, such that the Zeeman splitting is larger than the thermal energy. This way the spins reach their thermodynamical ground state in which they are aligned with the magnetic field, and therefore a strong polarization is achieved. Second, spin-polarized currents can be injected. The injection of spins from ferromagnetic semiconductors into normal semiconductors has been reported with polarizations up to 90% [8,9]. In addition, initialization of single spins can be achieved using a spin filter (see 1.2.4) or by optical schemes (see 1.2.5).

### 1.2.4 Single-spin detection

The magnetic moment of a single spin  $1/2$  is very small and therefore, hard to detect directly. For this reason there have been many proposals to detect spins based on the transfer of information stored in the spin to an orbital degree of freedom, called “spin-charge conversion” [10, 37, 38, 40–46]. The spin can be read using a spin filter, which is a device that only transmits electrons with a particular spin polarization and blocks the opposite polarization. Recher *et al.* [40] have proposed a spin-filter implementation consisting of a quantum dot in the Coulomb blockade regime, weakly coupled to two current leads. In a static magnetic field, the direction of the transmitted spin can be changed by tuning a gate voltage applied to the dot. Experimental demonstrations of a

spin filter have been achieved by Folk *et al.* [41], Potok *et al.* [42], Hanson *et al.* [37], and Elzerman *et al.* [38]. The first two of these implementations have demonstrated the spin-filtering effect with a GaAs quantum dot in the open [41] and in the Coulomb-blockade regime [42]. Another approach to the detection of spins is to perform an *n-shot* readout. This procedure consists in identically repeating  $n$  times the experiment, so that errors during the measurement can be statistically eliminated. There is a lower bound in the number  $n$  of measurements to be performed so that a statistical analysis can be done. This lower bound is given by

$$n > z_{1-\alpha}^2 \left( \frac{1}{\eta} - 1 \right)$$

where  $z_{1-\alpha}$  is the critical value of the standard normal distribution function,  $\Phi(z_{1-\alpha}) = 1 - \alpha = (1/2)[1 + \text{erf}(z_{1-\alpha}/\sqrt{2})]$ ,  $\alpha$  is called the infidelity, and

$$\eta = \left( \sqrt{p_{\uparrow}p_{\downarrow}} - \sqrt{(1-p_{\uparrow})(1-p_{\downarrow})} \right)^2 \quad (1.16)$$

can be interpreted as a measurement efficiency with  $\eta \in [0, 1]$ .  $p_{\uparrow}$  and  $p_{\downarrow}$  are the probabilities that the experimental readout of the spin states  $|\uparrow\rangle$  and  $|\downarrow\rangle$  respectively gives the correct result. Recently, *single-shot* readout of a single electron spin in a quantum dot has been experimentally demonstrated by Elzerman *et al.* [38].

### 1.2.5 Optical interaction, initialization and readout of spins

The currently very active field of ultrafast laser technology suggests that single spin states can be optically detected and manipulated within very short times (picoseconds or even femtoseconds), several orders of magnitude faster than in schemes based on the transport of electric charge. Via the absorption of a photon, an electron in a confined valence-band state can be excited to a confined conduction-band state. For such inter-band transitions, optical selection rules apply and establish conditions on the quantum numbers of the optically coupled states. Several methods have been developed to optically probe and manipulate states of *single* quantum dots [47]. Optical schemes have further been proposed to achieve initialization of electron spins, for the detection of the  $T_2$ -time of electron spins, for single-qubit gates, and for two-qubit gates. In these schemes and also in many other schemes exploiting the spin states of an electron, a quantum dot initially contains a single excess electron. Optical excitation of such a state creates a negatively charged exciton (sometimes also called “trion”) in the dot, i.e., a compound of two conduction-band electrons and one valence-band hole. If the quantum dot is in the so-called strong confinement regime, the (single-particle) confinement energies are much larger than the Coulomb interaction energies of the carriers in the dot. This criterion is typically satisfied for small self-assembled dots and colloidal dots. The two electrons then occupy the lowest single-particle level of the dot and form a spin singlet. Note that the excess electron initially occupies one of the available spin states. Due to the

Pauli principle, the absorption of a circularly polarized photon is only possible if the corresponding electron spin state is not already occupied. A  $\sigma^-$ -polarized photon can only be absorbed if the spin of the excess electron is in the state  $|\downarrow\rangle$ , whereas a  $\sigma^+$ -polarized photon can only be absorbed for  $|\uparrow\rangle$ . In the photoluminescence spectrum, the lines belonging to these two transitions coincide for zero magnetic field and split for non-zero magnetic fields. If a circularly polarized photon with an energy that matches the corresponding transition energy is absorbed, the initial spin state of the excess electron is identified. This experiment has recently been performed with a single InGaAs/GaAs dot by Högele *et al.* [48] using high-resolution laser absorption spectroscopy. Equivalently, the photoluminescence (which is only emitted after a successful photon absorption) could be detected instead of the absorption. One can also apply an electric field to the dot such that an electron and a hole tunnel out of the dot after a photon has been absorbed. Instead of the photoluminescence, the resulting electric current (the so-called photocurrent) can then be detected [49].

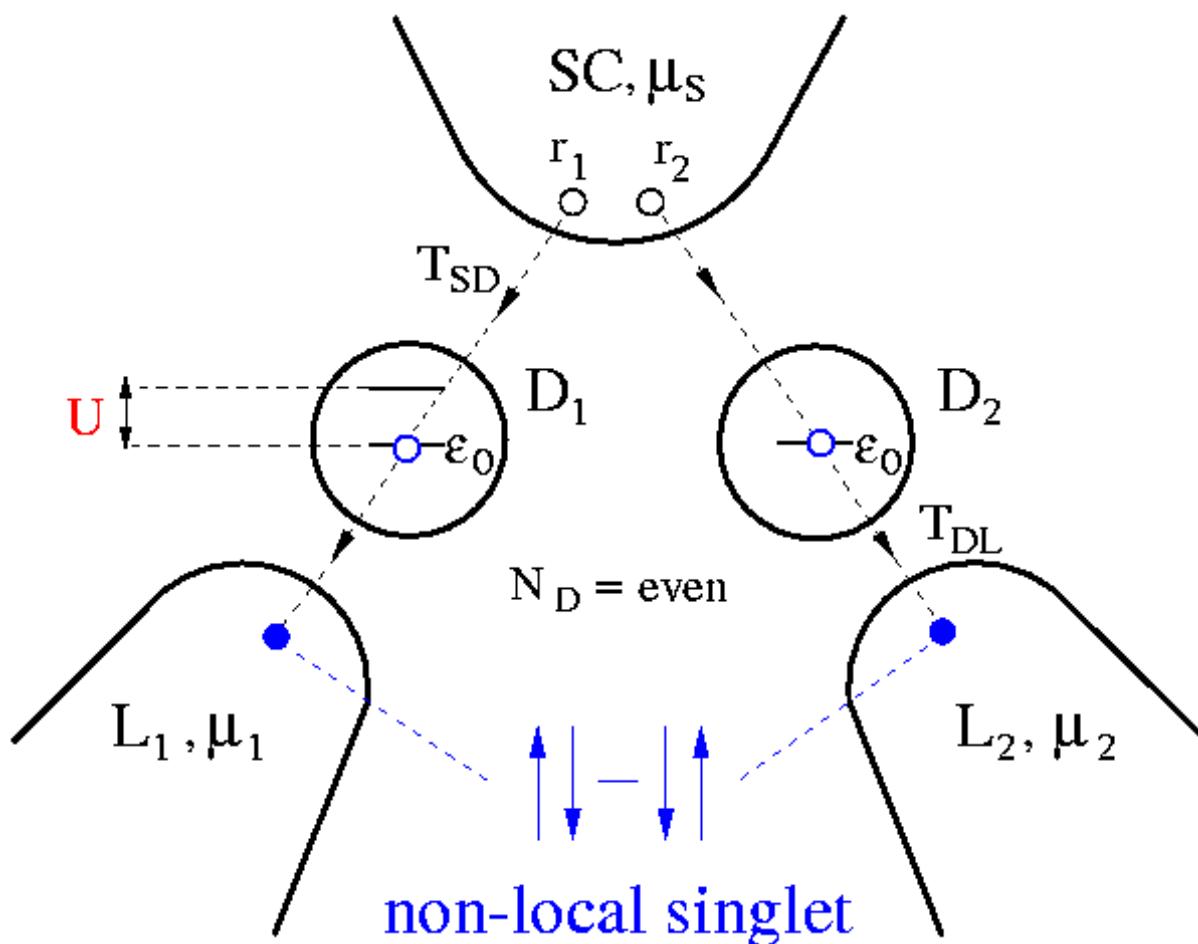


Figure 1.1: Setup for the Andreev entangler with quantum dots. To entangled electron from a Cooper pair in the semiconductor  $SC$  tunnel from  $\vec{r}_1$  and  $\vec{r}_2$  with amplitude  $T_{SD}$  to the quantum dots  $D_1$  and  $D_2$ . Then the electrons tunnel to normal Fermi liquid leads  $L_1$  and  $L_2$  with amplitude  $T_{DL}$ . The superconductor is kept at the chemical potential  $\mu_S$  and the leads at  $\mu_l$ . (Figure courtesy of P. Recher.)

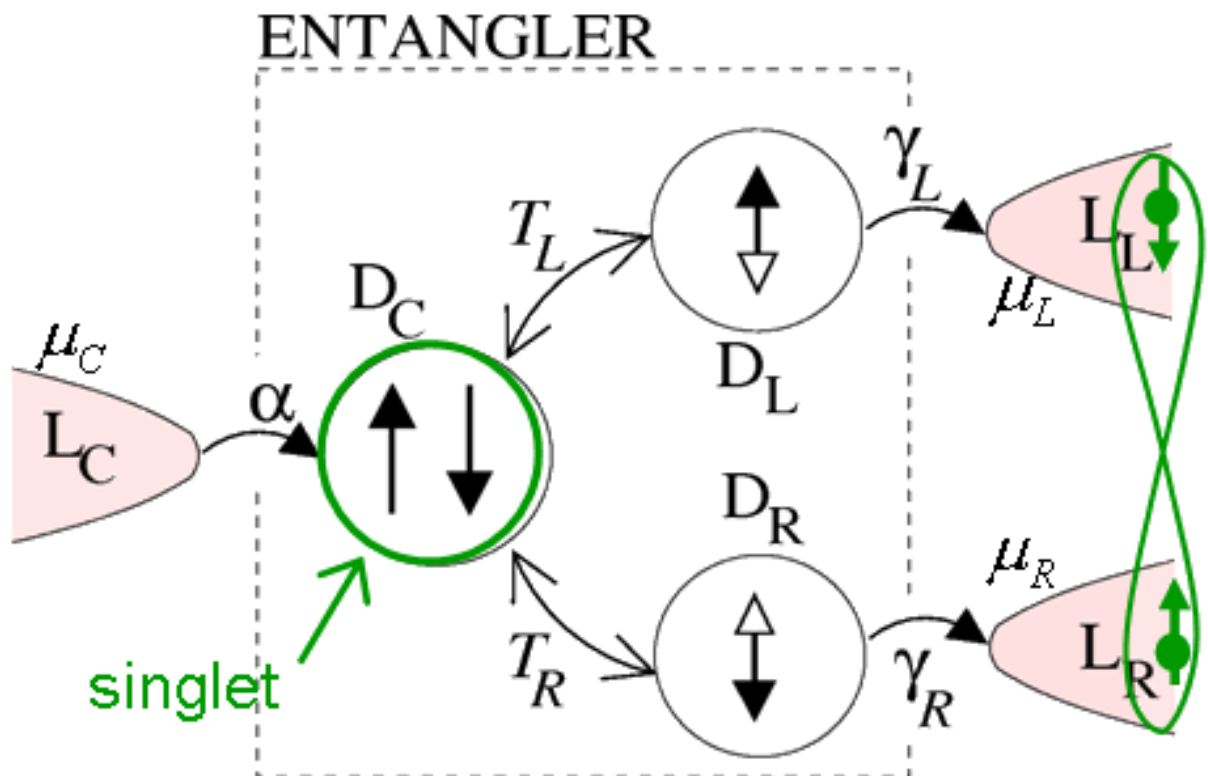


Figure 1.2: Setup for the triple-quantum dot entangler. The dot  $D_C$  can accept at most two electrons coming from the source lead at a rate  $\alpha$ . The two-electron ground state of the dot is the singlet. From the dot  $D_C$  the electrons can tunnel coherently with amplitude  $T_0$  to the dots  $D_L$  and  $D_R$ , which can only take 0 or 1 electrons. The secondary dots  $D_L$  and  $D_R$  act as energy filters, and from them the electrons can tunnel out to drain leads with at the rate  $\gamma$ . (Figure courtesy of D. Saraga.)

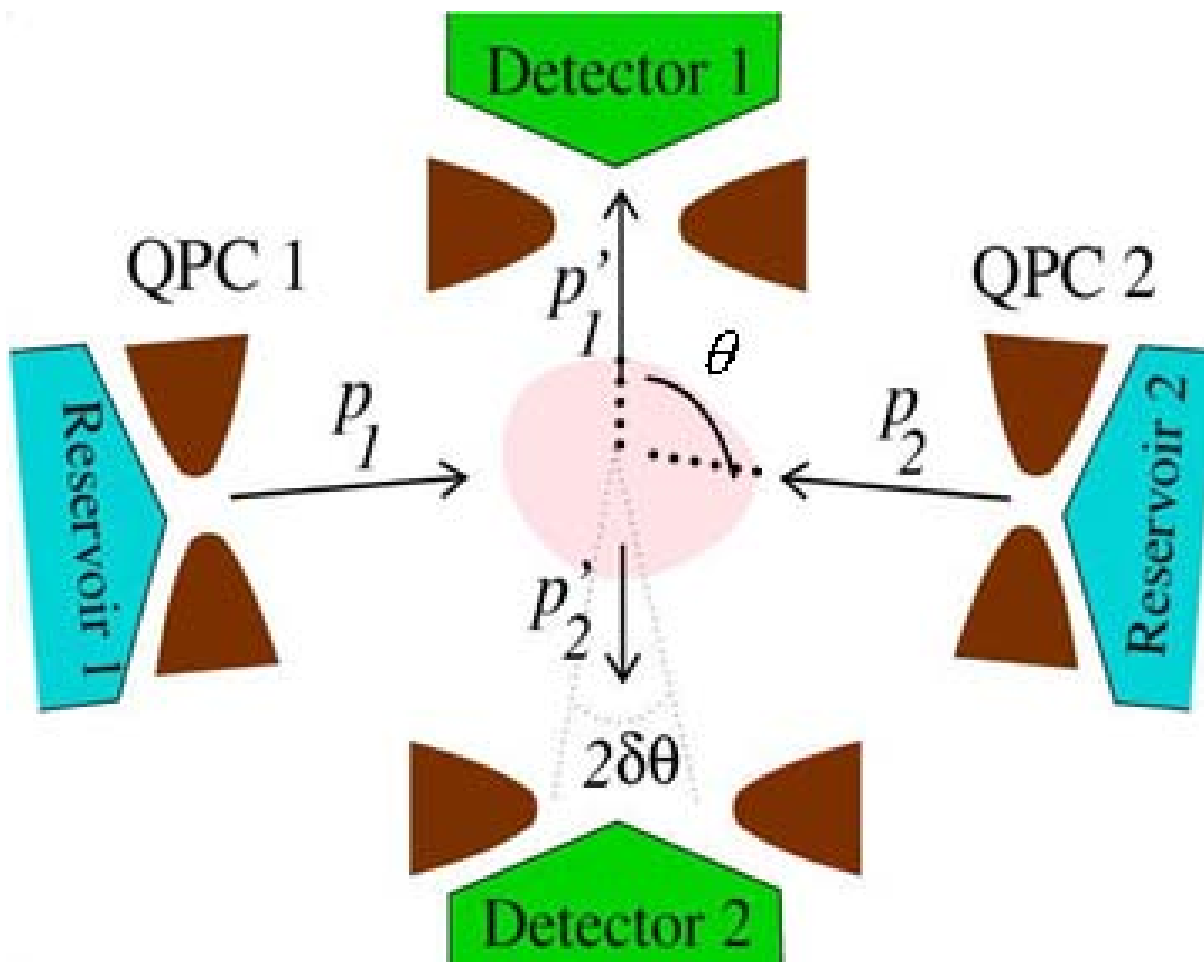


Figure 1.3: Setup for the Coulomb scattering entangler. Electrons coming from two sources are filtered by quantum point contacts such that they have momenta  $\vec{p}_1 \simeq -\vec{p}_2$ . They collide (shaded area) and scatter off from each other. Due to interference, at the scattering angle  $\pi/2$  only the singlet channel is allowed and the triplets are suppressed. The electrons of the singlet pair are collected each at a detector, positioned so that only electrons with scattering angles approximately equal to  $\pi/2$  are collected. (Figure courtesy of D. Saraga.)





# Chapter 2

## Entanglement transfer from electron spins to photons.

In this chapter we show that electron recombination in spin light-emitting diodes provides an efficient method to transfer entanglement from electron spins onto pairs of polarization-entangled photons. We also show the possibility to create 4-photon states of the GHZ type. From the GHZ state, two fully entangled photons can be obtained by a measurement of two photons in the linear polarization basis, even for quantum dots with observable fine structure splitting for neutral excitons and significant exciton spin decoherence. Due to the interplay of quantum mechanical selection rules and interference, maximally entangled electron pairs are converted into maximally entangled photon pairs with unit fidelity for a continuous set of observation directions. We model the dynamics of the conversion process using a master-equation approach and show that the implementation of our scheme is feasible with current experimental techniques. In Section 2.2 we concentrate on the electron-spins along their transport trough Fermi leads, describe their state before they enter the structures where they recombine, and give a rate for this whole injection-recombination process. In Section 2.3 we focus on the recombination process and analyze the optical output. Finally, in Section 2.4 we draw our conclusions.

### 2.1 Introduction

Spin light-emitting diodes (spin-LEDs), [1, 8, 9, 39, 50–53] in which electron recombination is accompanied by the emission of a photon with well-defined circular polarization, provide an efficient interface between electron spins and photons. The operation of such devices at the single-photon level would allow one to convert the quantum state of an electron encoded in its spin state into that of a photon with a wide range of possible applications. In view of quantum information schemes, converting spin into photon quantum states corresponds to a conversion of localized into flying qubits, which can be transmitted over long distances and could overcome limitations caused by the short-range nature of the electron exchange interaction [1]. On a more fundamental level, the photon polarization

can be readily measured experimentally such that an interface between spins and photons will allow one to measure quantum properties of the spin system via the photons generated on recombination. More specifically, entanglement of electron spins could be demonstrated not only in current noise [54,55] but also by measurements of photon polarizations which allows one to test Bell's inequalities [21] without the stringent limitations posed by decoherence in a solid state environment. In addition to its applications in quantum communication, this transfer can be used to characterize the output of an electron spin entangler [11–18] in a setup as shown in Fig. 2.1. The entangler injects the electrons of the entangled pair into separate leads. Subsequently, the electrons recombine optically in quantum dots located within two spin-LEDs (denoted by  $L$  and  $R$ ), and two photons are emitted. In the following, we also use the labels  $L$  and  $R$  for the two dots where optical recombination occurs. Such a setup can further act as a deterministic source of polarization-entangled photon pairs. Recently, the decay of biexcitons in single quantum dots has been proposed for the production of entangled photons [56,57]. However, several experiments [58–62] have only shown polarization correlation but not entanglement of the photons. The fine structure splitting  $\delta_{\text{ehx}}$  of the bright exciton ground state [63] has been identified to be crucial for the lack of entanglement: Firstly, the polarization-entangled photons are also entangled in energy if  $\delta_{\text{ehx}}$  is larger than the exciton line-width [64]. Secondly, for  $\delta_{\text{ehx}} \neq 0$  the exciton spin relaxation rate due to phonons  $1/T_{1,X}$  is enhanced [65] and leads to an increased decoherence rate  $1/T_{2,X} = 1/2T_{1,X} + 1/T_{\varphi,X}$ , where  $1/T_{\varphi,X}$  is the pure decoherence time. To overcome these difficulties we propose to use positively charged excitons ( $X^+$ ), for which  $\delta_{\text{ehx}} = 0$  up to small corrections. Moreover, we demonstrate that the antisymmetric hole ground state of the  $X^+$  enables the production of entangled four-photon states. By calculating the von Neumann entropy we study the transfer of entanglement for different photon emission directions. Due to quantum mechanical interference, the fidelity of this process approaches unity not only for photon emission along the spin quantization axis, but for a continuous set of observation directions.

## 2.2 Electrons injection and recombination

The effective Hamiltonian of the system is given by

$$H = H_L + H_R + H_{\text{rad}} + H_{\text{int}}, \quad (2.1)$$

where  $H_\alpha = \mathbf{p}^2/2m + V_{\text{qd}}(\mathbf{r})$  is the Hamiltonian of the quantum dot  $\alpha = L, R$  with confinement potential  $V_{\text{qd}}(\mathbf{r})$ . For convenience, we use the labels  $L$  and  $R$  for the two dots involved in the recombination. The Hamiltonian of the electromagnetic field is  $H_{\text{rad}} = \sum_{\mathbf{k},\lambda} \hbar\omega_k a_{\mathbf{k}\lambda}^\dagger a_{\mathbf{k}\lambda} + \frac{1}{2}$  and  $H_{\text{int}} = -e\mathbf{A} \cdot \mathbf{p}/m_0c = H_{\text{em}} + h.c.$  is the optical interaction term, which is linear in both the vector potential  $\mathbf{A}$  and the electron momentum  $\mathbf{p}$  and can be decomposed into a photon emission term  $H_{\text{em}}$  and its hermitian conjugate. For simplicity, we assume that the dots  $L$  and  $R$  are identical, with cubic crystal structure and

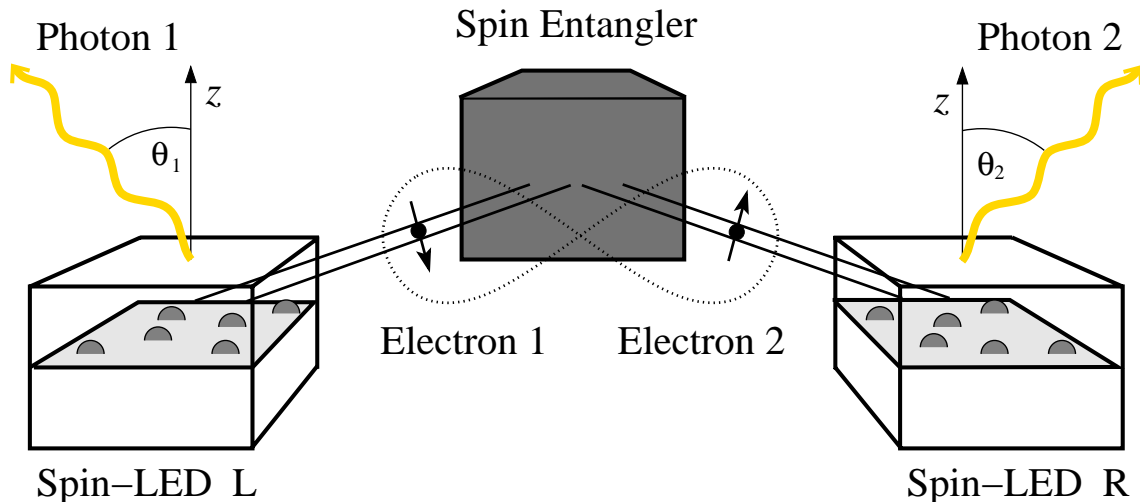


Figure 2.1: Schematic setup for the transfer of entanglement between electrons and photons. An electron entangler (gray box) injects a pair of spin-entangled electrons into two current leads. The electrons then recombine individually in one of the quantum dots located in the left (L) or the right (R) spin-LED and give rise to the emission of two photons.

with aligned main crystal axes. We choose the  $z$  axes parallel to the quantum dot growth direction (e.g., [001]). If the quantum dot confinement is stronger in the  $z$  direction than in the  $xy$  plane,  $z$  defines the spin quantization axis and heavy-hole (hh) and light-hole (lh) states are energetically split by  $\Delta_{\text{hh-lh}}$  (typically  $\Delta_{\text{hh-lh}} \sim 10$  meV). Alternatively, uniaxial strain can define a spin quantization axis and also lifts the degeneracy of hh and lh states [66]. We consider a hh ground state, with angular momentum projection  $\pm 3/2$  in terms of electron quantum numbers. We further focus on the strong-confinement regime, where the dot radius is smaller than the exciton Bohr radius. Then, for the recombination of a single electron, optical selection rules ensure a one-to-one correspondence of electron spin polarization and circular photon polarization if (and only if) the photon is emitted along the spin quantization axis, but not for the general case of photon emission into an arbitrary direction  $(\theta, \phi)$ , where  $\theta$  and  $\phi$  are the polar and the azimuthal angle, respectively.

The quantum dots in both spin-LEDs are prepared in a state  $|\chi_\alpha\rangle$ , where two excess holes occupy the lowest hh level in each dot. This initial state, which can be generated by applying an appropriate bias voltage across the LED, has several advantages. Firstly, electrons with arbitrary spin states can recombine optically, as demonstrated for electron spin detection in a recent experiment [52]. Secondly, the  $z$  component of the total hole spin vanishes. This is a consequence of the fact that in quantum dots the electron-hole exchange energy  $\Delta_{\text{ehx}}$  (typically  $\Delta_{\text{ehx}} < 0.1$  meV) is smaller than  $\Delta_{\text{hh-lh}}$ . Thus, circularly polarized  $X^+$  luminescence is obtained from the injected electron recombining with a hh, up to corrections of order  $\Delta_{\text{ehx}}/\Delta_{\text{hh-lh}}$ . This remains true for dots with asymmetric confinement in the  $xy$  plane, in stark contrast to the case with an electron and only one

hole in the dot [63], where the good exciton eigenstates are horizontally polarized and are split in energy typically by  $\delta_{ehx} \simeq 0.1$  meV, due to the electron-hole exchange interaction. Therefore, the electron-hole exchange interaction can be neutralized in anisotropic dots by initially providing *two* holes. The scheme we propose here equally works for initial states with more than two holes, as long as the total hole angular momentum along  $z$  vanishes. Inter-band mixing of hh and lh states (e.g., present in anisotropic dots) reduces the maximum circular polarization of photons emitted from spin-polarized electrons [51] and reduces the fidelity of our scheme. However, because the inter-band transition probability for lh states is three times smaller than that for hh states and hh-lh mixing is typically controlled by some small parameter in elliptical dots [63], we neglect lh transitions.

We first describe the dynamics of the electron injection and recombination in the two spin-LEDs using a master equation. The rate for the injection and the subsequent relaxation of electrons into the conduction band ground state in the dot  $\alpha$  is denoted by  $W_{e\alpha}$ . It has been demonstrated that this entire process is spin-conserving and occurs much faster than the optical recombination [52, 53], which is described by the rates  $W_{p\alpha}$ . Typically,  $W_{p\alpha} \sim 1$  ns $^{-1}$  and  $W_{e\alpha} \sim 0.1$  ps $^{-1}$  for the incoherent transition rates. We solve the master equation for the classical occupation probabilities and obtain the probability that two photons are emitted after the injection of two electrons into the dots at  $t = 0$ ,

$$P_{2p} = \prod_{\alpha=L,R} \frac{W_{e\alpha}(1 - e^{-tW_{p\alpha}}) - W_{p\alpha}(1 - e^{-tW_{e\alpha}})}{W_{e\alpha} - W_{p\alpha}}. \quad (2.2)$$

For  $W_{p\alpha} \ll W_{e\alpha}$ ,  $P_{2p} \approx \prod_{\alpha=L,R} (1 - e^{-tW_{p\alpha}})$ . After photon emission, bipartite photon entanglement is achieved by a measurement of the hole spins as we describe in Section 2.3 and the initial state is finally restored by injection of two holes into each of the two dots. We estimate the production rate of entangled photons in a setup to test some of the proposed electron entanglers [11–18]. For example, pairs of entangled electrons in a spin singlet state  $|\Psi^-\rangle = (|\uparrow\downarrow\rangle - |\downarrow\uparrow\rangle)/\sqrt{2}$  are produced by the Andreev entangler [11] with an average time separation  $\Delta t \sim 10^{-5}$ s, while for the entangler based on three quantum dots [16],  $\Delta t \sim 10^{-8}$ s. The two spin-entangled electrons of a pair typically are injected into the current leads with a relative time delay  $\tau \simeq 10^{-11}$  s and  $\tau \simeq 10^{-13}$  s for the Andreev and the three-dots entangler respectively. Because  $\tau, W_{p\alpha}^{-1} \ll \Delta t$ , photons originating from a single pair of entangled electrons can be identified with high reliability. In the steady state, the generation rate of entangled photons is determined by the rate at which entangled electron pairs leave the entangler,  $1/\Delta t$ .

### 2.2.1 Two-spin dynamics

The effect of relaxation and decoherence is taken into account for the two spins by the single-spin Bloch equation [67]. Given that the electrons are in different leads, they interact with independent environments (during times  $t$  and  $t'$ , respectively). Therefore, we consider different magnetic fields  $\mathbf{h}$  and  $\mathbf{h}'$ , enclosing an angle  $\beta$ , acting each on an individual spin. We calculate the two-spin density matrix  $\chi(t, t')$ , which is given in

Ref. [67] for  $t = t'$  and  $\beta = 0$ . We apply the Bloch equation directly to the first electron, for which we choose  $\mathbf{h} \parallel \hat{z}$ . Along  $\hat{z}$  we define the spin basis  $\{\uparrow, \downarrow\}$ . For the second electron the same Bloch equation is valid in the basis  $\{+, -\}$  of the spin states which are defined along  $\mathbf{h}'$ . Therefore, for the second electron a change of base has to be applied after evolving its density matrix with the Bloch equation, in order to get a transformation into the base of the first spin. The change of base reads

$$\begin{aligned}\rho_{++} &= \frac{1}{2} [(\rho_{\uparrow\uparrow} + \rho_{\downarrow\downarrow}) + \cos\beta (\rho_{\uparrow\uparrow} - \rho_{\downarrow\downarrow}) - \sin\beta (\rho_{\uparrow\downarrow} + \rho_{\downarrow\uparrow})], \\ \rho_{+-} &= \frac{1}{2} [\sin\beta (\rho_{\uparrow\uparrow} - \rho_{\downarrow\downarrow}) + (\rho_{\uparrow\downarrow} - \rho_{\downarrow\uparrow}) + \cos\beta (\rho_{\uparrow\downarrow} + \rho_{\downarrow\uparrow})], \\ \rho_{-+} &= \frac{1}{2} [\sin\beta (\rho_{\uparrow\uparrow} - \rho_{\downarrow\downarrow}) - (\rho_{\uparrow\downarrow} - \rho_{\downarrow\uparrow}) + \cos\beta (\rho_{\uparrow\downarrow} + \rho_{\downarrow\uparrow})], \\ \rho_{--} &= \frac{1}{2} [(\rho_{\uparrow\uparrow} + \rho_{\downarrow\downarrow}) - \cos\beta (\rho_{\uparrow\uparrow} - \rho_{\downarrow\downarrow}) + \sin\beta (\rho_{\uparrow\downarrow} + \rho_{\downarrow\uparrow})].\end{aligned}\quad (2.3)$$

After some algebra, the elements for the density matrix of the second spin for time  $t'$  in terms of the initial density matrix at time  $t' = 0$  can be obtained:

$$\begin{aligned}\rho_{\uparrow\uparrow}(t') &= \frac{1}{2} [\cos\beta f'_1 + \sin\beta f_A + [\rho_{\uparrow\uparrow}(0) + \rho_{\downarrow\downarrow}(0)] (1 - \cos\beta)], \\ \rho_{\uparrow\downarrow}(t') &= \frac{1}{2} (\cos\beta f_A - \sin\beta f'_1 + \sin\beta [\rho_{\uparrow\uparrow}(0) + \rho_{\downarrow\downarrow}(0)] + f_B), \\ \rho_{\downarrow\uparrow}(t') &= \frac{1}{2} (\cos\beta f_A - \sin\beta f'_1 + \sin\beta [\rho_{\uparrow\uparrow}(0) + \rho_{\downarrow\downarrow}(0)] - f_B), \\ \rho_{\downarrow\downarrow}(t') &= \frac{1}{2} [-\cos\beta f'_1 - \sin\beta f_A + [\rho_{\uparrow\uparrow}(0) + \rho_{\downarrow\downarrow}(0)] (1 + \cos\beta)],\end{aligned}\quad (2.4)$$

where

$$\begin{aligned}f'_1 &= (\rho_{\uparrow\uparrow}(0) + \rho_{\downarrow\downarrow}(0)) (1 + a'P') + e^{-t'/T'_1} (\cos\beta [\rho_{\uparrow\uparrow}(0) - \rho_{\downarrow\downarrow}(0)] - \sin\beta [\rho_{\uparrow\downarrow}(0) + \rho_{\downarrow\uparrow}(0)]), \\ f_A &= e^{-t'/T'_2} \left\{ \cos(\tilde{h}t') (\cos\beta [\rho_{\uparrow\downarrow}(0) + \rho_{\downarrow\uparrow}(0)] + \sin\beta [\rho_{\uparrow\uparrow}(0) - \rho_{\downarrow\downarrow}(0)]) \right. \\ &\quad \left. + i \sin(\tilde{h}t') [\rho_{\uparrow\downarrow}(0) - \rho_{\downarrow\uparrow}(0)] \right\}, \\ f_B &= e^{-t'/T'_2} \left\{ \cos(\tilde{h}t') [\rho_{\uparrow\downarrow}(0) - \rho_{\downarrow\uparrow}(0)] + i \sin(\tilde{h}t') (\cos\beta [\rho_{\uparrow\downarrow}(0) + \rho_{\downarrow\uparrow}(0)] \right. \\ &\quad \left. + \sin\beta [\rho_{\uparrow\uparrow}(0) - \rho_{\downarrow\downarrow}(0)]) \right\}.\end{aligned}\quad (2.5)$$

Here,  $T'_1$  and  $T'_2$  are the relaxation and decoherence times for the second spin respectively,  $a' = 1 - e^{-t'/T'_1}$  and  $P'$  is the stationary spin-polarization for the second spin.

In order to describe the time evolution of the two-spin density matrix in the basis  $\{\uparrow, \downarrow\}$  for both electrons, we decompose the initial singlet state. This will be done as follows: first, we will decompose the initial state (singlet) in terms of the two-spin basis  $\{|\uparrow\uparrow\rangle, |\uparrow\downarrow\rangle, |\downarrow\uparrow\rangle, |\downarrow\downarrow\rangle\}$  in the following way

$$\chi(t, t' = 0) = \frac{1}{2}(\chi_{(a)} - \chi_{(b)} - \chi_{(c)} + \chi_{(d)}). \quad (2.6)$$

Here,

$$\begin{aligned} \chi_{(a)} &= \rho_{\uparrow\uparrow}^{(1)} \otimes \rho_{\downarrow\downarrow}^{(2)}, \\ \chi_{(b)} &= \rho_{\uparrow\downarrow}^{(1)} \otimes \rho_{\downarrow\uparrow}^{(2)}, \\ \chi_{(c)} &= \rho_{\downarrow\uparrow}^{(1)} \otimes \rho_{\uparrow\downarrow}^{(2)}, \\ \chi_{(d)} &= \rho_{\downarrow\downarrow}^{(1)} \otimes \rho_{\uparrow\uparrow}^{(2)}. \end{aligned} \quad (2.7)$$

The transformation is now applied to the two-spin state via the corresponding single-spin transformations in each Hilbert space. Explicitly,

$$\begin{aligned} \chi(t, t') = \Lambda(t, t')[\chi(0, 0)] &= \frac{1}{2} (\Lambda_1(t) \otimes \Lambda_2(t')[\chi_{(a)}(0, 0)] - \Lambda_1(t) \otimes \Lambda_2(t')[\chi_{(b)}(0, 0)] \\ &\quad - \Lambda_1(t) \otimes \Lambda_2(t')[\chi_{(c)}(0, 0)] + \Lambda_1(t) \otimes \Lambda_2(t')[\chi_{(d)}(0, 0)]) \end{aligned} \quad (2.8)$$

where  $\Lambda_1(t)$  describes the time evolutions due to the Bloch equation for the first spin,

$$\begin{aligned} &\Lambda_1(t)[\rho^{(1)}(0)] \quad (2.9) \\ &= \begin{pmatrix} \frac{1}{2}(\rho_{\uparrow\uparrow}^{(1)} + \rho_{\downarrow\downarrow}^{(1)})(1 + a(t)P) + \frac{1}{2}(\rho_{\uparrow\uparrow}^{(1)} - \rho_{\downarrow\downarrow}^{(1)})e^{-t/T_1} & e^{-t/T_2 + iht} \rho_{\uparrow\downarrow}^{(1)} \\ e^{-t/T_2 - iht} \rho_{\downarrow\uparrow}^{(1)} & \frac{1}{2}(\rho_{\uparrow\uparrow}^{(1)} + \rho_{\downarrow\downarrow}^{(1)})(1 - a(t)P) - \frac{1}{2}(\rho_{\uparrow\uparrow}^{(1)} - \rho_{\downarrow\downarrow}^{(1)})e^{-t/T_1} \end{pmatrix} \end{aligned}$$

and  $\Lambda_2(t')$  is the corresponding transformation for the second spin obtained in Eq. (2.4). The full matrix elements of the two-spin state after the transformation are given in Appendix A.

From Eq.( 2.8), the fidelity  $f = 4\langle\Psi^-|\chi(t, t')|\Psi^-\rangle$  of the singlet is calculated, for the moment right before the electrons are injected into the spin-LEDs. We obtained

$$f = 1 - \cos\beta aa'PP' + e_1 [e_2'\sin^2\beta \cos(h't') + e_1'\cos^2\beta] + e_2e_1'\sin^2\beta \cos(ht) + e_2e_2' [2\cos\beta \sin(ht)\sin(h't') + (\cos^2\beta + 1)\cos(ht)\cos(h't')],$$

where for the first (second) spin  $e_i = e^{-t/T_i}$  ( $e_i' = e^{-t'/T_i'}$ ),  $a = 1 - e_1$  ( $a' = 1 - e_1'$ ),  $P$  ( $P'$ ) is the equilibrium polarization, and  $T_2$  and  $T_1$  ( $T_2'$  and  $T_1'$ ) are the spin decoherence and relaxation times, respectively. For  $t \ll T_1, T_2$  and  $t' \ll T_1', T_2'$  (in bulk GaAs  $T_2 \sim 100$  ns and typically  $T_1 \gg T_2$ ), the electrons form a non-local spin-entangled state after their injection into the dots  $L$  and  $R$  and after their subsequent relaxation to the single-electron orbital ground states  $\phi_{c\alpha}(\mathbf{r}_{c\alpha}, \sigma)$ . A local rotation of one of the two spins (for  $\mathbf{h} \neq \mathbf{h}'$ ) enables a transformation of  $|\Psi^-\rangle$  into another (maximally entangled) Bell state  $|\Psi^+\rangle = (|\uparrow\downarrow\rangle + |\downarrow\uparrow\rangle)/\sqrt{2}$  or  $|\Phi^\pm\rangle = (|\uparrow\uparrow\rangle \pm |\downarrow\downarrow\rangle)/\sqrt{2}$ . This can be achieved, e.g., by controlling the local Rashba spin-orbit interaction<sup>1</sup> in the current leads [55, 67].

## 2.3 Recombination process and optical output

We next turn to a microscopic description of the optical recombination process of the two electrons which occur independently, except for the entanglement of the spin wave functions. We consider now one single branch  $\alpha = L, R$  of the apparatus and omit the index  $\alpha$ . The state of the single quantum dot which is charged with two hhs in the orbital ground state and into which a single electron with spin  $\sigma$  has been injected is given by

$$|e, \sigma\rangle = \int d^3r_c \phi_c^*(\mathbf{r}_c, \sigma) b_{c\sigma}^\dagger |\chi\rangle. \quad (2.10)$$

Here,  $b_{n\sigma}^\dagger$  creates an electron with spin  $S_z = \sigma/2 = \pm 1/2$  in the state  $n$  of the dot,  $|\chi\rangle = \sum_{\tau \neq \tau'} \int d^3r_{v1} d^3r_{v2} \phi_v(\mathbf{r}_{v1}, \tau; \mathbf{r}_{v2}, \tau') b_{v\tau} b_{v\tau'} |g\rangle$ , where  $|g\rangle$  is the electro-statically neutral ground state of the quantum dot, and  $\phi_v(\mathbf{r}_{v1}, \tau; \mathbf{r}_{v2}, \tau')$  is the orbital part of the two-hole wave function. In the strong-confinement regime where Coulomb correlations are negligible,  $\phi_v$  is a product of the single-particle valence band states. The labels  $\tau, \tau'$  denote the hh spin component  $S_z = \tau/2 = \pm 1/2$  that factor out for angular momentum  $J_z = \pm 3/2$ . We now calculate the emission matrix element [68]  $\langle f | H_{\text{em}} | i \rangle$  with initial state  $|i\rangle = |e, \sigma\rangle \otimes |\dots, n_{\mathbf{k}\lambda}, \dots\rangle$  and final state  $|f\rangle = b_{v\tau'} |g\rangle \otimes |\dots, n_{\mathbf{k}\lambda} + 1, \dots\rangle$ , where  $|\dots, n_{\mathbf{k}\lambda}, \dots\rangle$  is a Fock state of the electromagnetic field, typically the photon vacuum. Because of quantum mechanical selection rules, the optical transitions connect only states with the same spin such that  $\tau = \sigma$  and  $\tau' \neq \sigma$ . We apply the envelope-function approximation for the single-particle levels and write  $\phi_n(\mathbf{r}_n, \sigma) = \psi_n(\mathbf{r}_n) u_{n\sigma}(\mathbf{r}_n)$ , where  $u_{n\sigma}(\mathbf{r}_n)$  is a Bloch function and  $\psi_n(\mathbf{r}_n)$  an envelope function determined by  $V_{\text{qd}}(\mathbf{r})$ , where  $n = c, v_1, v_2$ . The c band Bloch wave function is an  $s$ -type function  $|s\rangle$ , whereas the hh band has a  $p$ -type function  $|x + iy\rangle$ . In the dipole approximation, we obtain [68]

<sup>1</sup>This interaction provides an effective momentum-dependent magnetic field, which produces a spin precession.

$$|\langle f|H_{\text{em}}|i\rangle| = \frac{e}{m_0 c} A_0(\omega_k) \sqrt{n_{\mathbf{k}\lambda} + 1} |\mathbf{e}_{\mathbf{k}\lambda}^* \cdot \mathbf{p}_{cv}^* C_{eh}|, \quad (2.11)$$

where  $\mathbf{p}_{cv}^* = \mathbf{p}_{vc}$  is the inter-band momentum matrix element,  $\mathbf{e}_{\mathbf{k}\lambda} = (\cos\theta \cos\phi - i\lambda \sin\phi, \cos\theta \sin\phi + i\lambda \cos\phi, -\sin\theta)/\sqrt{2}$  is the unit polarization vector with  $\lambda = \pm 1$  for circular polarization  $|\sigma_{\pm}\rangle$ ,  $A_0(\omega_k) = (\hbar/2\epsilon\epsilon_0\omega_k V)^{1/2}$ , and  $C_{eh} = \int d^3r \psi_c^*(\mathbf{r}, \sigma) \psi_v(\mathbf{r}, \sigma)$ . For cubic symmetry,  $\mathbf{e}_{\mathbf{k}\lambda}^* \cdot \mathbf{p}_{cv}^* = p_{cv}(\cos\theta - \sigma\lambda)e^{-i\sigma\phi}/2 \equiv p_{cv}m_{\sigma\lambda}(\theta, \phi)$ , where  $p_{cv} = \langle s|p_x|x\rangle$ . With the transition  $|e, \sigma\rangle \rightarrow b_{v-\sigma}|g\rangle$ , a photon in the state

$$|\sigma, \theta, \phi\rangle = N(\theta)(m_{\sigma,+1}(\theta, \phi)|\sigma_+\rangle + m_{\sigma,-1}(\theta, \phi)|\sigma_-\rangle) \quad (2.12)$$

is emitted into the direction  $(\theta, \phi)$ . Here,  $N(\theta) = [2/(1 + \cos^2\theta)]^{1/2}$  is a normalization factor. Equation (2.12) shows that for  $\theta = 0$ , a spin up ( $\sigma = +1$ ) electron generates a  $|\sigma_-\rangle$  photon, whereas a  $|\sigma_+\rangle$  photon is obtained from a spin down ( $\sigma = -1$ ) electron which ensures a one-to-one correspondence between spin and photon polarization. The admixture of the opposite circular polarization increases with  $\theta$ , leading to elliptical polarization for  $\theta \in (0, \pi/2)$  and linear polarization for  $\theta = \pi/2$ . For  $\theta \neq 0$ , the spin-inverted states  $|+1, \theta, \phi\rangle$  and  $|-1, \theta, \phi\rangle$  have interchanged coefficients for  $|\sigma_+\rangle$  and  $|\sigma_-\rangle$ , up to a relative phase which is determined by the global phase factors  $\exp(-i\sigma\phi)$  of the single-photon states. Note that in two-photon states the azimuthal angles thus can provide a *relative* phase as we exploit below.

The two photons produced at recombination are entangled with the two holes which remain in the dots, due to the antisymmetric hole ground state. By injecting a pair of electrons with spins polarized in the  $xy$  plane into the dots<sup>2</sup>, a four-photon state of the Greenberger-Horne-Zeilinger (GHZ) type can be produced if  $T_{1,X}$  and  $T_{2,X}$  exceed the exciton lifetime  $\tau_X$ . For circularly polarized photons emitted along  $z$ , the electron Bell states give rise to the photon states

$$|\Psi^{\pm}\rangle \rightarrow |\sigma_+\sigma_-\sigma_-\sigma_+\rangle \pm |\sigma_-\sigma_+\sigma_+\sigma_-\rangle, \quad (2.13)$$

$$|\Phi^{\pm}\rangle \rightarrow |\sigma_-\sigma_-\sigma_+\sigma_+\rangle \pm |\sigma_+\sigma_+\sigma_-\sigma_-\rangle, \quad (2.14)$$

where the first two entries indicate the first photon pair (L,R) and the third and fourth entry the second photon pair (L,R), respectively. Normalization has been omitted for simplicity. Yet, the second photon pair is generated by neutral excitons and is thus exposed to the same problems as the biexciton decay cascade in asymmetric quantum dots. Here, a cavity can be used to maintain the GHZ state since the energy entanglement of the second photon pair can be erased [64] and  $\tau_X$  can be shortened due to the Purcell

---

<sup>2</sup>To switch between the production of entangled and polarized electron pairs, a double quantum dot with tunable exchange splitting  $J$  can be used, to which an in-plane magnetic field  $B_{\perp}$  is applied [54]. For  $J$  smaller (larger) than the Zeeman energy, the two-electron ground state is a triplet with spins along  $B_{\perp}$  (a singlet). Alternatively, for subsequent injection of *two* entangled electron pairs,  $\pm \rightarrow +$  on the right-hand side of Eqs. (2.13)–(2.16).



effect to reduce exciton polarization decoherence. Full *bipartite* photon entanglement of the first photon pair is obtained, e.g., by directing the second photon pair via secondary optical paths to a linear polarization measurement which is performed *before* the first photon pair is measured<sup>3</sup>, see Fig. 2.2. Even different bases  $\{|H\rangle, |V\rangle\}$  and  $\{|H'\rangle, |V'\rangle\}$  can be chosen for the two photons of the second pair. Note that the electron-hole exchange interaction in elliptical dots assists this projection into a linear basis, and even loss of the (linear) polarization coherence is tolerable. Still, quantum dots with  $T_{1,X} > \tau_X$  [65] are required for entanglement of the first photon pair. If the second photon pair is measured in the state  $|HH'\rangle$  or  $|VV'\rangle$ , the electron Bell states have given rise to the two-photon states

$$|\Psi^\pm\rangle \rightarrow | +1, \theta_1, \phi_1 \rangle_L | -1, \theta_2, \phi_2 \rangle_R \pm | -1, \theta_1, \phi_1 \rangle_L | +1, \theta_2, \phi_2 \rangle_R, \quad (2.15)$$

$$|\Phi^\pm\rangle \rightarrow | +1, \theta_1, \phi_1 \rangle_L | +1, \theta_2, \phi_2 \rangle_R \pm | -1, \theta_1, \phi_1 \rangle_L | -1, \theta_2, \phi_2 \rangle_R. \quad (2.16)$$

Here, normalization has been omitted for simplicity. If the second photon pair is measured as  $|HV'\rangle$  or  $|VH'\rangle$ ,  $\pm$  is replaced by  $\mp$  on the right-hand side of Eqs. (2.15) and (2.16). Obviously, the two-photon states (2.15) and (2.16) are maximally entangled for  $\theta_1 = \theta_2 = 0$ . For  $\theta_1 = \theta_2 \in (0, \pi/2)$ , the total relative phase factor between the two-photon states in Eq. (2.15) is  $\exp(i\gamma + 2i\Delta\phi)$ . Here,  $\Delta\phi = \phi_1 - \phi_2$ ,  $\gamma = \pi$  for  $|\Psi^-\rangle$ , and  $\gamma = 0$  for  $|\Psi^+\rangle$ . For Eq. (2.16), the relative phase factor is  $\exp[i\gamma + 2i(\phi_1 + \phi_2)]$ , with  $\gamma = \pi$  for  $|\Phi^-\rangle$  and  $\gamma = 0$  for  $|\Phi^+\rangle$ . By tuning the relative phase factors in Eqs. (2.15) and (2.16) to  $-1$ , two circularly polarized photons can be recovered for  $\theta_1 = \theta_2 \in (0, \pi/2)$  from the elliptically polarized single-photon states due to quantum mechanical interference<sup>4</sup>. Thus, maximal entanglement is transferred from two electron spins to the polarizations of two photons for certain ideal emission angles. For  $|\Psi^-\rangle$  ( $|\Psi^+\rangle$ ),  $\Delta\phi = 0$  ( $\Delta\phi = \pi/2$ ) needs to be satisfied  $\text{mod}\pi$ , whereas the condition for  $|\Phi^-\rangle$  ( $|\Phi^+\rangle$ ) is  $\phi_1 + \phi_2 = 0$  ( $\phi_1 + \phi_2 = \pi/2$ )  $\text{mod}\pi$ . Note that for  $\theta_1 = \theta_2 = \pi/2$  these two-photon states vanish completely due to destructive interference.

For arbitrary emission directions of the two photons, the degree of polarization entanglement can be quantified by the von Neumann entropy  $E = -\text{tr}_2(\tilde{\rho} \log_2 \tilde{\rho})$ . Here,  $\tilde{\rho} = \text{tr}_1 \rho$  is the reduced density matrix of the two-photon state  $\rho$  with the trace  $\text{tr}_1$  taken over photon 1. For a maximally entangled two-photon state  $E = 1$ , while  $E = 0$  represents a pure state  $\tilde{\rho}$  (which implies the absence of bipartite entanglement). If the two electrons recombine after times much shorter than the spin lifetimes  $T_1, T_1', T_2, T_2'$ ,  $E$  oscillates for Eq. (2.15) as a function of the relative azimuthal angle  $\Delta\phi$  of the two emitted photons between a minimal value [68],

<sup>3</sup>An alternative suggestion by A. Imamoglu (private communication) is to perform a Hadamard operation on the hh states which are left in the dots after emission of the first photon pair [e.g., via an optical Raman transition, see A. Imamoglu *et al.*, Phys. Rev. Lett. **83**, 4204 (1999)], followed by a hole-spin measurement along  $z$ , e.g., via state-selective absorption of circularly polarized photons.

<sup>4</sup>Such ideal angles can analogously be found for the four-photon GHZ states.

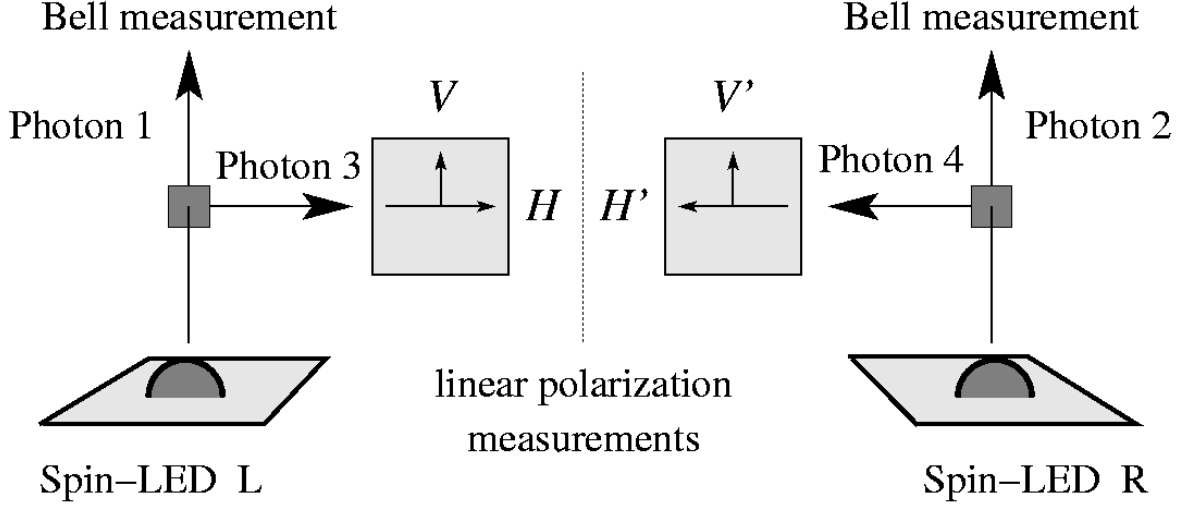


Figure 2.2: Schematic setup to obtain bipartite entanglement of photon 1 and 2 by measuring the photons 3 and 4 of the GHZ state in bases of linear polarizations  $H, V$  and  $H', V'$ , respectively (see text).

$$E_{\min} = \log_2(1 + x_1x_2) - \frac{x_1x_2}{1 + x_1x_2} \log_2(x_1x_2), \quad (2.17)$$

and a maximal value that is (only) obtained for the ideal angles  $\phi_1$  and  $\phi_2$  mentioned above, see Fig. 2.3. Explicitly,

$$E_{\max} = \log_2(x_1 + x_2) - \frac{x_1 \log_2(x_1)}{x_1 + x_2} - \frac{x_2 \log_2(x_2)}{x_1 + x_2}, \quad (2.18)$$

where  $x_i = \cos^2\theta_i$ . For Eq. (2.16),  $E$  oscillates between  $E_{\min}$  and  $E_{\max}$  as a function of  $\phi_1 + \phi_2$ . As expected,  $E_{\max} = 1$  for all  $\theta_1 = \theta_2 \in [0, \pi/2)$ . Note that the discontinuity in  $E_{\max}$  for  $\theta_1 = \theta_2 = \pi/2$  is due to the vanishing two-photon state.

Taking into account that photo-detectors collect photons from a finite solid angle, we allow for small deviations  $\delta\theta = \theta_1 - \theta_2$  and  $\delta\phi = \phi_1 - \phi_2$  from the ideal emission angles. Here, the large refraction index of the capping material of the dots (typically GaAs) compared to air strongly limits the possible deviations. We expand the two-photon density matrix in  $\delta\phi$  and  $\delta\theta$  and recalculate the von Neumann entropy. We obtain

$$E(\theta, \delta\theta, \delta\phi) \approx 1 - \frac{1}{2} \log_2(f_-(\theta, \delta\theta, \delta\phi)f_+(\theta, \delta\theta, \delta\phi)) + \frac{1}{2} (f_+(\theta, \delta\theta, \delta\phi) - 1) \times \log_2\left(\frac{f_-(\theta, \delta\theta, \delta\phi)}{f_+(\theta, \delta\theta, \delta\phi)}\right), \quad (2.19)$$

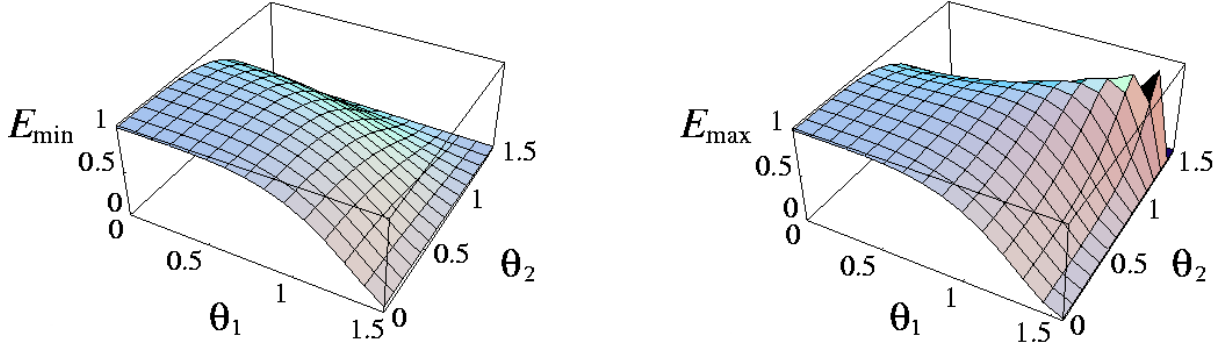


Figure 2.3: The von Neumann entropy (a)  $E = E_{min}$  and (b)  $E = E_{max}$  as a function of the polar angles  $\theta_1$  and  $\theta_2$  for photon emission. Depending on the azimuthal angles  $\phi_1$  and  $\phi_2$ ,  $E$  oscillates between (a) and (b). The photon-polarization entanglement is maximal for  $\theta_1 = \theta_2 = 0$ , whereas for  $\theta_i = \pi/2$  entanglement is absent. (a)  $E_{min}$  slowly decreases with increasing  $\theta_i$ . In (b),  $E_{max} = 1$  for the continuous set of directions  $\theta_1 = \theta_2 \in [0, \pi/2)$ .

where  $f_{\pm}(\theta, \delta\theta, \delta\phi) = 1 \pm \text{tg}\theta \sqrt{\delta\theta^2 + \delta\phi^2 \sin^2\theta}$ . In Fig. 2.4, the von Neumann entropy is plotted as a function of  $\delta\phi$  and  $\delta\theta$  for different values of the polar angle  $\theta$ . Since for  $\delta\theta = \delta\phi = 0$  we recover the ideal angular configuration, for which the entanglement is exactly one, we can directly observe in the graphs the loss of entanglement due to the angular variations. The values of  $\theta$  used in the plots were chosen according to the deviations from the normal direction ( $\theta = 0$ ) which can be expected in experimental setups. We find that the von Neumann entropy is only reduced by less than 6% from its maximal value due to variations in the photon emission angles from the ideal configuration.

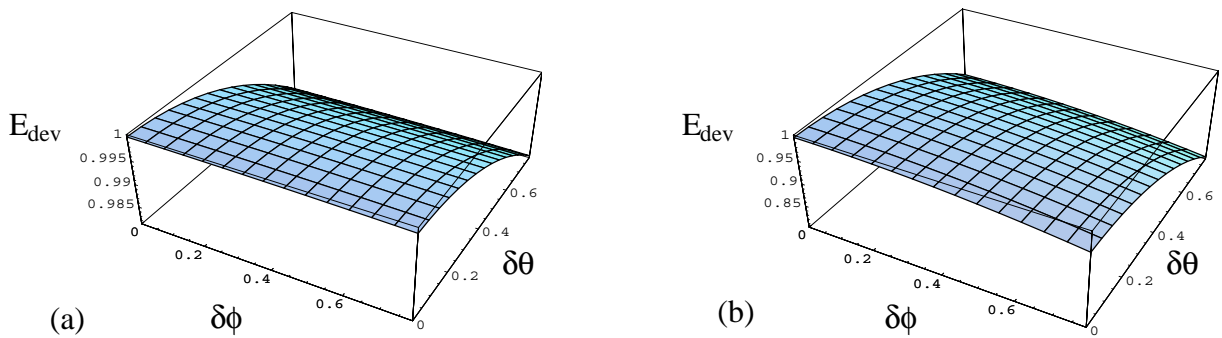


Figure 2.4: The von Neumann entropy for the cases  $\theta_1 = \theta_2 = \theta$  and  $\phi_1 = \phi_2 = \phi$  including small angular deviations from this configuration,  $\delta\theta$  and  $\delta\phi$ , for (a)  $\theta = \pi/16$ ,  $\phi = 0$  and (b)  $\theta = \pi/6$ ,  $\phi = 0$ . For these parameters, a variation in  $\phi$  has a negligible effect on  $E_{dev}$ .

## 2.4 Conclusions

In this chapter we have studied the transfer of entanglement from electron spins to photon polarizations. We have discussed the generation of entangled four-photon and two-photon states using quantum dots charged with two excess holes. We have proposed a scheme to achieve complete entanglement transfer from two electron spins to two photons with quantum dots, in spite of an exciton exchange splitting. We have shown the dependence of the entanglement obtained for the photons as a function of the emission angles and identified the conditions under which this entanglement is maximal. This offers the possibility to efficiently test Bell's inequalities for electron spins. In addition, our results show that a continuous set of directions exist along which entanglement is maximal. We have also discussed the influence of deviations from the ideal configuration. We have estimated that the loss of entanglement under realistic experimental conditions is smaller than a few percents. Finally, the scheme we have discussed here can also be realized for the efficient and deterministic production of entangled photons with two tunnel-coupled dots [69] instead of two isolated dots. In such a setup, entanglement of the two electron spins is provided from the singlet ground state of the delocalized electrons and is transferred to the photons as described in this work.

# Chapter 3

## Coherent spin transfer in coupled quantum dots

Time-resolved Faraday rotation has recently demonstrated coherent transfer of electron spin between quantum dots coupled by conjugated molecules. In this chapter, using a transfer Hamiltonian ansatz for the coupled quantum dots, we calculate the Faraday rotation signal as a function of the probe frequency in a pump-probe setup using neutral quantum dots. Additionally, we study the signal of one spin-polarized excess electron in the coupled dots. We show that, in both cases, the Faraday rotation angle is determined by the spin transfer probabilities and the Heisenberg spin exchange energy.

The chapter is organized as follows. In Sec. 3.1 we shortly describe the experiment that motivated this work. In Sec. 3.2 we discuss the model used for the calculations. In Sec. 3.3, we calculate the time-resolved Faraday rotation (FR) signal for an electron wave function which is delocalized over quantum dots  $A$  and  $B$ . In Sec. 3.4, we calculate the FR angle as a function of probe energy for an initial spin polarization created by optical pumping. We take into account both electron transfer processes and the Coulomb interaction and show that these terms give rise to an exchange splitting of the two-exciton eigenstates. In Sec. 3.5, we perform the related analysis for a system in which an initial spin polarization is created not by optical pumping but by doping of the quantum dots. In Sec. 3.6, we discuss our results for the parameters of CdSe quantum dots coupled by benzene molecules [70], calculate the transfer matrix element and spin transfer probabilities. In Sec. 3.7, we draw our conclusions.

### 3.1 Introduction

The past years have evidenced rapid experimental progress in the field of spintronics [50, 71]. Coherent transport of electron spins in semiconductors has been demonstrated over several micrometers [6], nourishing hopes that the electron spin may be used as carrier of information similar to the electron charge. Such applications of the spin degree of freedom for classical or quantum information processing [10] require control of the electron spin not

only in extended systems such as 2DEG's, but rather also for spins localized in quantum dots (QD's). Recently, coherent transfer of electron spin has been observed between QD's with different radii  $r_A \simeq 1.7$  nm (QD *A*) and  $r_B \simeq 3.5$  nm (QD *B*) coupled by a benzene ring [70]. The different QD size allows one to pump and probe selectively the spin polarization for QD's of species *A* and *B*. The main result of Ref. [70] is that an electron spin polarization created by optical pumping in QD *B* is transferred 'instantaneously' to QD *A*. The efficiency of this transfer mechanism is of order 10% at low temperatures  $T < 50$  K and increases to approximately 20% for  $T \gtrsim 100$  K. The observed shift of the exciton energies to lower values compared to isolated QD's is also consistent with a coherent delocalization of the electron or hole over the system formed by the QD's and the bridging molecule. In the following Subsection we give an overview of this experiment, which motivated our work.

### 3.1.1 Experimental motivation

The system used in the experiment is an artificial solid made of layers of CdSe quantum dots of different radii. The dots are bridged by conjugated molecules (1,4-benzenedimethanethiol)(schematically depicted in Fig. 3.1). Different structures can be achieved by selecting the sequence of layers of dots, for instance, an *AB* structure is a bilayer made of one layer of dots of type *A* and subsequently a layer of dots of type *B*. The first exciton energy-separations are  $E_{gA} = 2.41$  eV and  $E_{gB} = 2.06$  eV for *A* and *B* respectively. Because the dots are different, and so are their corresponding excitation energies, they can be individually addressed with a laser. The laser used in the experiment to selectively excite the dots is a 150-fs pulsed laser with tunable energy ( $E_{pump}$ ). After a delay time  $\Delta t$  of exciting the dots, a linearly polarized probe pulse measures the spin magnetization ( $S_x$ ) along the laser propagation direction in either quantum dot. The energy of the probe pulse ( $E_{probe}$ ) is tuned independently of the pumping energy.

The spin magnetization  $S_x$  along the laser probe pulse is proportional to the angle  $\theta_F$  that the linear polarization of the probe pulse has rotated after interacting with the dots. This effect is known as the Faraday effect. In the experiment the time-resolved Faraday rotation is measured. This means that an in-plane magnetic field  $B$  is applied. The spins precess around the direction of this magnetic field, and therefore the Faraday rotation signal oscillates. The oscillation frequency  $\nu$  depends on the sample. An initial electron spin polarization is created in the quantum dots *B* by optical pumping. The spin magnetization is then probed in the quantum dots *A* by the time-resolved measurement of the Faraday rotation angle. In Fig. 3.2 the time resolved FR data from a *ABAABA* and its FFT spectra is shown for different probing energies, as well as the normalized FFT spectra of the time resolved Faraday rotation data as a function of  $\nu$  and the probe energy. As it can be seen, although the dots of type *B* were excited, at certain probing energies one finds spin magnetization in the dots of type *A*, since the FFT has maximal values at the corresponding frequency for these dots.

The purpose of the work exposed in this chapter is to show that a two-site Hamilto-

nian with a transfer term captures some of the essential experimental features. We aim at calculating the dependence of the experimentally observed Faraday rotation (FR) signal as a function of probe energy on microscopic parameters such as spin transfer probabilities. The FR angle is proportional to the difference in refractive indices for  $\sigma^\pm$  circularly polarized light which is determined by the difference of the dielectric response functions. We calculate the dielectric response functions of coupled QD's and derive an analytical expression for the FR angle in terms of electron transfer probabilities and Heisenberg exchange splittings. The experimental data provide strong evidence that the spin transfer is mediated by the  $\pi$ -conjugated molecule. We do not aim to describe this transfer mechanism microscopically, but consider the transfer matrix elements for electrons and holes as parameters of the Hamiltonian.

## 3.2 The theoretical model

For CdSe QD's with radii  $r_A$  and  $r_B$ , the single-particle level spacing for electrons and holes is large compared to the temperatures  $T \leq 200$  K explored experimentally. This allows us to restrict our attention to the lowest orbital levels in the conduction and valence band of both QD's. A possible admixing of higher orbital levels caused by the Coulomb interaction is determined by the parameter  $r_{A,B}/a_X$ , where  $a_X \simeq 5.4$  nm is the exciton radius for CdSe [72]. For the small QD's in Ref. [70], the Coulomb interaction is small compared to the single-particle level spacing, such that the admixing of higher orbital levels to the ground state is small as well. (For details on experimental parameters, see Sec. 3.6.) This allows us to describe the coupled QD's by the Hamiltonian

$$\hat{H} = \hat{H}_0 + \hat{H}_{\text{Coul}} + \hat{H}_T, \quad (3.1)$$

where

$$\hat{H}_0 = \sum_{\nu=A,B;\sigma=\pm} (E_c^\nu \hat{c}_{c,\sigma}^{\nu\dagger} \hat{c}_{c,\sigma}^\nu + E_v^\nu \hat{c}_{v,\sigma}^{\nu\dagger} \hat{c}_{v,\sigma}^\nu) \quad (3.2)$$

contains the single-particle levels of uncoupled QD's  $\nu = A, B$ . The operators  $\hat{c}_c^{\nu,\sigma}$  and  $\hat{c}_v^{\nu,\sigma}$  annihilate an electron in the lowest level  $E_c^\nu$  of the conduction band with spin quantum number  $s_z = \sigma/2$  and the highest level in the valence band,  $E_v^\nu$ , with angular momentum  $j_z = \sigma/2$ , respectively, where  $\sigma = \pm$ . Here, we have adopted a simple model for the change in the band structure of CdSe due to the QD confinement. We assume a spherical QD shape and a splitting of the  $j = 3/2$  valence band at the  $\Gamma$  point into the heavy hole (hh) and light hole (lh) subband with total angular momentum projection  $j_z = \pm 3/2$  and  $j_z = \pm 1/2$ , respectively, as obtained, e.g., from the Luttinger Hamiltonian with an additional anisotropy term for the crystal field of the hexagonal lattice [73]. The lh subband will be neglected in the following. The Coulomb interaction energy is

$$\hat{H}_{\text{Coul}} = \sum_{\nu=A,B} \frac{U_\nu}{2} [\hat{n}_c^\nu (\hat{n}_c^\nu - 1) + \hat{n}_v^\nu (\hat{n}_v^\nu - 1) - 2\hat{n}_c^\nu \hat{n}_v^\nu], \quad (3.3)$$

where  $\hat{n}_c^\nu = \sum_{\sigma=\pm} \hat{c}_{c,\sigma}^{\nu\dagger} \hat{c}_{c,\sigma}^\nu$  and  $\hat{n}_v^\nu = \sum_{\sigma=\pm} \hat{c}_{v,\sigma}^\nu \hat{c}_{v,\sigma}^{\nu\dagger}$  are the number operators for electrons in the conduction band level and holes in the valence band level.  $U_\nu \simeq e^2/4\pi\epsilon\epsilon_0 r_\nu$  is the characteristic charging energy of QD  $A$  and  $B$ , respectively. Transfer of spin and charge between the QD's is accounted for by the transfer Hamiltonian

$$\hat{H}_T = \sum_{\sigma=\pm} (t_c \hat{c}_{c,\sigma}^{A\dagger} \hat{c}_{c,\sigma}^B + t_v \hat{c}_{v,\sigma}^{A\dagger} \hat{c}_{v,\sigma}^B + h.c.), \quad (3.4)$$

where we assume that transfer of electrons through the  $\pi$ -conjugated molecule conserves the electron spin both in the conduction and the valence band.

The ansatz for the Hamiltonian in Eqs. (3.1)–(3.4) is a model in which the biexciton shift, the exciton fine structure, and the electrostatic coupling between the QD's have been neglected. We will justify this in Sec. 3.6 below where we discuss our results for the experimental parameters of Ref. [70]. Because the focus of this work is to calculate the FR angle that results from transfer of electrons between the QD's, we assume for simplicity that the symmetry axis of the QD's with hexagonal crystal structure is parallel to the direction of pump and probe laser pulses. The effect of a random QD orientation will be discussed in Sec. 3.6.

In the following, we analyze the results of Ref. [70] based on the Hamiltonian Eq. (3.1).

### 3.3 Time resolved Faraday rotation for coupled Quantum Dots

Before we calculate the FR angle for the general Hamiltonian Eq. (3.1) in Secs. 3.4 and 3.5 below, we first consider time-resolved FR for a particularly simple case in which a single electron is in a coherent superposition of states in QD's  $A$  and  $B$  at time  $t = 0$ ,  $|\psi(0)\rangle = (\hat{c}_{c,+}^{B\dagger} + \alpha \hat{c}_{c,+}^{A\dagger})|0\rangle/\sqrt{1 + \alpha^2}$ . We further assume  $t_{c,v} = 0$  and  $E_c^A = E_c^B$  in Eq. (3.1) for  $t > 0$ . Here,  $|0\rangle$  denotes the vacuum state in which the valence band in both QD's is filled and the conduction band states are empty. This simple scenario, although unrealistic because transfer matrix elements are assumed to vanish after the initial state  $|\psi_0\rangle$  has been prepared, will allow us to derive simple analytical expressions for the FR angle even in presence of a magnetic field. The simplifying assumptions  $t_{c,v} = 0$  and  $E_c^A = E_c^B$  will be lifted in the microscopic discussion in Secs. 3.4 and 3.5.

The different radii  $r_A$  and  $r_B$  of the CdSe QD's lead to different  $g$ -factors and different Larmor precession frequencies  $\omega_\nu = g_\nu \mu_B B_{ext}/\hbar$  [74–76], where  $B_{ext}$  is an external magnetic field perpendicular to the spin quantization axis which is given by the symmetry axis of the CdSe QD's, and  $g_\nu$  are the electron  $g$ -factors for  $\nu = A, B$ . At time  $t$ ,

$$|\psi(t)\rangle = \frac{1}{\sqrt{1 + \alpha^2}} \left[ \cos(\omega_B t/2) \hat{c}_{c,+}^{B\dagger} - i \sin(\omega_B t/2) \hat{c}_{c,-}^{B\dagger} + \alpha \cos(\omega_A t/2) \hat{c}_{c,+}^{A\dagger} - i \alpha \sin(\omega_A t/2) \hat{c}_{c,-}^{A\dagger} \right] |0\rangle. \quad (3.5)$$



This time evolution of the electron spin can be detected by FR because the FR angle  $\theta_F$  is determined by the population imbalance between the  $s_z = \pm 1/2$  conduction band states in this situation [77–79]. For probe pulse frequency  $E/h$ ,  $\theta_F$  is proportional to the difference of the real parts of the dielectric response functions  $\epsilon(E)$  for  $\sigma^\pm$  circularly polarized light [77]. With the spectral representation of the response functions,  $\theta_F(E)$  is expressed in terms of the transition matrix elements between the state  $|\psi(t)\rangle$  with energy  $E_0$  and all intermediate states  $|\psi_i\rangle$  which are virtually excited by the probe pulse,

$$\theta_F(E, t) = CE \sum_{|\psi_i\rangle} \frac{E - (E_i - E_0)}{[E - (E_i - E_0)]^2 + \Gamma^2} \times \left( \left| \langle \psi_i | \hat{P}_+ | \psi(t) \rangle \right|^2 - \left| \langle \psi_i | \hat{P}_- | \psi(t) \rangle \right|^2 \right).$$

The polarization operators  $\hat{P}_\pm = d_A \hat{c}_{c,\pm}^{A\dagger} \hat{c}_{v,\pm}^A + d_B \hat{c}_{c,\pm}^{B\dagger} \hat{c}_{v,\pm}^B$  couple to the  $\sigma^\mp$  circularly polarized components of the probe pulse.  $d_\nu$  are the dipole transition matrix elements for transition from the  $j_z = \pm 3/2$  valence band states to the  $s_z = \pm 1/2$  conduction band states in QD's  $A$  and  $B$ .  $E_0 = E_c^B$  and  $E_i$  are the energy eigenvalues of the initial state and the intermediate state  $|\psi_i\rangle$ , respectively, and the level broadening  $\Gamma$  accounts for a finite lifetime of the orbital levels. The prefactor  $C \propto L/(hc n_0)$  is determined by the size  $L$  of the sample and the refraction index  $n_0$  of bulk CdSe.

Because we have assumed an initial state  $|\psi(0)\rangle$  with one electron, all intermediate states  $|\psi_i\rangle$  in Eq. (3.6) are energy eigenstates with two electrons and one hole. For  $t_{c,v} = 0$  in Eq. (3.1), these are of the form  $|\psi_i\rangle = \hat{c}_{c,\sigma}^{\nu\dagger} \hat{c}_{v,\sigma}^\nu \hat{c}_{c,\sigma'}^{\nu'\dagger} |0\rangle$  with  $\sigma, \sigma' = \pm$  and  $\nu, \nu' = A, B$ . Pauli blocking prohibits the creation of an exciton with electron spin  $\sigma 1/2$  if the conduction band level is already occupied by an electron with the same spin. The resulting difference in transition matrix elements for  $\hat{P}_+$  and  $\hat{P}_-$  is proportional to the population imbalance of the  $s_z = \pm 1/2$  levels. For a probe pulse at time  $t$ , from Eq. (3.6) we obtain directly

$$\theta_F(E, t) = \frac{CE}{1 + \alpha^2} \left[ d_B^2 \frac{E - E_X^B}{(E - E_X^B)^2 + \Gamma^2} \cos(\omega_B t) + \alpha^2 d_A^2 \frac{E - E_X^A}{(E - E_X^A)^2 + \Gamma^2} \cos(\omega_A t) \right], \quad (3.6)$$

where  $E_X^\nu = E_c^\nu - E_v^\nu - U_\nu$  is the exciton energy for QD  $\nu$ .  $\theta_F(E, t)$  shows coherent oscillations with frequencies  $\omega_A$  and  $\omega_B$  caused by the electron spin precessing around the external magnetic field. In reality, these coherent oscillations are exponentially damped with a spin dephasing rate  $\Gamma_S$  which is typically much smaller than the orbital dephasing rate,  $\Gamma_S \ll \Gamma$ . Taking into account spin dephasing, the Fourier transform of the time-resolved FR signal as a function of the probe pulse energy  $E$  and the Fourier frequency  $\omega$  is

$$\theta_F(E, \omega) = \frac{CE}{1 + \alpha^2} \times \left[ d_B^2 \frac{E - E_X^B}{(E - E_X^B)^2 + \Gamma^2} \frac{\Gamma_S}{(\omega - \omega_B)^2 + \Gamma_S^2} + \alpha^2 d_A^2 \frac{E - E_X^A}{(E - E_X^A)^2 + \Gamma^2} \frac{\Gamma_S}{(\omega - \omega_A)^2 + \Gamma_S^2} \right]. \quad (3.7)$$

$\theta_F(E, \omega)$  shows characteristic features for  $E \simeq E_X^A$  and  $\omega \simeq \omega_\nu$ . The two terms in Eq. (3.7) describe the dielectric response due to virtual creation of an exciton in QD  $A$  and  $B$ , respectively. For  $E_X^B \leq E \leq E_X^A$ , they have different sign and may cancel. Figure 3.3(a) shows a grayscale plot of  $|\theta_F(E, \omega)|$  for the experimental values  $E_X^B = 2.06$  eV,  $E_X^A = 2.41$  eV,  $\Gamma = 0.05$  eV, and  $\Gamma_S/2\pi = 0.5$  GHz, assuming  $d_A^2/d_B^2 = 1$  and  $\alpha^2 = 0.2$ . For Fig. 3.3(b),  $\Gamma = 0.035$  eV, and  $\Gamma_S/2\pi = 1.2$  GHz, and  $\alpha^2 = 0.4$ . One of the most characteristic features of the experimental data (Fig. 2D in Ref. [70]) is that  $|\theta_F(E, \omega)|$  vanishes and reappears as a function of probe pulse frequency  $E$  for  $\omega \simeq \omega_\nu$ . This can also be clearly seen in the theoretical result.

Above, we have assumed that the electron delocalized over both QD's at  $t = 0$  retains spatial coherence. For rapid decoherence of the orbital part of the wave function, the initial state is described by the density matrix  $\hat{\rho} = \left( \hat{c}_{c,+}^{B\dagger} |0\rangle \langle 0| \hat{c}_{c,+}^B + \alpha^2 \hat{c}_{c,+}^{A\dagger} |0\rangle \langle 0| \hat{c}_{c,+}^A \right) / (1 + \alpha^2)$ . The FR signal in this case is the incoherent superposition of the FR signals for QD  $A$  and  $B$ , and is identical to the results in Eqs. (3.6) and (3.7). Hence, a FR signal as shown in Fig. 3.3 does not allow one to distinguish coherent from incoherent spatial superpositions.

### 3.4 Optical spin injection

In the preceding section,  $\theta_F(E)$  was calculated for the simple case of a single electron delocalized over the coupled QD's. So far, we have also neglected that all intermediate states  $|\psi_i\rangle$  in Eq. (3.6) that are virtually excited by the probe pulse will be modified by finite transfer energies  $t_{c,v}$ . We next turn to a microscopic analysis in which we take into account  $t_{c,v} \neq 0$  also for the intermediate states.

In Ref. [70], the initial state prepared by optical pumping is a one-exciton state. Similar to the analysis in Sec. 3.3 above, the FR angle as a function of probe energy is proportional to the difference of dielectric response functions for  $\sigma^\pm$  circularly polarized light [Eq. (3.6)]. In order to evaluate this expression, both the initial one-exciton state and all intermediate two-exciton states which are virtually excited by the probe pulse must be calculated for the coupled QD's. In this section, we first calculate the one-exciton energy eigenstate of the coupled QD's prepared by the pump pulse and subsequently identify all two-exciton eigenstates  $|\psi_i\rangle$  which are virtually excited by the probe pulse. Our analysis is based on perturbation theory in the transfer energies and is valid if  $|t_{c,v}|$  is the smallest energy scale,  $|t_{c,v}| \ll \delta E_c, |\delta E_v|, U_A, U_B, |\delta E_{c,v} \pm U_{A,B}|$ . Here, we have defined the energy differences  $\delta E_c = E_c^A - E_c^B \geq 0$  and  $\delta E_v = E_v^A - E_v^B \leq 0$  between the conduction and valence band levels of QD's  $A$  and  $B$ .

In Ref. [70], an initial spin polarization was created by optical pumping. For  $t_{c,v} = 0$ , the states  $\hat{c}_{c,\sigma}^{\nu\dagger}\hat{c}_{v,\sigma}^{\nu}|0\rangle$  are one-exciton eigenstates with energy eigenvalues

$$E_X^{\nu(0)} = E_c^\nu - E_v^\nu - U_\nu \quad (3.8)$$

which are prepared by absorption of a  $-\sigma$  circularly polarized pump pulse. To first order in the transfer energies  $t_{c,v}$ , the energy eigenstates are

$$|X_{A,\sigma}\rangle = \hat{c}_{c,\sigma}^{A\dagger}\hat{c}_{v,\sigma}^A|0\rangle + \left( \frac{t_c}{\delta E_c - U_A}\hat{c}_{c,\sigma}^{B\dagger}\hat{c}_{v,\sigma}^A + \frac{t_v}{\delta E_v + U_A}\hat{c}_{c,\sigma}^{A\dagger}\hat{c}_{v,\sigma}^B \right) |0\rangle, \quad (3.9a)$$

$$|X_{B,\sigma}\rangle = \hat{c}_{c,\sigma}^{B\dagger}\hat{c}_{v,\sigma}^B|0\rangle + \left( -\frac{t_c}{\delta E_c + U_B}\hat{c}_{c,\sigma}^{A\dagger}\hat{c}_{v,\sigma}^B - \frac{t_v}{\delta E_v - U_B}\hat{c}_{c,\sigma}^{B\dagger}\hat{c}_{v,\sigma}^A \right) |0\rangle, \quad (3.9b)$$

with eigenenergies

$$E_X^A = E_X^{A(0)} + \frac{t_c^2}{\delta E_c - U_A} - \frac{t_v^2}{\delta E_v + U_A}, \quad (3.10a)$$

$$E_X^B = E_X^{B(0)} - \frac{t_c^2}{\delta E_c + U_B} + \frac{t_v^2}{\delta E_v - U_B}. \quad (3.10b)$$

As expected, the eigenenergies are shifted due to the delocalization of electrons and holes over the coupled QD's. The exciton states in Eq. (3.9) are the only one-exciton states which can be prepared by the absorption of a photon with circular polarization  $-\sigma$  if the photon is incident along the hexagonal axis of the CdSe crystal structure. However, a photon with energy  $E \simeq E_X^B$  no longer creates an exciton only in QD B, but an exciton in which electron and hole are delocalized over the coupled QD system. This delocalization of the quantum mechanical wave function is consistent with the short time-scale for spin transfer observed experimentally [70].

We now turn to the calculation of the FR angle, assuming that the pump pulse has prepared an initial state  $|\psi\rangle = |X_{B,+}\rangle$ . The evaluation of the dielectric response function will require us to calculate all two-exciton states that are virtually excited by the probe pulse. Interesting features in the FR signal effected by spin transfer are of order  $t_{c,v}^2$ . In order to keep the following expressions simple, we assume that spin is transferred between the conduction band states and set  $t_v = 0$ . Then, only the seven states  $|A_+B_+\rangle$ ,  $|T_0\rangle$ ,  $|S\rangle$ ,  $|B_+B_-\rangle$ ,  $|\tilde{T}_0\rangle$ ,  $|\tilde{S}\rangle$ , and  $|\widetilde{B_+B_-}\rangle$  listed below and in Appendix B have finite matrix elements up to  $\mathcal{O}(t_c^2)$  with  $\hat{P}_\pm|X_{B,+}\rangle$ . For  $\delta E_v + U_A \neq 0$ , only the eigenenergies of  $|A_+B_+\rangle$ ,  $|T_0\rangle$ , and  $|S\rangle$  are close to the excitation energy of a probe pulse with frequency  $E/h \simeq E_X^A/h$ . Hence, these states dominate the spectral representation in Eq. (3.6)<sup>1</sup>.

The polarization operator  $\hat{P}_+$  induces transitions from the initial state  $|X_{B,+}\rangle$  to

---

<sup>1</sup>Two-exciton eigenstates which are energetically offset compared to  $E + E_X^B$  will also contribute to the FR signal. However, their contribution varies slowly as a function of probe energy and leads at most to an offset in the results derived below. See also Appendix B.

$$|A_+B_+\rangle = \hat{c}_{c,+}^{A\dagger}\hat{c}_{c,+}^{B\dagger}\hat{c}_{v,+}^A\hat{c}_{v,+}^B|0\rangle \quad (3.11)$$

with energy eigenvalue

$$E_{A_+B_+} = E_X^{A(0)} + E_X^{B(0)}. \quad (3.12)$$

The notation indicates that two electrons with the same spin  $s_z = 1/2$  occupy the conduction band states in QD's A and B, respectively, and form a spin triplet state.  $|A_+B_+\rangle$  is an exact eigenstate of the Hamiltonian even for  $t_c \neq 0$  because transfer of the conduction band electrons is blocked by Pauli's exclusion principle. The matrix element  $\langle A_+B_+|\hat{P}_+|X_{B_+}\rangle$  is the only finite matrix element of the operator  $\hat{P}_+$ .

Finite matrix elements for  $\hat{P}_-$  come from the states in which the electrons in the conduction band level form a spin triplet and singlet, respectively,

$$|T_0\rangle = \frac{1}{\sqrt{2}} \left( \hat{c}_{c,-}^{A\dagger}\hat{c}_{c,+}^{B\dagger} + \hat{c}_{c,+}^{A\dagger}\hat{c}_{c,-}^{B\dagger} \right) \hat{c}_{v,-}^A\hat{c}_{v,+}^B|0\rangle, \quad (3.13a)$$

$$|S\rangle \propto \frac{1}{\sqrt{2}} \left( \hat{c}_{c,-}^{A\dagger}\hat{c}_{c,+}^{B\dagger} - \hat{c}_{c,+}^{A\dagger}\hat{c}_{c,-}^{B\dagger} \right) \hat{c}_{v,-}^A\hat{c}_{v,+}^B|0\rangle \quad (3.13b)$$

$$+ \sqrt{2} \left( \frac{t_c}{\delta E_c + U_B} \hat{c}_{c,+}^{A\dagger}\hat{c}_{c,-}^{A\dagger} - \frac{t_c}{\delta E_c - U_A} \hat{c}_{c,+}^{B\dagger}\hat{c}_{c,-}^{B\dagger} \right) \times \hat{c}_{v,-}^A\hat{c}_{v,+}^B|0\rangle,$$

and the holes with  $j_z = -3/2$  and  $j_z = +3/2$  are localized in QD's A and B, respectively. Note that the projection of the total conduction band spin onto the spin-quantization axis vanishes for the triplet state  $|T_0\rangle$ . The normalization constant for  $|S\rangle$  is defined by  $\langle S|S\rangle = 1$ . The eigenenergies

$$E_{T_0} = E_X^{A(0)} + E_X^{B(0)}, \quad (3.14a)$$

$$E_S = E_X^{A(0)} + E_X^{B(0)} + 2t_c^2 \left( \frac{1}{\delta E_c - U_A} - \frac{1}{\delta E_c + U_B} \right)$$

show an energy offset which is caused by the inter-dot exchange coupling [10, 68]. The energies of  $|A_+B_+\rangle$  and  $|T_0\rangle$  are not shifted by electron transfer because of Pauli blocking and destructive interference of transfer paths, respectively.

The state

$$|B_+B_-\rangle \propto \left[ \hat{c}_{c,+}^{B\dagger}\hat{c}_{c,-}^{B\dagger} + \frac{t_c}{\delta E_c - U_A} \left( \hat{c}_{c,-}^{A\dagger}\hat{c}_{c,+}^{B\dagger} - \hat{c}_{c,+}^{A\dagger}\hat{c}_{c,-}^{B\dagger} \right) \right. \\ \left. + \frac{2t_c^2\hat{c}_{c,+}^{A\dagger}\hat{c}_{c,-}^{A\dagger}}{(\delta E_c - U_A)(2\delta E_c - U_A + U_B)} \right] \hat{c}_{v,-}^A\hat{c}_{v,+}^B|0\rangle \quad (3.15)$$

with

$$E_{B_+B_-} = E_X^{B(0)} + E_c^B - E_v^A - 2\frac{t_c^2}{\delta E_c - U_A} \quad (3.16)$$

is offset in energy from  $E_X^{A(0)} + E_X^{B(0)}$  even to zeroth order in  $t_c$  and does not contribute significantly to  $\theta_F(E)$  for  $E \simeq E_X^A$ . The three states in Eqs. (3.13) and (3.15) provide the dominant terms in the spectral representation for  $\theta_F$  in Eq. (3.6). In particular, they exhaust the sum rule  $\sum_{|\psi_i\rangle} |\langle\psi_i|\hat{c}_{c,-}^{A\dagger}\hat{c}_{v,-}^A|X_{B,+}\rangle|^2 = 1$  up to  $\mathcal{O}(t_c^2)$ . In Fig. 3.4, the spin configurations for  $|A_+B_+\rangle$ ,  $|S\rangle$ , and  $|T_0\rangle$  are shown schematically.

From Eqs. (3.9b)–(3.16), the FR angle  $\theta_F$  is readily evaluated. We denote the electron transfer probability from QD  $\nu$  to QD  $\nu'$  by  $p_{\nu\rightarrow\nu'}$ . We obtain

$$p_{A\rightarrow B} = \left(\frac{t_c}{\delta E_c - U_A}\right)^2, \quad (3.17a)$$

$$p_{B\rightarrow A} = \left(\frac{t_c}{\delta E_c + U_B}\right)^2. \quad (3.17b)$$

For the transition matrix elements of the dipole operators in Eq. (3.6), we obtain in terms of the transfer probabilities

$$|\langle A_+B_+|\hat{P}_+|X_{B,+}\rangle|^2 = (1 - p_{B\rightarrow A})d_A^2, \quad (3.18a)$$

$$|\langle T_0|\hat{P}_-|X_{B,+}\rangle|^2 = \frac{1 - p_{B\rightarrow A}}{2}d_A^2, \quad (3.18b)$$

$$|\langle S|\hat{P}_-|X_{B,+}\rangle|^2 = \frac{1 + p_{B\rightarrow A} - 2p_{A\rightarrow B}}{2}d_A^2, \quad (3.18c)$$

$$|\langle B_+B_-|\hat{P}_-|X_{B,+}\rangle|^2 = p_{A\rightarrow B}d_A^2. \quad (3.18d)$$

Because of the exchange splitting  $E_{T_0} - E_S$  between conduction band triplet and singlet states, finite transfer probabilities  $p_{A\rightarrow B}$  and  $p_{B\rightarrow A}$  lead to pronounced features in the FR angle as a function of the probe pulse frequency  $E/h$ . For probe energies  $E_{T_0B} = E_{T_0} - E_X^B \leq E \leq E_{SB} = E_S - E_X^B$ , the FR signal varies strongly with energy and is given by

$$\theta_F(E) = \frac{CEd_A^2}{2} \left[ (1 - p_{B\rightarrow A}) \frac{E - E_{T_0B}}{(E - E_{T_0B})^2 + \Gamma^2} - (1 + p_{B\rightarrow A} - 2p_{A\rightarrow B}) \frac{E - E_{SB}}{(E - E_{SB})^2 + \Gamma^2} \right]. \quad (3.19)$$

For  $|E - E_{SB}| \gtrsim |E_{T_0} - E_S|$ , Eq. (3.19) simplifies to

$$\theta_F(E) \simeq CE d_A^2 \frac{E - E_X^{A(0)}}{\left(E - E_X^{A(0)}\right)^2 + \Gamma^2} (p_{A \rightarrow B} - p_{B \rightarrow A}). \quad (3.20)$$

This result is surprising because the FR angle is not only determined by the probability  $p_{B \rightarrow A}$  that the electron created by the pump pulse has been transferred to QD  $A$ . Rather, even the *sign* of the FR angle depends on the parameters  $\delta E_c$  (and  $\delta E_v$  if transfer between valence band states is included) and  $U_{A,B}$ .  $\theta_F \geq 0$  for  $|\delta E_c - U_A| \geq |\delta E_c + U_B|$ , and  $\theta_F \leq 0$  for  $|\delta E_c - U_A| \leq |\delta E_c + U_B|$ . Although counterintuitive at first sight, this can be readily understood from the one- and two-exciton eigenstates. The matrix element for the virtual creation of an exciton with  $s_z = 1/2$ ,  $j_z = 3/2$  in QD  $A$  is reduced by the probability  $p_{B \rightarrow A}$  that the conduction band electron created by the pump pulse in  $B$  has been transferred to  $A$ . In this case, it blocks the creation of a second exciton with the same spin. The transition matrix element for the creation of an exciton with  $s_z = -1/2$ ,  $j_z = -3/2$  is reduced by the probability  $p_{A \rightarrow B}$  that the electron with spin  $s_z = -1/2$  in the conduction band state of QD  $A$  is transferred to QD  $B$ . This transfer process is not prohibited by Pauli blocking and leads to the virtual occupation of  $|B_+ B_- \rangle$  which is energetically far off resonance. The interplay of both processes results in Eq. (3.20).

Our derivation of Eq. (3.20) was based on the assumption that  $t_c$  is the smallest energy scale in the system. As will be discussed in Sec. 3.6 below, for the experimental parameters in Ref. [70],  $\delta E_v + U_A \simeq 0$ . For  $t_v = 0$ , this does not lead to divergences in the perturbative expansion in  $t_c$ . However, these special parameters require that two additional two-exciton states are taken into account for the calculation of  $\theta_F(E)$  because they are nearly degenerate with  $|A_+ B_+ \rangle$ ,  $|S \rangle$ , and  $|T_0 \rangle$  (see Fig. 3.5). The states  $|\tilde{S} \rangle$  and  $|\tilde{T}_0 \rangle$  defined in Eq. (B.1) have finite overlap matrix elements with  $\hat{P}_- |X_{B,+} \rangle$ ,

$$|\langle \tilde{T}_0 | \hat{P}_- |X_{B,+} \rangle|^2 = \frac{p_{B \rightarrow A} d_B^2}{2}, \quad (3.21a)$$

$$|\langle \tilde{S} | \hat{P}_- |X_{B,+} \rangle|^2 = \frac{p_{B \rightarrow A} d_B^2}{2}. \quad (3.21b)$$

The spin configuration for the states  $|\tilde{S} \rangle$  and  $|\tilde{T}_0 \rangle$  are shown schematically in Fig. 3.6(a). Note that both holes occupy the valence band states of QD  $B$ . The accidental degeneracy of  $|\tilde{S} \rangle$  and  $|\tilde{T}_0 \rangle$  with  $|S \rangle$  and  $|T_0 \rangle$  arises because, for the parameters of Ref. [70], the decrease in orbital energy  $\delta E_v$  is comparable to the increase in Coulomb energy  $U_A$ . Transitions between an initial state  $|X_{B,+} \rangle$  and  $|\tilde{S} \rangle$ ,  $|\tilde{T}_0 \rangle$ , are two-step processes. A  $\sigma^+$  polarized probe photon creates an exciton with  $s_z = -1/2$  and  $j_z = -3/2$  in  $B$ , and one of the conduction band electrons in  $B$  is subsequently transferred to  $A$ . These processes are shown schematically in Fig. 3.6(b).

Taking into account all two-exciton states with energies

$$\left| E_i - \left( E_X^{A(0)} + E_X^{B(0)} \right) \right| \lesssim \max[|\delta E_v + U_A|, |E_{T_0} - E_S|],$$

the FR angle is

$$\begin{aligned} \theta_F(E) = \frac{CE}{2} \left\{ d_A^2 \left[ (1 - p_{B \rightarrow A}) \frac{E - E_{T_0B}}{(E - E_{T_0B})^2 + \Gamma^2} \right. \right. \\ \left. \left. - (1 + p_{B \rightarrow A} - 2p_{A \rightarrow B}) \frac{E - E_{SB}}{(E - E_{SB})^2 + \Gamma^2} \right] \right. \\ \left. - d_B^2 p_{B \rightarrow A} \left[ \frac{E - E_{\tilde{T}_0B}}{(E - E_{\tilde{T}_0B})^2 + \Gamma^2} + \frac{E - E_{\tilde{S}B}}{(E - E_{\tilde{S}B})^2 + \Gamma^2} \right] \right\}. \end{aligned} \quad (3.22)$$

The energy differences  $E_{\tilde{T}_0B} = E_{\tilde{T}_0} - E_X^B$  and  $E_{\tilde{S}B} = E_{\tilde{S}} - E_X^B$  are given by the eigenenergies in Eq. (B.2). For  $|E - E_{T_0B}|, |E - E_{SB}| \ll |E - E_{\tilde{T}_0B}|, |E - E_{\tilde{S}B}|$ , Eq. (3.22) simplifies to Eq. (3.19).<sup>2</sup>

Above, we have only considered  $t_c \neq 0$  and  $t_v = 0$ , i.e., a scenario in which electrons in the valence band remain localized in the QD's while electrons in conduction band states can be transferred. The case  $t_v \neq 0$  and  $t_c = 0$  can be mapped onto the problem discussed above by mapping electrons onto holes, i.e., by interchanging c and v in above expressions. In particular, Eqs. (3.19) and (3.20) remain valid if the transfer probabilities for electrons are replaced by the corresponding values for holes, e.g.,  $p_{A \rightarrow B} = [t_c / (\delta E_v + U_A)]^2$ , and the energy eigenvalues are calculated for transfer in the valence rather than the conduction band.

In the limit of small QD's with similar sizes,  $U_{A,B} \gg t_{c,v} \gg \delta E_c, |\delta E_v|$ , configurations in which electrons and holes occupy different QD's are strongly suppressed. If  $t_{c,v}/U_{A,B} \simeq 0$  but  $t_c t_v / U_{A,B} (E_X^{A(0)} - E_X^{B(0)})$  remains finite, a joint transfer of electron and hole via a virtual intermediate state is possible. Evidence for this coherent delocalization of an exciton has been reported for QD's of similar sizes [80, 81]. The observation of incoherent exciton tunneling between QD's has also been reported [82–85].

### 3.5 Doping of coupled Quantum Dots

In the last section, we have analyzed the FR angle for an initial spin population created by optical pumping, the method used in Ref. [70]. We now calculate the FR angle  $\theta_F(E)$  for the case that the initial spin density is carried by an excess electron rather than the exciton. Spin injection could be achieved, e.g., by doping one CdSe QD with a single donor atom. For a chemical potential  $E_c^B \leq \mu \leq E_c^A, E_c^B + U_B$ , the conduction band level of QD  $B$  is filled with one electron while QD  $A$  remains empty. The excess electron can be spin polarized by cooling in presence of a magnetic field. Again, we set  $t_v = 0$  to keep our results transparent.

---

<sup>2</sup>In order to calculate  $\theta_F(E)$  for arbitrary energies  $E$ , also virtual transitions to  $|B_+ B_- \rangle, |\widetilde{B_+ B_-} \rangle$ , and the vacuum state  $|0\rangle$  have to be taken into account. The corresponding expression is omitted here, but can be directly obtained from Eq. (3.6).

The transfer matrix element for the conduction band level leads to the delocalization of the excess electron in QD  $B$ ,

$$|e_{B,\sigma}\rangle = \left[ 1 + \left( \frac{t_c}{\delta E_c} \right)^2 \right]^{-1/2} \left( \hat{c}_{c,\sigma}^{B\dagger} - \frac{t_c}{\delta E_c} \hat{c}_{c,\sigma}^{A\dagger} \right) |0\rangle \quad (3.23)$$

with eigenenergy  $E^B = E_c^B - t_c^2/\delta E_c$ . Note that the energy shift is different from the one found for the exciton because there is no Coulomb attraction between electron and hole in the present case.

We calculate the FR angle for an initial state  $|e_{B,+}\rangle$  and probe energy  $E \simeq E_X^A$ . Similar to the analysis in Sec. 3.4, three intermediate states dominate the spectral representation for  $\theta_F(E)$ . These states are the following.

$$|A_+B_+\rangle = \hat{c}_{c,+}^{A\dagger} \hat{c}_{c,+}^{B\dagger} \hat{c}_{v,+}^A |0\rangle \quad (3.24)$$

with energy eigenvalue

$$E_{A_+B_+} = E_X^{A(0)} + E_c^B \quad (3.25)$$

is populated by creation of an exciton with conduction and valence band spins  $s_z = 1/2$  and  $j_z = 3/2$ , respectively<sup>3</sup>. Virtual creation of an exciton with  $s_z = -1/2$  and  $j_z = -3/2$  leads to transitions to the spin triplet and singlet states

$$|T_0^-\rangle = \frac{1}{\sqrt{2}} \left( \hat{c}_{c,-}^{A\dagger} \hat{c}_{c,+}^{B\dagger} + \hat{c}_{c,+}^{A\dagger} \hat{c}_{c,-}^{B\dagger} \right) \hat{c}_{v,-}^A |0\rangle \quad (3.26a)$$

$$\begin{aligned} |S^-\rangle &\propto \frac{1}{\sqrt{2}} \left( \hat{c}_{c,-}^{A\dagger} \hat{c}_{c,+}^{B\dagger} - \hat{c}_{c,+}^{A\dagger} \hat{c}_{c,-}^{B\dagger} \right) \hat{c}_{v,-}^A |0\rangle \\ &+ \sqrt{2} \left( \frac{t_c}{\delta E_c} \hat{c}_{c,+}^{A\dagger} \hat{c}_{c,-}^{A\dagger} - \frac{t_c}{\delta E_c - U_A - U_B} \hat{c}_{c,+}^{B\dagger} \hat{c}_{c,-}^{B\dagger} \right) \\ &\quad \times \hat{c}_{v,-}^A |0\rangle, \end{aligned} \quad (3.26b)$$

where the normalization constant for  $|S^-\rangle$  is determined by  $\langle S^- | S^- \rangle = 1$ . The eigenenergies

$$E_{T_0^-} = E_X^{A(0)} + E_c^B, \quad (3.27a)$$

$$E_{S^-} = E_X^{A(0)} + E_c^B + 2t_c^2 \left( \frac{1}{\delta E_c - U_A - U_B} - \frac{1}{\delta E_c} \right)$$

are split by the exchange coupling of the conduction band levels. Further, there are several states with energies differing from  $E_X^{A(0)} + E_c^B$  (see Appendix C). For probe pulse

---

<sup>3</sup>The superscript distinguishes the states with two electrons and one hole from the two-exciton states discussed in Sec. 3.4.



energies  $E \simeq E_X^{A(0)}$  and  $|\delta E_v + U_A - U_B| \gtrsim \Gamma$ ,  $\theta_F(E)$  is dominated by virtual excitations into the states  $|A_+B_+^- \rangle$ ,  $|T_0^- \rangle$ , and  $|S^- \rangle$ . In this case, all other energy eigenstates with two conduction band electrons and one hole listed in Appendix C are energetically far off resonance and can be neglected.

The transition matrix elements of the polarization operators  $\hat{P}_\pm$  between  $|e_{B,+} \rangle$  and the states Eqs. (3.24) and (3.26) are readily evaluated. The probabilities for electron transfer between the QD's are now given by

$$p_{B \rightarrow A}^- = \left( \frac{t_c}{\delta E_c} \right)^2, \quad (3.28a)$$

$$p_{A \rightarrow B}^- = \left( \frac{t_c}{\delta E_c - U_A - U_B} \right)^2. \quad (3.28b)$$

Then,

$$|\langle A_+B_+^- | \hat{P}_+ | e_{B,+} \rangle|^2 = (1 - p_{B \rightarrow A}^-) d_A^2, \quad (3.29a)$$

$$|\langle T_0^- | \hat{P}_- | e_{B,+} \rangle|^2 = \frac{1 - p_{B \rightarrow A}^-}{2} d_A^2, \quad (3.29b)$$

$$|\langle S^- | \hat{P}_- | e_{B,+} \rangle|^2 = \frac{1 + p_{B \rightarrow A}^- - 2p_{A \rightarrow B}^-}{2} d_A^2. \quad (3.29c)$$

Inserting these matrix elements into the spectral representation of  $\theta_F(E)$ , Eq. (3.6), we find for the FR angle

$$\begin{aligned} \theta_F(E) = \frac{CEd_A^2}{2} & \left[ (1 - p_{B \rightarrow A}^-) \frac{E - E_{T_0B}^-}{(E - E_{T_0B}^-)^2 + \Gamma^2} \right. \\ & \left. - (1 + p_{B \rightarrow A}^- - 2p_{A \rightarrow B}^-) \frac{E - E_{SB}^-}{(E - E_{SB}^-)^2 + \Gamma^2} \right] \end{aligned} \quad (3.30)$$

for probe energies  $E \simeq E_X^{A(0)}$ , in close analogy to Eq. (3.19) for optical spin injection. The energy differences are defined by  $E_{T_0B}^- = E_{T_0}^- - E^B$  and  $E_{SB}^- = E_{S^-} - E^B$ . Because of the exchange splitting between  $|T_0^- \rangle$  and  $|S^- \rangle$ ,  $\theta_F(E)$  will in general exhibit several peaks and lack point inversion symmetry. The functional dependence on probe energy is determined by the transfer probabilities and the energy differences  $E_{T_0B}^-$  and  $E_{SB}^-$ . For a more detailed analysis which takes into account all finite transition matrix elements up to  $\mathcal{O}(t_c^2)$ , see Appendix C.

Experiments on doped QD's could provide valuable information supplementing the experimental data obtained for optical pumping. The main advantage over optical spin injection is that spin decoherence times are expected to be substantially longer because

they are not limited by electron-hole recombination. Even more importantly, FR measurements on doped coupled QD's can clarify whether spin transfer occurs predominantly between the conduction or valence band levels because, for  $t_c = 0$  and  $t_v \neq 0$ ,  $\theta_F(E) \simeq 0$  for probe energies  $E \simeq E_X^{A(0)}$ .

### 3.6 Comparison with experiment

In order to compare the results of Sec. 3.4 with experimental data from Ref. [70], we first provide numerical values for  $\delta E_c$ ,  $\delta E_v$ ,  $U_A$ , and  $U_B$ . The energy level spectrum of CdSe QD's is well established both experimentally and theoretically [86, 87]. The absorption energies  $E_X^{A(0)} = 2.41$  eV and  $E_X^{B(0)} = 2.06$  eV in Ref. [70] are consistent with  $r_A \simeq 2.0$  nm and  $r_B \simeq 3.5$  nm, and we will use these radii for the following calculations. From Ref. [86],  $\delta E_c \simeq 0.30$  eV and  $\delta E_v \simeq -0.10$  eV.

From the bulk values for the static dielectric constant,  $\epsilon = 9.7$ , and the band masses in the conduction and valence band,  $m_c/m_e = 0.12$  and  $m_v/m_e = 0.45$ , one obtains the exciton radius 5.4 nm [72, 88–90]. The exciton radius is larger than  $r_{A,B}$ , and electrons and holes are strongly confined in the QD's as assumed in Eq. (3.1). The characteristic energy scale of the Coulomb interaction is  $U_\nu \simeq e^2/4\pi\epsilon\epsilon_0 r_\nu$ . For the given values of  $r_A$  and  $r_B$ ,  $U_A = 0.07$  eV and  $U_B = 0.04$  eV.

The Hamiltonian Eq. (3.1) does not take into account biexciton shifts, the exciton fine structure, and inter-dot Coulomb interactions. For CdSe QD's with radii 1.5–4 nm, the biexciton shift is of order 0.01–0.02 eV (Ref. [91]) and the characteristic energy splitting between bright and dark excitons is smaller than 0.01 eV [92]. The characteristic energy scale for inter-dot Coulomb interactions is  $U_{AB} \simeq e^2/4\pi\epsilon_0\epsilon(r_A + r_B) \leq 0.03$  eV. However, it is relevant only if neither of the two QD's is electrically neutral. The most important effect of the inter-dot Coulomb interaction is to lower the energy eigenvalues of  $|\tilde{T}_0\rangle$  and  $|\tilde{S}\rangle$  [Eq. (B.1)] by  $U_{AB}$ . All these energy scales are small compared to the level broadening  $\Gamma$  and can safely be neglected.

In the following, we assume that only electrons in conduction band levels are transferred between the QD's while valence band electrons remain localized. As discussed in Sec. 3.5, this assumption can be tested by experiments on doped QD's. Mediated by electron transfer through the molecular bridge, the lowest conduction band level in QD  $B$  hybridizes with the lowest conduction band level in QD  $A$ . Comparing the observed energy shift  $E_X^B - E_X^{B(0)} = -0.02$  eV with Eq. (3.10), we find

$$t_c = \sqrt{\left(E_X^{B(0)} - E_X^B\right) (\delta E_c + U_B)} = 0.082 \text{ eV}. \quad (3.31)$$

Our theory predicts that the exciton absorption peak for QD  $A$  is shifted to larger energies for the coupled QD's, in contrast to the experimental result  $E_X^A - E_X^{A(0)} < 0$ . The most likely explanation for this is that the lowest conduction band level in QD  $A$  hybridizes

also with higher excited levels in QD  $B$  which are nearly degenerate with  $E_c^A$ <sup>4</sup>. In order to account for quantitative changes effected by this hybridization, the energy  $E_X^{A(0)}$  must be replaced by the true value of the hybridized state in all expressions for the two-exciton eigenenergies. This value can be obtained from  $E_X^{A(0)} + t_c^2/(\delta E_c + U_A) \simeq 2.36$  eV, where the latter is the experimental value for the exciton absorption edge of QD  $A$  in the coupled QD's. Hence,  $E_X^{A(0)} \rightarrow 2.33$  eV.

From these parameters, we calculate for the transfer probabilities between the lowest conduction band states  $p_{A \rightarrow B} = 0.13$  and  $p_{B \rightarrow A} = 0.06$ . The energy differences between the two-exciton states and the initial state are  $E_{T_0B} = 2.35$  eV,  $E_{SB} = 2.37$  eV,  $E_{\tilde{T}_0B} = 2.32$  eV,  $E_{\tilde{S}B} = 2.31$  eV. The oscillator strength for exciton creation, proportional to  $d_{A,B}^2$ , is independent of the QD size in the strong confinement regime and proportional to the QD volume for weak confinement. Because both QD's are close to the strong confinement limit, we assume a weak scaling  $d_B^2/d_A^2 = 2$  for the following Figures.

In Fig. 3.7(a), we show the FR angle calculated from Eq. (3.20) as a function of probe energy for different values of  $\Gamma$ ,  $\Gamma = 0.05$  eV (solid),  $0.02$  eV (dashed), and  $0.08$  eV (dotted). We note that even qualitative features depend strongly on the microscopic parameters such as  $\Gamma$ . For small  $\Gamma$ , additional peaks emerge because the contributions from the individual two-exciton states can be resolved.

In spite of the dependence on microscopic parameters, some pronounced features in  $\theta_F(E)$  are generally present: (i)  $\theta_F(E)$  does not exhibit point-inversion symmetry, in stark contrast to the FR angle expected from virtual transitions to a single state. (ii)  $\theta_F$  has in general more than two maxima or minima. The positions and heights of the extrema are determined by the interplay of the transfer probabilities  $p_{A \rightarrow B}$  and  $p_{B \rightarrow A}$ , and the energy splittings between the different two-exciton states. Experiments have demonstrated the strong dependence of the FR angle on the probe energy  $E$ , including a fine structure of the resonance [93].

In Fig. 3.7(b), we compare the calculated FR signal for coupled QD's  $A$  and  $B$  with the corresponding result for uncoupled QD's  $A$  pumped at resonance. For a probe energy  $E \simeq 2.42$  eV, the FR signal for coupled QD's  $A$  and  $B$  is significantly smaller than the FR signal of the  $AA$  system, consistent with experimental observations [70].

So far, we have assumed that the symmetry axis of the CdSe QD's with hexagonal crystal structure is parallel to the propagation direction of pump and probe laser pulses. However, in experiment the QD's are randomly oriented. We discuss next how the random orientation changes our results. The propagation direction of pump and probe laser pulse is  $\hat{\mathbf{z}}$ , the polarization vector of the probe pulse  $\hat{\mathbf{x}}$ , and the symmetry axes of QD's  $A$  and  $B$  are denoted by  $\hat{\mathbf{c}}_A$  and  $\hat{\mathbf{c}}_B$ , respectively. We define the azimuthal angles  $\phi_A = \angle(\hat{\mathbf{x}}, \hat{\mathbf{c}}_A)$  and  $\phi_B = \angle(\hat{\mathbf{x}}, \hat{\mathbf{c}}_B)$ , and the angle enclosed by the two symmetry axes  $\phi_{AB} = \angle(\hat{\mathbf{c}}_A, \hat{\mathbf{c}}_B)$  [see Fig. 3.8(a)]. The conduction band spin eigenstates with quantization axis  $\hat{\mathbf{c}}_{A,B}$  are denoted by  $|\uparrow_{A,B}\rangle$  and  $|\downarrow_{A,B}\rangle$ .

---

<sup>4</sup>This hybridization with higher lying levels in QD  $B$  does not invalidate our calculation of the FR angle in Sec. 3.4 because the pump pulse leads to occupation of the lowest conduction band level in QD  $B$  only.

For arbitrary angle  $\angle(\hat{\mathbf{z}}, \hat{\mathbf{c}}_B)$ , the probability for the circularly polarized pump pulse to create a net spin polarization in the conduction band level decreases from its maximum value at  $\angle(\hat{\mathbf{z}}, \hat{\mathbf{c}}_B) = 0$  to zero at  $\angle(\hat{\mathbf{z}}, \hat{\mathbf{c}}_B) = \pi/2$ . For  $\angle(\hat{\mathbf{z}}, \hat{\mathbf{c}}_B) < \pi/2$ , the majority of conduction band electrons is in spin state  $|\uparrow_B\rangle$ , with the quantization axis defined by  $\hat{\mathbf{c}}_B$ . On transfer to QD  $A$ , the conduction band electron retains its spin state because states with  $s_z = \pm 1/2$  are degenerate in both QD's and  $t_c$  is spin-independent. The characteristic level spacing of valence band states is large compared to the crystal field splitting in bulk CdSe, which allows us to treat the latter as a small perturbation, following Ref. [91].

In the following, we calculate the FR angle for a random orientation of QD's assuming that the pump pulse has created a conduction band electron with spin  $|\uparrow_B\rangle$ . The random orientation of QD's affects the FR of the probe pulse in two ways. Firstly, the matrix elements for transitions from the  $j_z = \pm 3/2$  valence band levels to the  $s_z = \pm 1/2$  conduction band levels in QD  $A$  ( $B$ ) decrease by  $\sin \phi_A$  ( $\sin \phi_B$ ) compared to the oriented sample [91]. More importantly, also the relative orientation of  $\hat{\mathbf{c}}_A$  and  $\hat{\mathbf{c}}_B$  modifies the FR angle. For illustration, consider two QD's with  $t_c = 0$ , and a conduction band electron in spin state  $|\uparrow_B\rangle$  in  $B$ . The  $\sigma^-$  circularly polarized component of the probe pulse with  $E \simeq E_X^A$  excites a virtual exciton in  $A$ , with a conduction band electron in spin state  $|\uparrow_A\rangle$ . Note that the spin direction is defined by  $\hat{\mathbf{c}}_A$ , the symmetry axis of  $A$ . Expanding  $|\uparrow_A\rangle = \cos(\phi_{AB}/2)|\uparrow_B\rangle + i \sin(\phi_{AB}/2)|\downarrow_B\rangle$  in terms of the eigenstates along quantization axis  $\hat{\mathbf{c}}_B$ , the product state of the two excitons contains terms in which the two conduction band spins are antiparallel and have a finite overlap with the spin singlet state. This is in stark contrast to the oriented sample, where the two conduction band electrons would always form a triplet.

The analogous analysis for coupled QD's must take into account both the reduced transition matrix elements for the probe pulse and the relative orientation of QD's  $A$  and  $B$ . Because virtual transitions to  $|\tilde{T}_0\rangle$  and  $|\tilde{S}\rangle$  involve excitation of QD  $B$  which was populated by the pump pulse, the matrix elements in Eq. (3.21) are reduced by a factor  $|\sin \phi_B|$  which is independent of the relative orientation of  $\hat{\mathbf{c}}_A$  and  $\hat{\mathbf{c}}_B$ . In contrast, virtual transitions in QD  $A$  probe the spin polarization relative to the quantization axis  $\hat{\mathbf{c}}_A$  after an electron with spin pointing along  $\hat{\mathbf{c}}_B$  has been transferred, and the transition matrix elements depend also on  $\phi_{AB}$  [Fig. 3.8(b)]. For the FR angle, we find

$$\theta_F(E) = \frac{CE}{2} \left\{ d_A^2 \cos \phi_{AB} \sin^2 \phi_A \left[ (1 - p_{B \rightarrow A}) \frac{E - E_{T_0B}}{(E - E_{T_0B})^2 + \Gamma^2} \right. \right. \quad (3.32)$$

$$\left. \left. - (1 + p_{B \rightarrow A} - 2p_{A \rightarrow B}) \frac{E - E_{SB}}{(E - E_{SB})^2 + \Gamma^2} \right] - d_B^2 \sin^2 \phi_B p_{B \rightarrow A} \left[ \frac{E - E_{\tilde{T}_0B}}{(E - E_{\tilde{T}_0B})^2 + \Gamma^2} \right. \right.$$

$$\left. \left. + \frac{E - E_{\tilde{S}B}}{(E - E_{\tilde{S}B})^2 + \Gamma^2} \right] \right\}.$$

The dependence on the relative orientation of the two QD's,  $\phi_{AB}$ , is readily understood. For  $\phi_{AB} = \pi/2$ , the first and second term in the expression for  $\theta_F(E)$  vanish because the conduction band spin created in QD  $B$  is perpendicular to the spin quantization axis in

QD  $A$ . A laser pulse probing QD  $A$  does not show any FR because the net spin along  $\hat{\mathbf{c}}_A$  vanishes [Fig. 3.8(b)].

In experiment,  $\hat{\mathbf{c}}_A$  and  $\hat{\mathbf{c}}_B$  are randomly distributed over the unit sphere. Performing this average in Eq. (3.33), we find for the FR angle

$$\begin{aligned} \overline{\theta}_F(E) = \frac{CE}{2} \left\{ \frac{3}{16} d_A^2 \left[ (1 - p_{B \rightarrow A}) \frac{E - E_{T_0B}}{(E - E_{T_0B})^2 + \Gamma^2} \right. \right. \\ \left. \left. - (1 + p_{B \rightarrow A} - 2p_{A \rightarrow B}) \frac{E - E_{SB}}{(E - E_{SB})^2 + \Gamma^2} \right] \right. \\ \left. - \frac{2}{3} d_B^2 p_{B \rightarrow A} \left[ \frac{E - E_{\tilde{T}_0B}}{(E - E_{\tilde{T}_0B})^2 + \Gamma^2} + \frac{E - E_{\tilde{S}B}}{(E - E_{\tilde{S}B})^2 + \Gamma^2} \right] \right\}. \end{aligned} \quad (3.33)$$

Note that the spectral weight of the last term increases compared to the oriented sample.

## 3.7 Conclusions

We have calculated the Faraday rotation angle for coupled QD's as a function of the probe pulse frequency. We have considered an initial spin polarization in neutral QD's (created by optical pumping) and of one excess electron in the two coupled QD's. Our results lead us to the following conclusions.

(i) The Faraday rotation angle shows a nontrivial functional dependence on the probe energy, the details of which depend on the spin exchange energy and spin transfer probabilities [see Eq. (3.20) and Fig. 3.7(a)]. Most notably, because several two-exciton states are separated in energy by a small spin exchange coupling,  $\theta_F(E)$  is not invariant under point inversion symmetry. Measurement of  $\theta_F(E)$  as a function of probe energy would allow one to identify the contributions of the various two-exciton states that are virtually excited by the probe pulse.

(ii) Experiments on doped QD's would allow one to determine whether spin transfer is mediated by transfer in the conduction or valence band states. In particular, from a vanishing Faraday rotation angle for probe pulse energies close to the resonance of QD  $A$  one could exclude that an excess electron injected into QD  $B$  has been transferred to  $A$ . In contrast, for optical spin injection, spin could be transferred both between conduction and valence band states.

(iii) In general, measurement of the Faraday rotation signal at a given probe frequency does not provide enough information to determine spin transfer probabilities between the QD's. However, from the experimentally observed energy shifts, we calculate a characteristic energy scale  $t_c = 0.08$  eV for spin transfer in the conduction band. Based on the transfer Hamiltonian ansatz, this implies a probability of 6% for electron spin to be transferred from QD  $B$  to QD  $A$ , and of 13% for the opposite direction.

The purpose of this work was to establish the connection between spin transfer and the Faraday rotation signal observed in experiment. Our analysis was based on a transfer

Hamiltonian ansatz. Some of the most interesting results of Ref. [70] remain to be explored theoretically. Most notably, the transfer Hamiltonian ansatz is based on the assumption that electrons are transferred between the QD's via the bridging benzene molecule. Microscopic work will have to clarify why conjugated molecules provide efficient transfer paths between QD's. Very recently, further studies of the problem were presented [94], the results of which provide support for the work described in this chapter.

The results obtained here can provide important guidance also for the identification of microscopic transfer mechanisms. The increase of the Faraday rotation signal at a fixed probe frequency has been interpreted as increase of the spin transfer efficiency for higher temperatures [70]. According to our results, an increase in the transfer matrix element  $t_c$  also leads to a shift of the exciton edge in absorption spectra toward lower energies. If the exciton absorption edge does not change with increasing temperature, the increased Faraday rotation signal is more likely effected, e.g., by additional incoherent transfer paths than by an increase of the transfer matrix element.

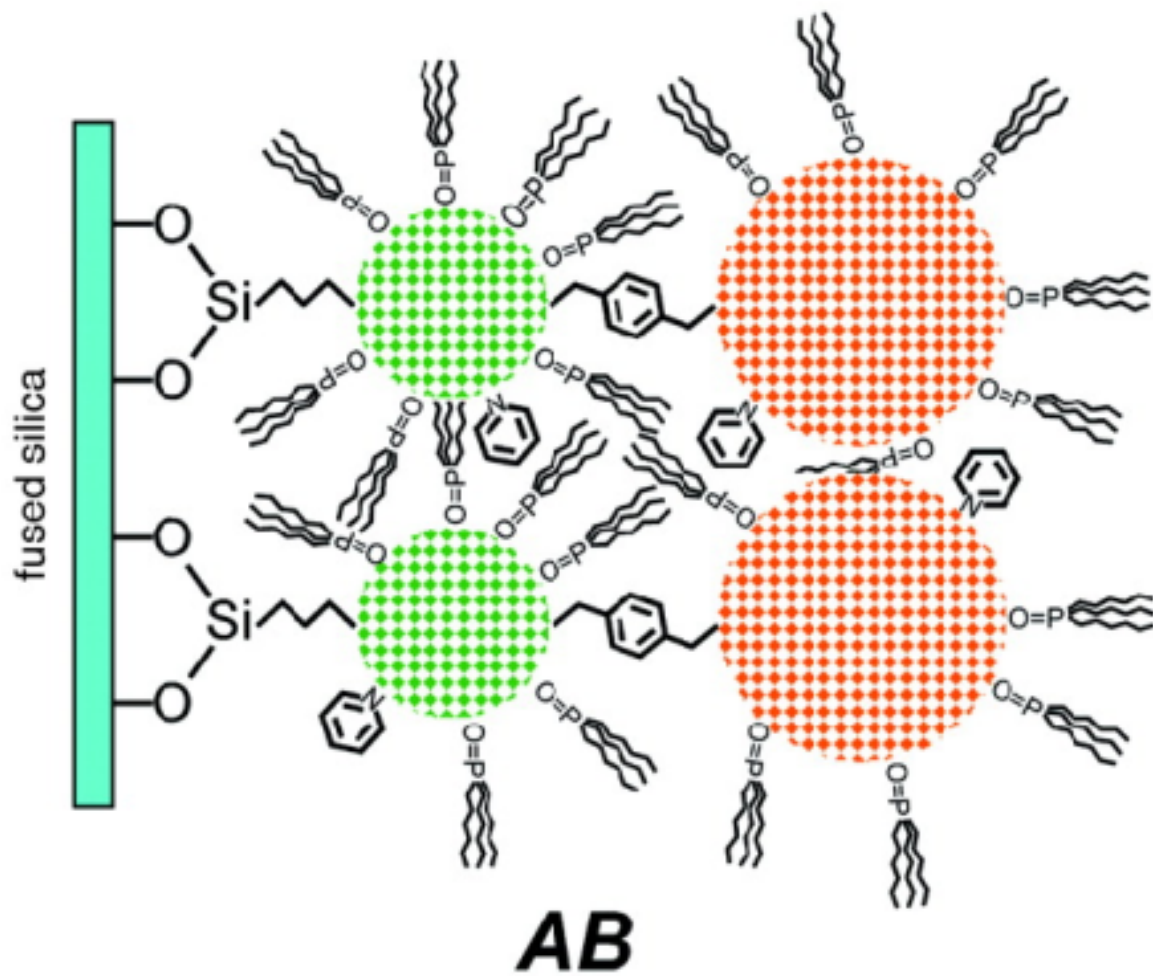


Figure 3.1: Schematic bilayer of the different types of dots *A* (size 3.4 nm) and *B* (size 7nm). The structure is denoted as *AB*.(Figure courtesy of M. Ouyang and D. D. Awschalom.)

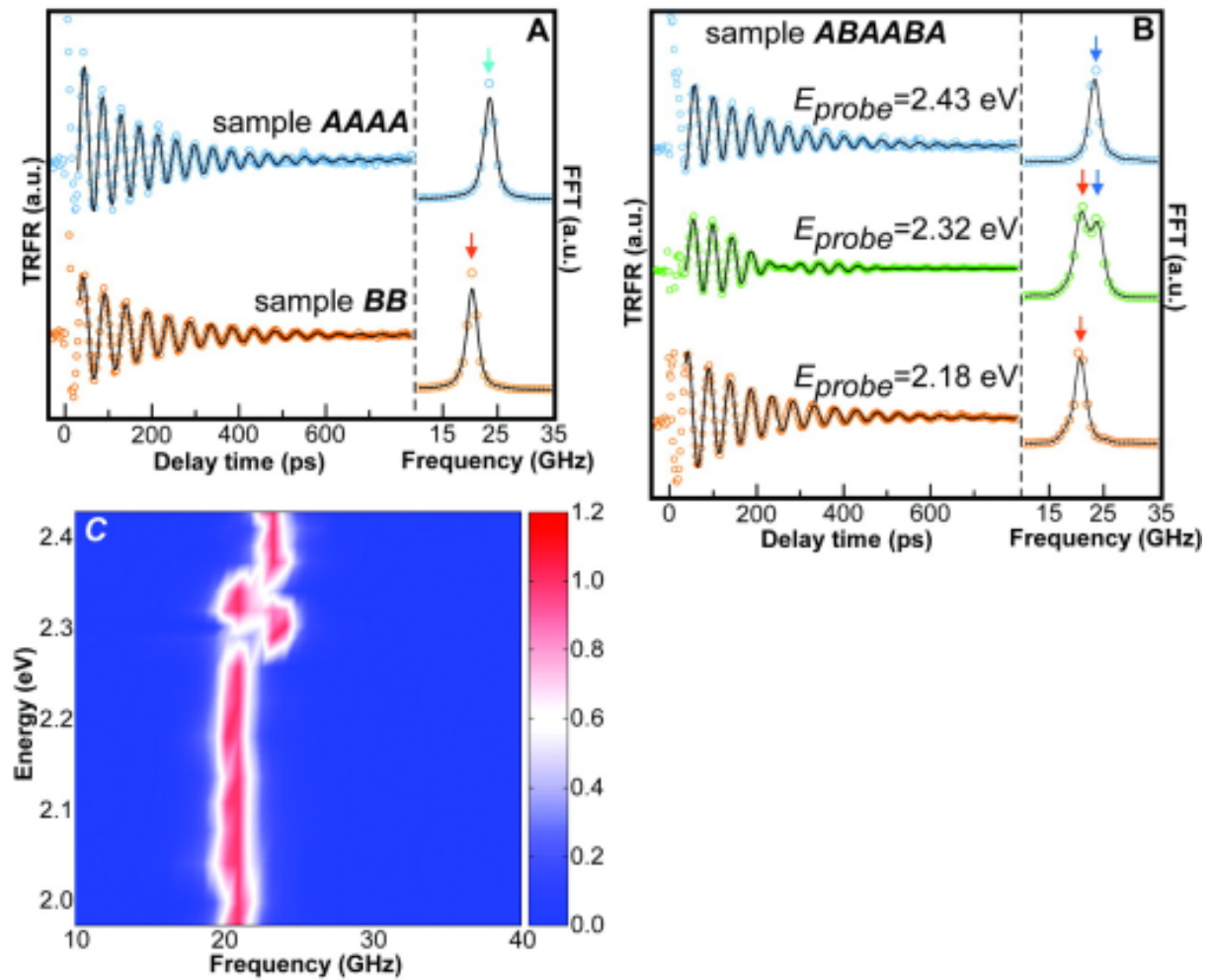
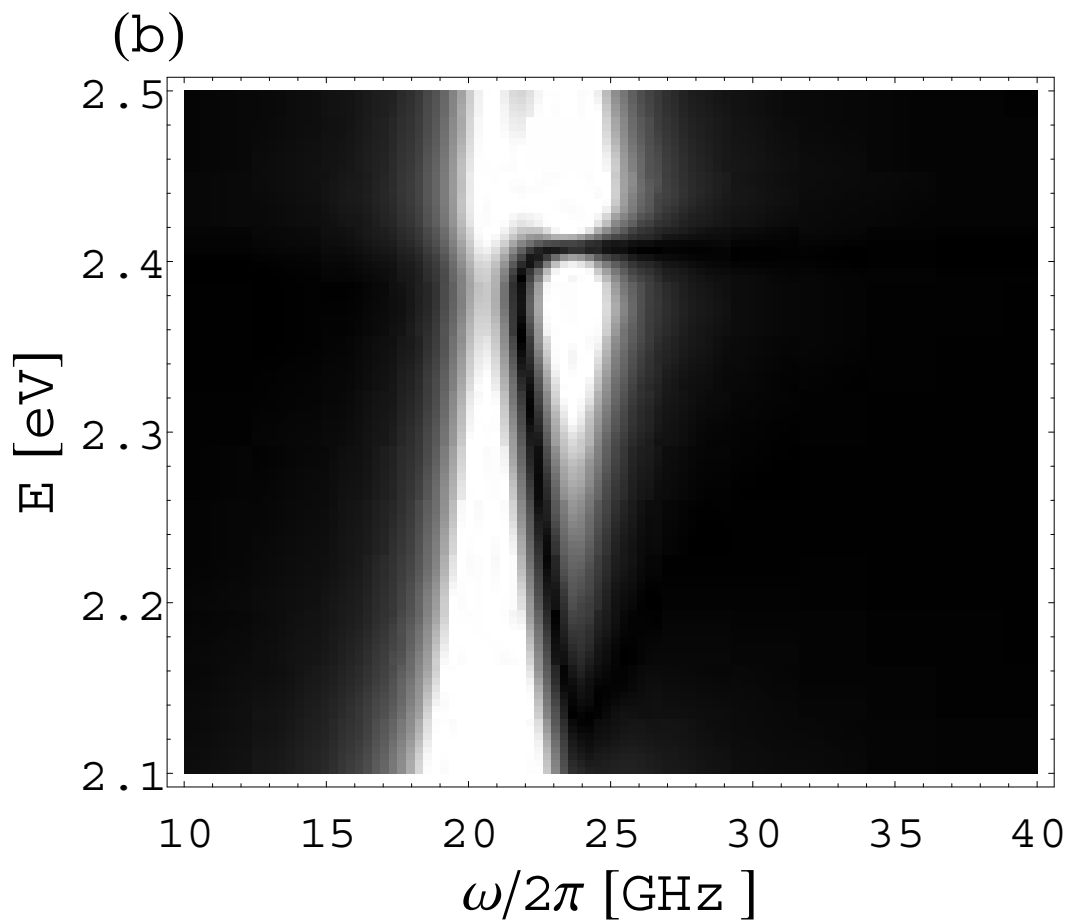
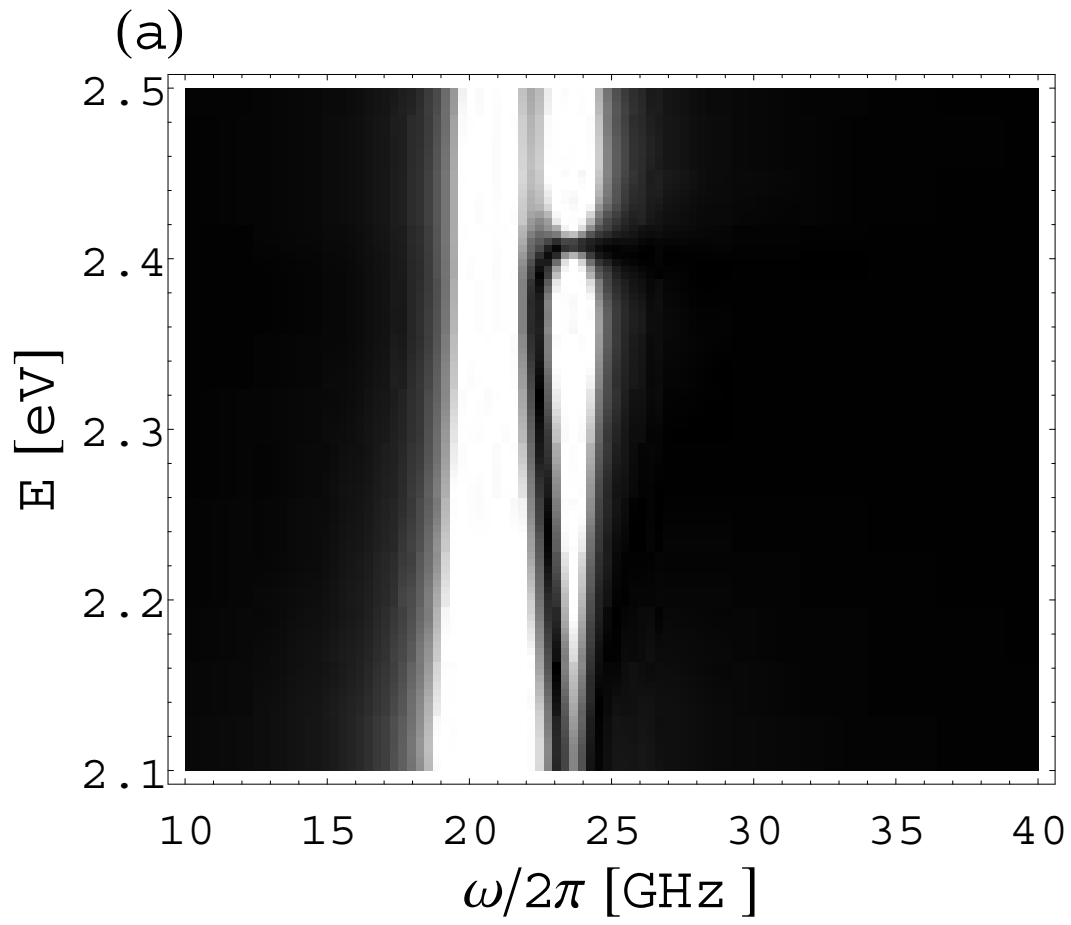


Figure 3.2: (A) Time resolved FR curves for structures *AAAA* and *BB* and their FFT spectra. These curves serve as control and reference, showing that at the pumping energy corresponding to *A* (*B*) a peak at the corresponding frequency is observed. (B) FR curves from a *ABAABA* sample for different probing energies. (Figure courtesy of M. Ouyang and D. D. Awschalom.)





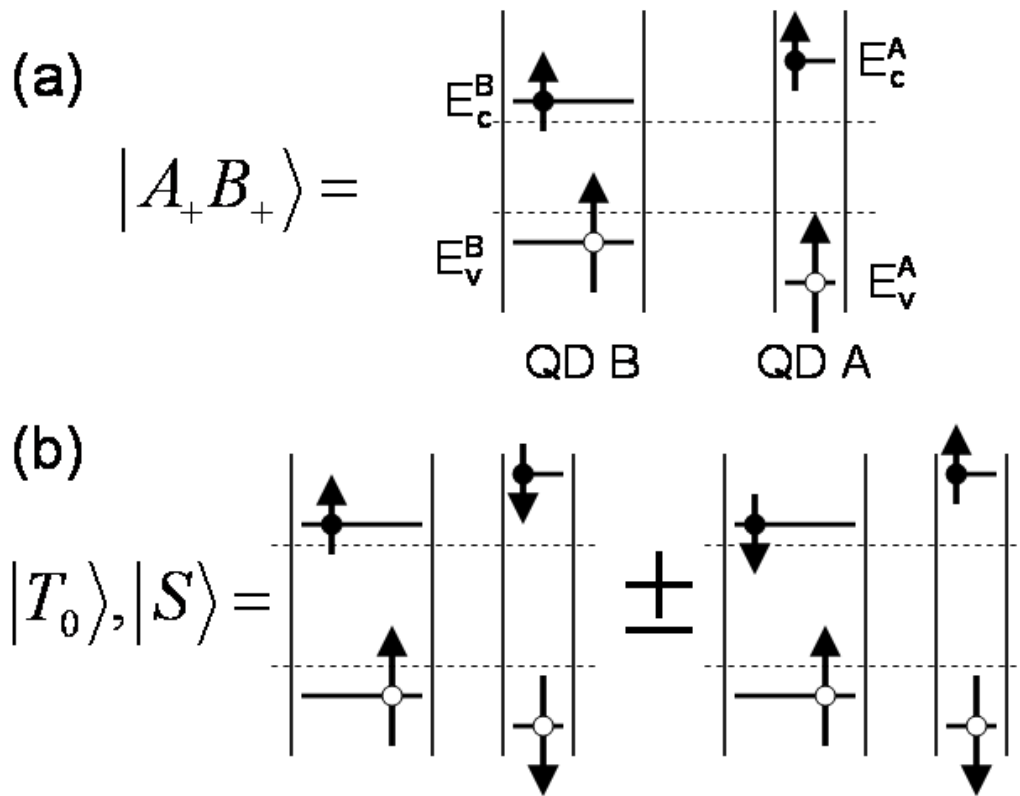


Figure 3.4: Schematic representation of the spin configurations (in the electron picture) for states (a)  $|A_+ B_+\rangle$  and (b)  $|S\rangle, |T_0\rangle$  to leading order in  $t_c$ . The dashed lines represent the conduction and valence band edge in bulk CdSe.

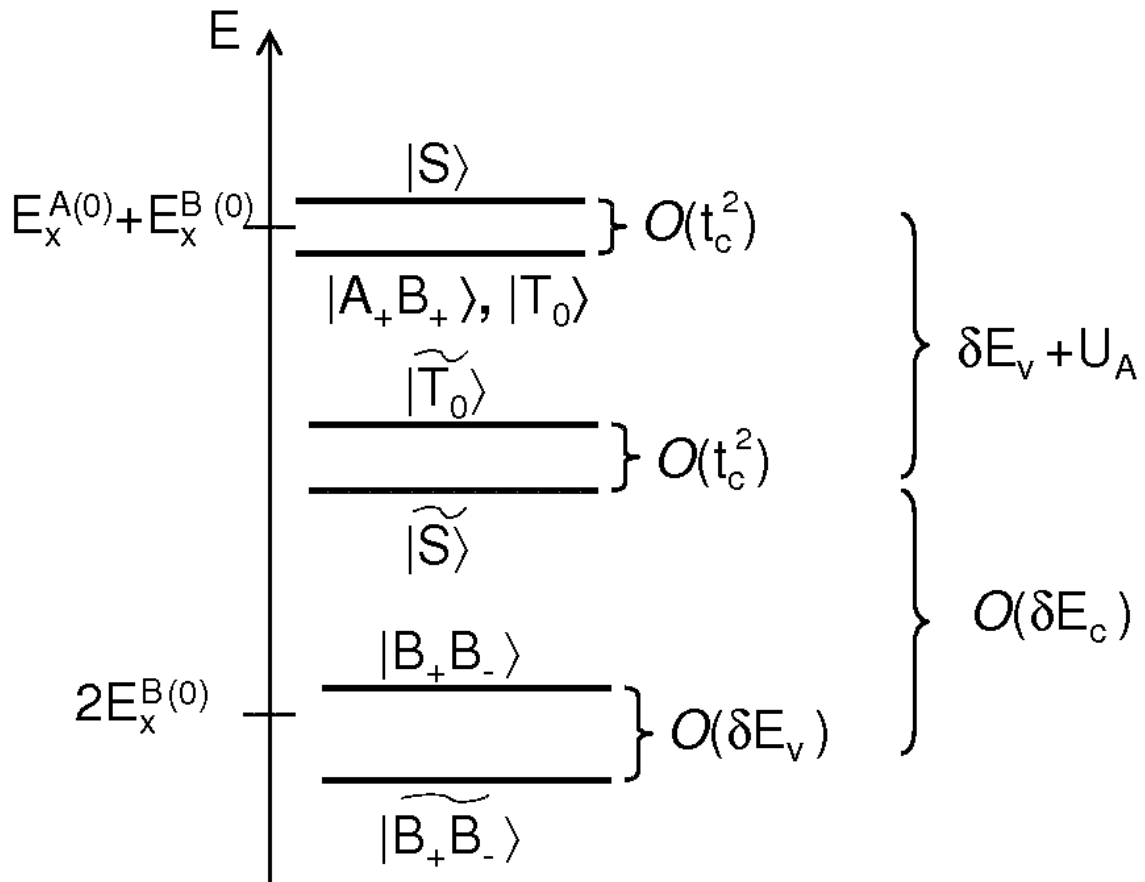


Figure 3.5: Energy level scheme of all two-exciton eigenstates discussed in the text. The eigenenergies fall into three groups which are split by terms of order  $O(t_c^2)$  or  $O(\delta E_v)$ . For the QD's used in Ref. [70],  $\delta E_v + U_A \simeq 0$ , and the five states  $|A_+B_+\rangle$ ,  $|T_0\rangle$ ,  $|S\rangle$ ,  $|\widetilde{T}_0\rangle$ , and  $|\widetilde{S}\rangle$  are nearly degenerate.

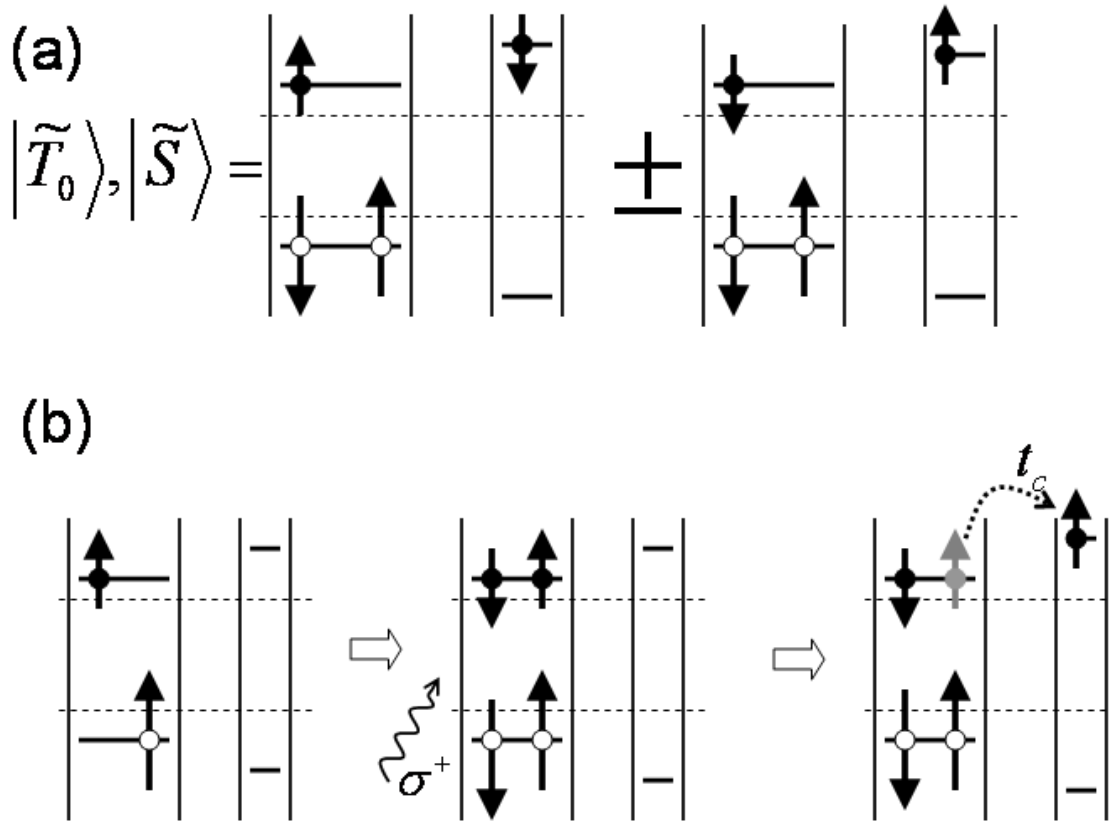


Figure 3.6: (a) Schematic representation of the spin configurations for the states  $|\tilde{S}\rangle$ ,  $|\tilde{T}_0\rangle$  to leading order in  $t_c$ . (b) Transitions between an initial state  $|X_{B,+}\rangle$  and  $|\tilde{S}\rangle$ ,  $|\tilde{T}_0\rangle$  are effected by the absorption of a  $\sigma^+$  polarized probe photon and subsequent tunneling of one conduction band electron.

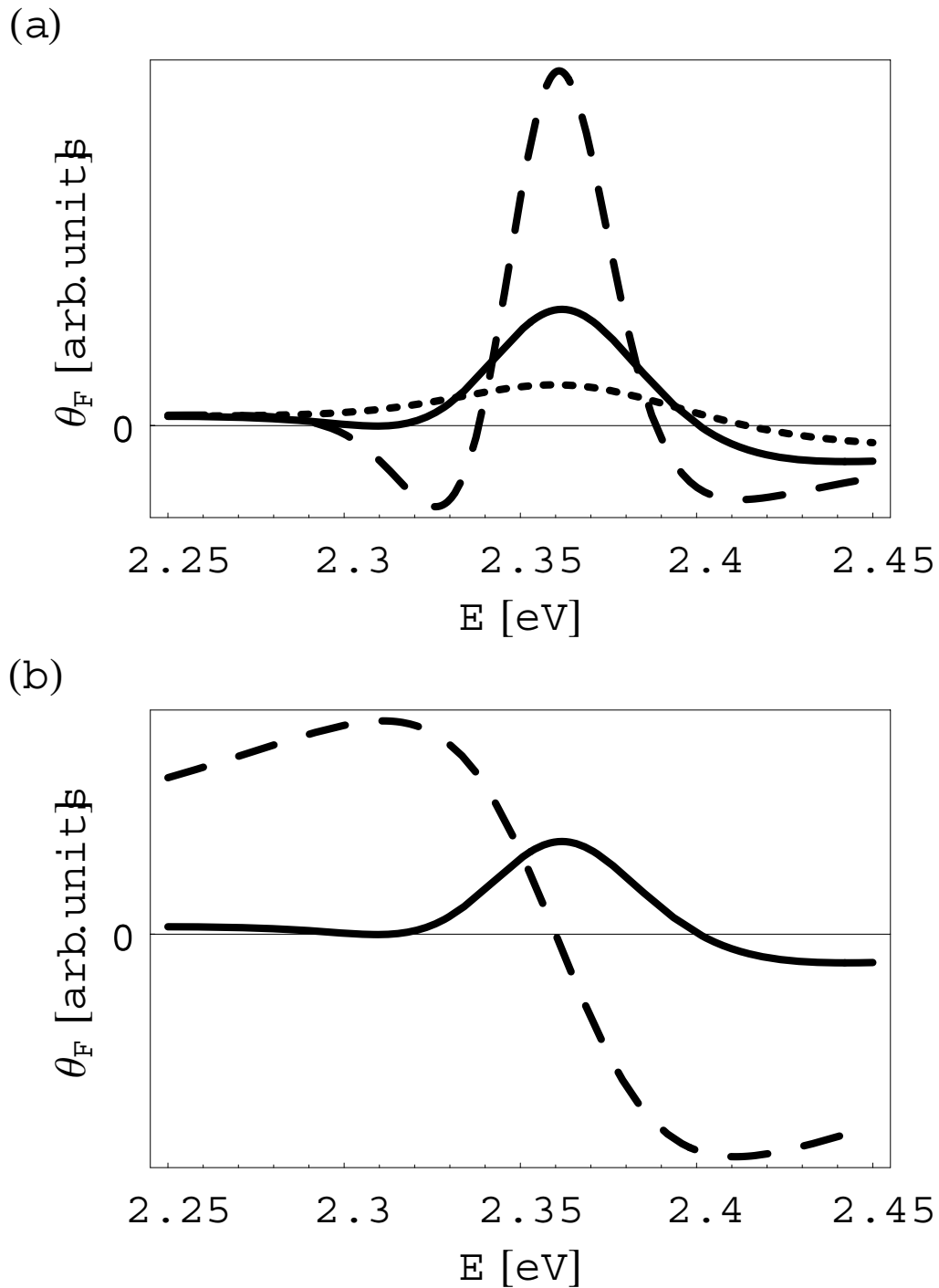


Figure 3.7: (a) Plot of the FR angle as a function of probe pulse frequency calculated from Eq. (3.20) for different level broadenings  $\Gamma = 0.05$  eV (solid), 0.02 eV (dashed), and 0.08 eV (dotted). All other parameters are as described in the text. For small  $\Gamma$ ,  $\theta_F(E)$  clearly shows the individual contributions from the various two-exciton states. (b) Comparison of the FR angle for coupled QD's for  $\Gamma = 0.05$  eV (solid) with the calculated signal for a AA structure (dashed).

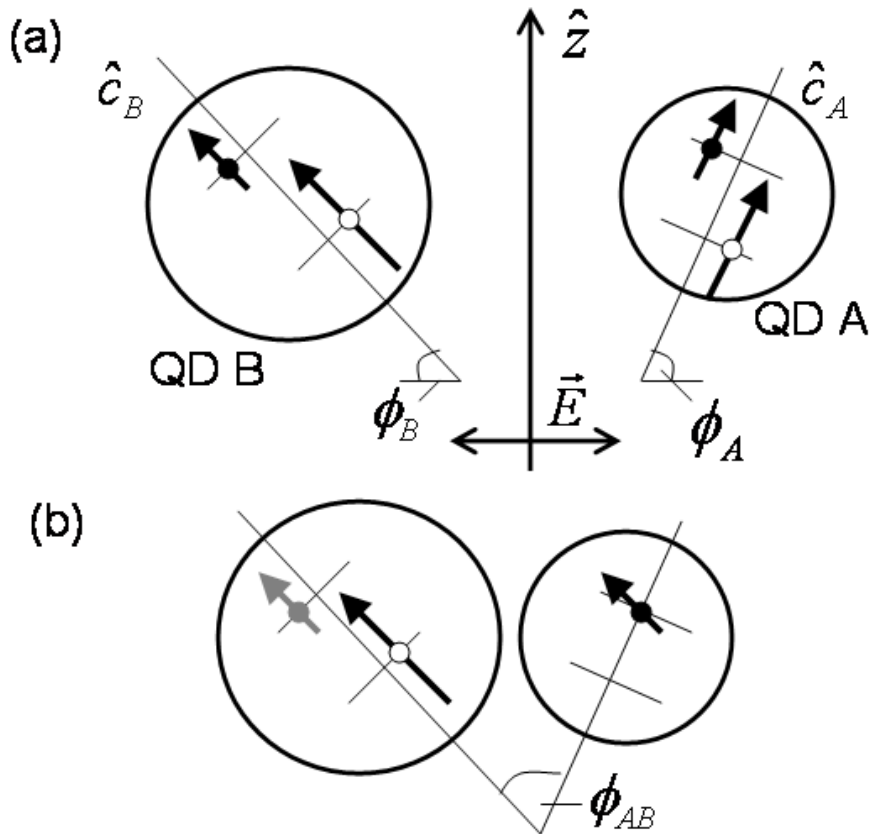


Figure 3.8: (a) The hexagonal symmetry axes of QD's  $A$  and  $B$  are in general oriented randomly relative to the direction of the laser pump and probe pulse. Because of the interband selection rules, a  $\sigma^-$  circularly polarized laser pulse generates a spin polarization along the symmetry axis of the respective QD. (b) A conduction band electron created in QD  $B$  retains its spin direction on transfer to QD  $A$ . FR in QD  $A$  probes the projection of this spin onto the symmetry axis  $\hat{c}_A$ , which gives rise to a factor  $\cos \phi_{AB}$  for the first and second term in Eq. (3.33).

# Appendix A

## Two-spin density matrix

In the following we show the density matrix for the two-spin state of the electrons right before injection into the spin-LEDs, obtained as described in Sec. 2.2.1.

$$\begin{aligned}
\chi_{\{\uparrow\uparrow,\uparrow\uparrow\}}(t, t') &= \frac{1}{4} \left\{ (1 + aP) [1 + a'P' \cos \beta] - e^{-t/T_1} \left[ e^{-t'/T_1'} \cos^2 \beta + e^{-t'/T_2'} \sin^2 \beta \cos(\tilde{h}t') \right] \right\} \\
\chi_{\{\uparrow\uparrow,\uparrow\downarrow\}}(t, t') &= \frac{\sin \beta}{4} \left\{ -a'P' (1 + aP) + e^{-(t/T_1+t'/T_1')} \cos \beta - e^{-(t/T_1+t'/T_2')} \left[ \cos \beta \cos(\tilde{h}t') + i \sin(\tilde{h}t') \right] \right\} \\
\chi_{\{\uparrow\uparrow,\downarrow\uparrow\}}(t, t') &= -\frac{\sin \beta}{4} e^{-t/T_2+iht} \left\{ -e^{-t'/T_1'} \cos \beta + e^{-t'/T_2'} \left[ \cos \beta \cos(\tilde{h}t') - i \sin(\tilde{h}t') \right] \right\} \\
\chi_{\{\uparrow\uparrow,\downarrow\downarrow\}}(t, t') &= -\frac{\sin^2 \beta}{4} e^{-t/T_2+iht} \left[ e^{-t'/T_1'} - e^{-t'/T_2'} \cos(\tilde{h}t') \right] \\
\chi_{\{\uparrow\downarrow,\uparrow\uparrow\}}(t, t') &= \frac{\sin \beta}{4} \left\{ -a'P' (1 + aP) + e^{-(t/T_1+t'/T_1')} \cos \beta + e^{-(t/T_1+t'/T_2')} \left[ -\cos \beta \cos(\tilde{h}t') + i \sin(\tilde{h}t') \right] \right\} \\
\chi_{\{\uparrow\downarrow,\uparrow\downarrow\}}(t, t') &= \frac{1}{4} \left\{ (1 + aP) [1 - a'P' \cos \beta] + e^{-t/T_1} \left[ e^{-t'/T_1'} \cos^2 \beta + e^{-t'/T_2'} \sin^2 \beta \cos(\tilde{h}t') \right] \right\} \\
\chi_{\{\uparrow\downarrow,\downarrow\uparrow\}}(t, t') &= -\frac{e^{-t/T_2+iht}}{4} \left\{ e^{-t'/T_1'} \sin^2 \beta + e^{-t'/T_2'} \left[ \cos(\tilde{h}t') (1 + \cos^2 \beta) - 2i \cos \beta \sin(\tilde{h}t') \right] \right\} \\
\chi_{\{\uparrow\downarrow,\downarrow\downarrow\}}(t, t') &= -\frac{\sin \beta}{4} e^{-t/T_2+iht} \left\{ e^{-t'/T_1'} \cos \beta + e^{-t'/T_2'} \left[ -\cos \beta \cos(\tilde{h}t') + i \sin(\tilde{h}t') \right] \right\} \\
\chi_{\{\downarrow\uparrow,\uparrow\uparrow\}}(t, t') &= -\frac{\sin \beta}{4} e^{-t/T_2-ih t} \left\{ -e^{-t'/T_1'} \cos \beta + e^{-t'/T_2'} \left[ \cos \beta \cos(\tilde{h}t') + i \sin(\tilde{h}t') \right] \right\} \\
\chi_{\{\downarrow\uparrow,\uparrow\downarrow\}}(t, t') &= -\frac{e^{-t/T_2-ih t}}{4} \left\{ e^{-t'/T_1'} \sin^2 \beta + e^{-t'/T_2'} \left[ \cos(\tilde{h}t') (1 + \cos^2 \beta) + 2i \cos \beta \sin(\tilde{h}t') \right] \right\} \\
\chi_{\{\downarrow\uparrow,\downarrow\uparrow\}}(t, t') &= \frac{1}{4} \left\{ (1 - aP) [1 + a'P' \cos \beta] + e^{-t/T_1} \left[ e^{-t'/T_1'} \cos^2 \beta + e^{-t'/T_2'} \sin^2 \beta \cos(\tilde{h}t') \right] \right\}
\end{aligned}$$

$$\begin{aligned}
\chi_{\{\downarrow\uparrow,\downarrow\downarrow\}}(t, t') &= \frac{\sin \beta}{4} \left\{ -a'P'(1 - aP) - e^{-(t/T_1+t'/T'_1)} \cos \beta + e^{-(t/T_1+t'/T'_2)} \left[ \cos \beta \cos(\tilde{h}t') + i \sin(\tilde{h}t') \right] \right\} \\
\chi_{\{\downarrow\downarrow,\uparrow\uparrow\}}(t, t') &= -\frac{\sin^2 \beta}{4} e^{-t/T_2-ih t} \left[ e^{-t'/T'_1} - e^{-t'/T'_2} \cos(\tilde{h}t') \right] \\
\chi_{\{\downarrow\downarrow,\uparrow\downarrow\}}(t, t') &= -\frac{\sin \beta}{4} e^{-t/T_2-ih t} \left\{ e^{-t'/T'_1} \cos \beta - e^{-t'/T'_2} \left[ \cos \beta \cos(\tilde{h}t') + i \sin(\tilde{h}t') \right] \right\} \\
\chi_{\{\downarrow\downarrow,\downarrow\uparrow\}}(t, t') &= \frac{\sin \beta}{4} \left\{ -a'P'(1 - aP) - e^{-(t/T_1+t'/T'_1)} \cos \beta + e^{-(t/T_1+t'/T'_2)} \left[ \cos \beta \cos(\tilde{h}t') - i \sin(\tilde{h}t') \right] \right\} \\
\chi_{\{\downarrow\downarrow,\downarrow\downarrow\}}(t, t') &= \frac{1}{4} \left\{ (1 - aP) [1 - a'P' \cos \beta] - e^{-t/T_1} \left[ e^{-t'/T'_1} \cos^2 \beta + e^{-t'/T'_2} \sin^2 \beta \cos(\tilde{h}t') \right] \right\}
\end{aligned}$$



# Appendix B

## Two-exciton eigenstates of coupled quantum dots

In order to evaluate the FR angle  $\theta_F(E)$  from Eq. (3.6) for arbitrary probe energies  $E$ , all two-exciton intermediate states  $|\psi_i\rangle$  with finite transition matrix elements  $\langle\psi_i|\hat{P}_\pm|X_{B,+}\rangle$  must be calculated. States with energies  $E_i \simeq E + E_X^{B(0)}$  lead to the dominant contributions in the expression for the FR angle, Eq. (3.6). The states  $|A_+B_+\rangle$ ,  $|S\rangle$ , and  $|T_0\rangle$  defined in Eqs. (3.11) and (3.13) have energy eigenvalues  $E_i$  with  $|E_X^{A(0)} + E_X^{B(0)} - E_i| \leq \mathcal{O}[t_c^2/(\delta E_c - U_A), t_c^2/(\delta E_c + U_A)]$ , and are the most important intermediate states for probe pulse energies  $E \simeq E_X^{A(0)}$ . However, for the experimental values of Ref. [70],  $\delta E_v + U_A$  is small and two additional two-exciton states must be taken into account.

The states

$$|\tilde{T}_0\rangle = \frac{1}{\sqrt{2}} \left( \hat{c}_{c,-}^{A\dagger} \hat{c}_{c,+}^{B\dagger} + \hat{c}_{c,+}^{A\dagger} \hat{c}_{c,-}^{B\dagger} \right) \hat{c}_{v,+}^B \hat{c}_{v,-}^B |0\rangle, \quad (\text{B.1a})$$

$$|\tilde{S}\rangle \propto \frac{1}{\sqrt{2}} \left( \hat{c}_{c,-}^{A\dagger} \hat{c}_{c,+}^{B\dagger} - \hat{c}_{c,+}^{A\dagger} \hat{c}_{c,-}^{B\dagger} \right) \hat{c}_{v,+}^B \hat{c}_{v,-}^B |0\rangle \\ + \sqrt{2} \left( \frac{t_c}{\delta E_c + U_A + 2U_B} \hat{c}_{c,+}^{A\dagger} \hat{c}_{c,-}^{A\dagger} - \frac{t_c}{\delta E_c + U_B} \hat{c}_{c,+}^{B\dagger} \hat{c}_{c,-}^{B\dagger} \right) \hat{c}_{v,+}^B \hat{c}_{v,-}^B |0\rangle \quad (\text{B.1b})$$

differ from the corresponding states in Eq. (3.13) in that both holes are localized in QD  $B$ . The normalization constant for  $|\tilde{S}\rangle$  is fixed by  $\langle\tilde{S}|\tilde{S}\rangle = 1$ . The eigenenergies

$$E_{\tilde{T}_0} = E_X^{A(0)} + E_X^{B(0)} + \delta E_v + U_A, \quad (\text{B.2a})$$

$$E_{\tilde{S}} = E_X^{A(0)} + E_X^{B(0)} + \delta E_v + U_A \\ + 2t_c^2 \left( \frac{1}{\delta E_c + U_B} - \frac{1}{\delta E_c + 2U_B + U_A} \right) \quad (\text{B.2b})$$

$ \psi_i\rangle$	$E_i$	$E_i - E_X^B$ [eV]
$ A_+B_+\rangle$	$E_X^{A(0)} + E_X^{B(0)}$	2.35
$ T_0\rangle$	$E_X^{A(0)} + E_X^{B(0)}$	2.35
$ S\rangle$	$E_X^{A(0)} + E_X^{B(0)}$	2.37
$ B_+B_-\rangle$	$E_c^B - E_v^A + E_X^{B(0)}$	2.06
$ \widetilde{T}_0\rangle$	$E_c^A - E_v^B + E_X^{B(0)}$	2.32
$ \widetilde{S}\rangle$	$E_c^A - E_v^B + E_X^{B(0)}$	2.33
$ \widetilde{B_+B_-}\rangle$	$2E_X^{B(0)}$	2.04

Table B.1: Two-exciton eigenstates  $|\psi_i\rangle$  which contribute to the FR angle up to second order in  $t_c$ . We also list the corresponding eigenenergies to  $\mathcal{O}(t_c^0)$  and evaluate them for the parameters discussed in Sec. 3.6. As noted in the main text, the degeneracy of  $|\widetilde{T}_0\rangle$ ,  $|\widetilde{S}\rangle$  with  $|T_0\rangle$ ,  $|S\rangle$  is a consequence of  $\delta E_v + U_A \simeq 0$  for the QD's used in experiment.

are shifted relative to  $E_{T_0}$  and  $E_S$  by  $\delta E_v + U_A$ .

The state

$$|\widetilde{B_+B_-}\rangle \propto \left[ \hat{c}_{c,+}^{B\dagger} \hat{c}_{c,-}^{B\dagger} + \frac{t_c}{\delta E_c + U_B} \left( \hat{c}_{c,-}^{A\dagger} \hat{c}_{c,+}^{B\dagger} - \hat{c}_{c,+}^{A\dagger} \hat{c}_{c,-}^{B\dagger} \right) + \frac{2t_c^2 \hat{c}_{c,+}^{A\dagger} \hat{c}_{c,-}^{A\dagger}}{(\delta E_c + U_B)(2\delta E_c + U_A + 3U_B)} \right] \hat{c}_{v,+}^B \hat{c}_{v,-}^B |0\rangle \quad (\text{B.3})$$

with

$$E_{\widetilde{B_+B_-}} = 2E_X^{B(0)} - 2 \frac{t_c^2}{\delta E_c + U_B} \quad (\text{B.4})$$

is energetically separated from  $E_{T_0}$  and  $E_S$  by  $E_X^{A(0)} - E_X^{B(0)}$ .

In Table B.1, we summarize all two-exciton eigenstates which contribute to the spectral representation of  $\theta_F(E)$  up to order  $t_c^2$ . We also list the formal expressions for their eigenenergies to leading order  $\mathcal{O}(t_c^0)$  and give the numerical values, taking into account terms up to  $\mathcal{O}(t_c^2)$  for the parameters discussed in Sec. 3.6.

# Appendix C

## Eigenstates of doped coupled quantum dots

Here, we calculate eigenstates and energy eigenvalues for states with two electrons and one hole in the coupled QD's. These are the intermediate states  $|\psi_i\rangle$  in Eq. (3.6) which have finite overlap matrix elements with  $\hat{P}_\pm|e_{B,+}\rangle$  and determine the FR angle for coupled QD's doped with a single excess electron.

In addition to the states  $|A_+B_+^-\rangle$ ,  $|S^-\rangle$ , and  $|T_0^-\rangle$  defined in Eqs. (3.24) and (3.26), five states have contributions of order  $t_c^2$  to the FR angle. These are

$$|B_+B_-^-\rangle \propto \left[ \hat{c}_{c,+}^{B\dagger} \hat{c}_{c,-}^{B\dagger} + \frac{t_c}{\delta E_c - U_A - U_B} \left( \hat{c}_{c,-}^{A\dagger} \hat{c}_{c,+}^{B\dagger} - \hat{c}_{c,+}^{A\dagger} \hat{c}_{c,-}^{B\dagger} \right) \right] \hat{c}_{v,-}^A |0\rangle, \quad (\text{C.1a})$$

$$|\widetilde{A_+B_+}^-\rangle = \hat{c}_{c,+}^{A\dagger} \hat{c}_{c,+}^{B\dagger} \hat{c}_{v,+}^B |0\rangle, \quad (\text{C.1b})$$

$$|\tilde{T}_0^-\rangle = \frac{1}{\sqrt{2}} \left( \hat{c}_{c,-}^{A\dagger} \hat{c}_{c,+}^{B\dagger} + \hat{c}_{c,+}^{A\dagger} \hat{c}_{c,-}^{B\dagger} \right) \hat{c}_{v,-}^B |0\rangle, \quad (\text{C.1c})$$

$$|\tilde{S}^-\rangle \propto \left[ \frac{1}{\sqrt{2}} \left( \hat{c}_{c,-}^{A\dagger} \hat{c}_{c,+}^{B\dagger} - \hat{c}_{c,+}^{A\dagger} \hat{c}_{c,-}^{B\dagger} \right) + \right. \quad (\text{C.1d})$$

$$\left. \sqrt{2} \left( \frac{t_c}{\delta E_c + U_A + U_B} \hat{c}_{c,+}^{A\dagger} \hat{c}_{c,-}^{A\dagger} - \frac{t_c}{\delta E_c} \hat{c}_{c,+}^{B\dagger} \hat{c}_{c,-}^{B\dagger} \right) \right] \hat{c}_{v,-}^B |0\rangle,$$

$$|\widetilde{B_+B_-}^-\rangle \propto \left[ \hat{c}_{c,+}^{B\dagger} \hat{c}_{c,-}^{B\dagger} + \frac{t_c}{\delta E_c} \left( \hat{c}_{c,-}^{A\dagger} \hat{c}_{c,+}^{B\dagger} - \hat{c}_{c,+}^{A\dagger} \hat{c}_{c,-}^{B\dagger} \right) \right] \hat{c}_{v,-}^B |0\rangle, \quad (\text{C.1e})$$

with the proportionality constants chosen to ensure normalization. The corresponding energy eigenvalues are

$$E_{B_+B_-} = 2E_c^B + U_B - E_v^A - 2\frac{t_c^2}{\delta E_c - U_A - U_B}, \quad (\text{C.2a})$$

$$E_{\widetilde{A_+B_+}^-} = E_X^{B(0)} + E_c^A, \quad (\text{C.2b})$$

$$E_{\widetilde{T_0}^-} = E_X^{B(0)} + E_c^A, \quad (\text{C.2c})$$

$$E_{\widetilde{S}^-} = E_X^{B(0)} + E_c^A + 2t_c^2 \left( \frac{1}{\delta E_c} - \frac{1}{\delta E_c + U_A + U_B} \right),$$

$$E_{\widetilde{B_+B_-}^-} = E_X^{B(0)} + E_c^B - 2\frac{t_c^2}{\delta E_c}. \quad (\text{C.2d})$$

From Eq. (C.1), we obtain the transition matrix elements in terms of the transfer probabilities defined in Eq. (3.28),

$$|\langle B_+B_- | \hat{P}_- | e_{B,+} \rangle|^2 = p_{A \rightarrow B}^- d_A^2, \quad (\text{C.3a})$$

$$|\langle \widetilde{A_+B_+}^- | \hat{P}_+ | e_{B,+} \rangle|^2 = p_{B \rightarrow A}^- d_B^2, \quad (\text{C.3b})$$

$$|\langle \widetilde{T_0}^- | \hat{P}_- | e_{B,+} \rangle|^2 = \frac{p_{B \rightarrow A}^-}{2} d_B^2, \quad (\text{C.3c})$$

$$|\langle \widetilde{S}^- | \hat{P}_- | e_{B,+} \rangle|^2 = \frac{p_{B \rightarrow A}^-}{2} d_B^2, \quad (\text{C.3d})$$

$$|\langle \widetilde{B_+B_-}^- | \hat{P}_- | e_{B,+} \rangle|^2 = (1 - p_{B \rightarrow A}^-) d_B^2. \quad (\text{C.3e})$$

These transition matrix elements and the eigenenergies allow one to calculate  $\theta_F(E)$  for arbitrary energies. However, the states in Eq. (C.1) are offset in energy from  $E_X^{A(0)} + E^B$ . For probe energies  $E \simeq E_X^{A(0)}$ , virtual transitions to the states  $|A_+B_+^- \rangle$ ,  $|S^- \rangle$ , and  $|T_0^- \rangle$  are dominant, and  $\theta_F(E)$  simplifies to the approximate expression given in Eq. (3.30).

In Table C.1, we list all states with two electrons and one hole which contribute to  $\theta_F(E)$  up to  $\mathcal{O}(t_c^2)$ . We also provide the general expressions for the eigenenergies to order  $\mathcal{O}(t_c^0)$  and evaluate them numerically for the parameters discussed in Sec. 3.6.

$ \psi_i\rangle$	$E_i$	$E_i - E_c^B$ [eV]
$ A_+B_+\rangle$	$E_X^{A(0)} + E_c^B$	2.34
$ T_0^-\rangle$	$E_X^{A(0)} + E_c^B$	2.34
$ S^-\rangle$	$E_X^{A(0)} + E_c^B$	2.36
$ B_+B_-\rangle$	$2E_c^B + U_B - E_v^A$	2.19
$ \widetilde{A_+B_-}\rangle$	$E_X^{B(0)} + E_c^A$	2.27
$ \widetilde{T_0^-\rangle}$	$E_X^{B(0)} + E_c^A$	2.27
$ \widetilde{S^-\rangle}$	$E_X^{B(0)} + E_c^A$	2.28
$ \widetilde{B_+B_-}\rangle$	$E_X^{B(0)} + E_c^B$	2.03

Table C.1: Eigenstates  $|\psi_i\rangle$  with two electrons and one hole which contribute to the FR angle up to second order in  $t_c$ . We also list the corresponding eigenenergies to  $\mathcal{O}(t_c^0)$  and evaluate them for the parameters discussed in Sec. 3.6.



# Bibliography

- [1] D.D. Awschalom, D. Loss, and N. Samarth. *Semiconductor Spintronics and Quantum Computation*. Springer, Berlin, 2002.
- [2] I. Žutić, J. Fabian, and S. Das Sarma. *Rev. Mod. Phys.*, 76:323, 2004.
- [3] V. Cerletti, W.A. Coish, O. Gywat, and D. Loss. *Nanotechnology*, 16:R27–R49, 2005.
- [4] M.N. Baibich, J.M. Broto, A. Fert, F. Nguyen Van Dau, F. Petroff, P. Etienne, G. Creuzet, A. Friederich, and J. Chazeles. *Phys. Rev. Lett.*, 61:2472, 1998.
- [5] S. Datta and B. Das. *Appl. Phys. Lett.*, 56:665, 1990.
- [6] J.M. Kikkawa, I.P. Smorchkova, N. Samarth, and D.D. Awschalom. *Science*, 277:1284, 1997.
- [7] J.M. Kikkawa and D.D. Awschalom. *Phys. Rev. Lett.*, 80:4313, 1998.
- [8] R. Fiederling, M. Keim, G. Reuscher, W. Ossau, G. Schmidt, A. Waag, and L.W. Molenkamp. *Nature*, 402:787, 1999.
- [9] Y. Ohno, D.K. Young, B. Beschoten, F. Matsukura, H. Ohno, and D.D. Awschalom. *Nature*, 402:790, 1999.
- [10] D. Loss and D.P. DiVincenzo. *Phys. Rev. A*, 57:120, 1998.
- [11] P. Recher, E.V. Sukhorukov, and D. Loss. *Phys. Rev. B*, 63:165314, 2001.
- [12] G.B. Lesovik, T. Martin, and G. Blatter. *Eur. Phys. J. B*, 24:287, 2001.
- [13] P. Recher and D. Loss. *Phys. Rev. B*, 65:165327, 2002.
- [14] C. Bena, S. Vishveshwara, L. Balents, and M.P.A. Fisher. *Phys. Rev. Lett.*, 89:037901, 2002.
- [15] V. Bouchiat, N. Chtchelkatchev, D. Feinberg, G.B. Lesovik, T. Martin, and J. Torrès. *Nanotechnology*, 14:77, 2003.
- [16] D.S. Saraga and D. Loss. *Phys. Rev. Lett.*, 90:166803, 2003.

- [17] P. Recher and D. Loss. *Phys. Rev. Lett.*, 91:267003, 2003.
- [18] D.S. Saraga, B.L. Altshuler, D. Loss, and R.M. Westervelt. *Phys. Rev. Lett.*, 92:246803, 2004.
- [19] A. Einstein, B. Podolsky, and N. Rosen. *Phys. Rev.*, 47:777, 1935.
- [20] N. Bohr. *Phys. Rev.*, 48:696, 1935.
- [21] J. Bell. *Physics*, 1:195, 1965.
- [22] J. Clauser, M. Horne, A. Shimony, and R. Holt. *Phys. Rev. Lett.*, 23:880, 1969.
- [23] A. Aspect, J. Dalibard, and G. Roger. *Phys. Rev. Lett.*, 49:1804, 1982.
- [24] G. Weihs, T. Jennewein, C. Simon, H. Weinfurter, and A. Zeilinger. *Phys. Rev. Lett.*, 81:5039, 1998.
- [25] M. Rowe, D. Kielpinski, V. Meyer, C. Sackett, W. Itano, C. Monroe, and D. Wineland. *Nature*, 409:791, 2001.
- [26] D. Greenberger, M. Horne, and A. Zeilinger. *Bell's Theorem, Quantum Theory, and Conceptions of the Universe*, page 69. Kluwer, Dordrecht, 1989.
- [27] H. Drexler, D. Leonard, W. Hansen, J.P. Kotthaus, and P.M. Petroff. *Phys. Rev. Lett.*, 73:2252, 1994.
- [28] S. Tarucha, D.G. Austing, T. Honda, R.J. van der Hage, and L.P. Kouwenhoven. *Phys. Rev. Lett.*, 77:3613, 1996.
- [29] R.J. Warburton, C. Schäfflein, D. Haft, F. Bickel, A. Lorke, K. Karrai, J.M. Garcia, W. Schoenfeld, and P.M. Petroff. *Nature*, 405:926, 2000.
- [30] M. Ciorga, A.S. Sachrajda, P. Hawrylak, C. Gould, P. Zawadzki, S. Jullian, Y. Feng, and Z. Wasilewski. *Phys. Rev. B*, 61:R16315, 2000.
- [31] J.M. Elzerman, R. Hanson, J.S. Greidanus, L.H. Willems van Beveren, S. De Franceschi, L.M.K. Vandersypen, S. Tarucha, and L.P. Kouwenhoven. *Phys. Rev. B*, 67:R161308, 2003.
- [32] M. Pioro-Ladrière, M. Ciorga, J. Lapointe, P. Zawadzki, M. Korkusiński, P. Hawrylak, and A.S. Sachrajda. *Phys. Rev. Lett.*, 91:026803, 2003.
- [33] J.R. Petta, A.C. Johnson, C.M. Marcus, M.P. Hanson, and A.C. Gossard, 2004. cond-mat/0408139.
- [34] T. Fujisawa, D.G. Austing, Y. Tokura, Y. Hirayama, and S. Tarucha. *Nature*, 419:278, 2002.



- [35] J.R. Petta, A.C. Johnson, A. Yacoby, C.M. Marcus, M.P. Hanson, and A.C. Gossard, 2004. cond-mat/0412048.
- [36] R. Hanson, L. H. Willems van Beveren, I. T. Vink, J. M. Elzerman, W. J. M. Naber, F. H. L. Koppens, L. P. Kouwenhoven, and L. M. K. Vandersypen, 2004. cond-mat/0412768.
- [37] R. Hanson, B. Witkamp, L. M. Vandersypen, L. H. van Beveren, J. M. Elzerman, and L. P. Kouwenhoven. Zeeman Energy and Spin Relaxation in a One-Electron Quantum Dot. *Physical Review Letters*, 91(19):196802, November 2003.
- [38] J. M. Elzerman, R. Hanson, L. H. Willems van Beveren, B. Witkamp, L. M. K. Vandersypen, and L. P. Kouwenhoven, November 2004. cond-mat/0411232.
- [39] M. Kroutvar Y. Ducommun, D. Heiss, M. Bichler, D. Schuh, G. Abstreiter, and J.J. Finleyand. *Nature*, 432:81, 2004.
- [40] P. Recher, E. V. Sukhorukov, and D. Loss. Quantum Dot as Spin Filter and Spin Memory. *Physical Review Letters*, 85:1962–1965, August 2000.
- [41] J. A. Folk, R. M. Potok, C. M. Marcus, and V. Umansky. A Gate-Controlled Bidirectional Spin Filter Using Quantum Coherence. *Science*, 299:679–682, January 2003.
- [42] R. M. Potok, J. A. Folk, C. M. Marcus, V. Umansky, M. Hanson, and A. C. Gossard. Spin and Polarized Current from Coulomb Blockaded Quantum Dots. *Physical Review Letters*, 91(1):016802, July 2003.
- [43] S. Cortez, O. Krebs, S. Laurent, M. Senes, X. Marie, P. Voisin, R. Ferreira, G. Bastard, J.-M. Gérard, and T. Amand. Optically Driven Spin Memory in n-Doped InAs-GaAs Quantum Dots. *Physical Review Letters*, 89(20):207401, October 2002.
- [44] A. Shabaev, A.L. Efros, D. Gammon, and I.A. Merkulov. *Phys. Rev. B*, 68:R201305, 2003.
- [45] H.-A. Engel and D. Loss. *Phys. Rev. Lett.*, 86:4648, 2001.
- [46] H.-A. Engel and D. Loss. *Phys. Rev. B*, 65:195321, 2002.
- [47] M. Grundmann, J. Christen, N.N. Ledentsov, J. Böhrer, D. Bimberg, S.S. Ruvimov, P. Werner, U. Richter, U. Gösele, J. Heydenreich, V.M. Ustinov, A.Y. Egorov A.E. Zhukov, P.S. Kop'ev, and Z. Alferov. *Phys. Rev. Lett.*, 74:4043, 1995.
- [48] A. Högele, M. Kroner, S. Seidl, K. Karrai, M. Atatüre, J. Dreiser, A. Imamoglu, R.J. Warburton, A. Badolato, B.D. Gerardot, and P.M. Petroff, 2004. cond-mat/0410506.
- [49] M. Baier, F. Findeis, A. Zrenner, M. Bichler, and G. Abstreiter. *Phys. Rev. B*, 64:195326, 2001.

- [50] Y. Chye, M.E. White, E. Johnston-Halperin, B.D. Gerardot, D.D. Awschalom, and P.M. Petroff. *Phys. Rev. B*, 66:R201301, 2002.
- [51] C.E. Pryor and M.E. Flatté. *Phys. Rev. Lett.*, 91:257901, 2003.
- [52] K. Gündoğdu, K.C. Hall, T.F. Boggess, D.G. Deppe, and O.B. Shchekin. *Appl. Phys. Lett.*, 84:2793, 2004.
- [53] J. Seufert, G. Bacher, H. Schömgig, A. Forchel, L. Hansen, G. Schmidt, and L.W. Molenkamp. *Phys. Rev. B*, 69:035311, 2004.
- [54] G. Burkard, D. Loss, and E.V. Sukhorukov. *Phys. Rev. B*, 61:R16303, 2000.
- [55] J.C. Egues, G. Burkard, and D. Loss. *Phys. Rev. Lett.*, 89:176401, 2002.
- [56] O. Benson, C. Santori, M. Pelton, and Y. Yamamoto. *Phys. Rev. Lett.*, 84:2513, 2000.
- [57] E. Moreau, I. Robert, L. Manin, V. Thierry-Mieg, J.M. Gérard, and I. Abram. *Phys. Rev. Lett.*, 87:183601, 2001.
- [58] A. Kiraz, S. Fälth, C. Becher, B. Gayral, W.V. Schoenfeld, P.M. Petroff, L. Zhang, E. Hu, and A. Imamoglu. *Phys. Rev. B*, 65:R161303, 2002.
- [59] C. Santori, D. Fattal, M. Pelton, G.S. Solomon, and Y. Yamamoto. *Phys. Rev. B*, 66:045308, 2002.
- [60] R.M. Stevenson, R.M. Thompson, A.J. Shields, I. Farrer, B.E. Kardynal, D.A. Ritchie, and M. Pepper. *Phys. Rev. B*, 66:R081302, 2002.
- [61] V. Zwiller, P. Jonsson, H. Blom, S. Jeppesen, M.-E. Pistol, L. Samuelson, A.A. Katznelson, E.Yu. Kotelnikov, V. Evtikhiev, and G. Björk. *Phys. Rev. A*, 66:053814, 2002.
- [62] S.M. Ulrich, S. Strauf, P. Michler, G. Bacher, and A. Forchel. *Appl. Phys. Lett.*, 83:1848, 2003.
- [63] T. Takagahara. *Phys. Rev. B*, 62:16840, 2000.
- [64] T.M. Stace, G.J. Milburn, and C.H.W. Barnes. *Phys. Rev. B*, 67:085317, 2003.
- [65] E. Tsitsishvili, R. v. Baltz, and H. Kalt. *Phys. Rev. B*, 67:205330, 2003.
- [66] E.L. Ivchenko and G.E. Pikus. *Superlattices and other Heterostructures*. Springer, Berlin, 1995.
- [67] G. Burkard and D. Loss. *Phys. Rev. Lett.*, 91:087903, 2003.

- [68] O. Gywat, G. Burkard, and D. Loss. *Phys. Rev. B*, 65:205329, 2002.
- [69] O. Gywat, 2005. PhD Thesis, University of Basel.
- [70] M. Ouyang and D.D. Awschalom. *Science*, 301:1074, 2003.
- [71] S.A. Wolf, D.D. Awschalom, R.A. Buhrman, J.M. Daughton, S. von Molnár, M.L. Roukes, A.Y. Chtchelkanova, and D.M. Treger. *Science*, 294:1488, 2001.
- [72] H. Fu, L.W. Wang, and A. Zunger. *Phys. Rev. B*, 59:5568, 1999.
- [73] A.L. Efros. *Phys. Rev. B*, 46:7448, 1992.
- [74] J.A. Gupta, D.D. Awschalom, A.L. Efros, and A.V. Rodina. *Phys. Rev. B*, 66:125307, 2002.
- [75] A.V. Rodina, A.L. Efros, and A.Y. Alekseev. *Phys. Rev. B*, 67:155312, 2003.
- [76] J. Schrier and K.B. Whaley. *Phys. Rev. B*, 67:235301, 2003.
- [77] S. Hugonnard-Bruyère, C. Buss, F. Vouilloz, R. Frey, and C. Flytzanis. *Phys. Rev. B*, 50:2200, 1994.
- [78] N. Linder and L.J. Sham. *Physica E*, 2:412, 1998.
- [79] L.J. Sham. *Journ. Mag. Mag. Mat*, 200:219, 1999.
- [80] G. Schedelbeck, W. Wegscheider, M. Bichler, and G. Abstreiter. *Science*, 278:1792, 1997.
- [81] M. Bayer, P. Hawrylak, K. Hinzer, S. Fafard, M. Korkusinski, Z.R. Wasilewski, O. Stern, and A. Forchel. *Science*, 291:451, 2001.
- [82] R. Heitz, I. Mukhametzhanov, P. Chen, and A. Madhukar. *Phys. Rev. B*, 58:10151, 1998.
- [83] A. Tackeuchi, T. Kuroda, K. Mase, Y. Nakata, and N. Yokoyama. *Phys. Rev. B*, 62:1568, 2000.
- [84] H.D. Robinson, B.B. Goldberg, and J.L. Merz. *Phys. Rev. B*, 64:075308, 2001.
- [85] J. Seufert, M. Obert, G. Bacher, A. Forchel, T. Passow, K. Leonardi, and D. Hommel. *Phys. Rev. B*, 64:121303, 2001.
- [86] A.I. Ekimov, F. Hache, M.C. Schanne-Klein, D. Ricard, C. Flytzanis, I.A. Kudryavtsev, T.V. Yazeva, A.V. Rodina, and A.L. Efros. *J. Opt. Soc. Am. B*, 10:100, 1993.
- [87] D.J. Norris, A. Sacra, C.B. Murray, and M.G. Bawendi. *Phys. Rev. Lett.*, 72:2612, 1994.

- [88] R.R. Reeber. *J. Mater Sci.*, 11:590, 1976.
- [89] R.G. Wheeler and J.O. Dimmock. *Phys. Rev.*, 125:1805, 1962.
- [90] R. Geick and C.H. Perry. *J. Appl. Phys.*, 37:1994, 1966.
- [91] A.L. Efros *et al.* *Phys. Rev. B*, 54:4843, 1996.
- [92] M. Achermann, J.A. Hollingsworth, and V.I. Klimov, 2003. cond-mat/0309712.
- [93] M. Ouyang. private communication.
- [94] J. Schrier and B. Whaley, 2005. cond-mat/0502080.

# Curriculum Vitae

von Verónica Cerletti

18.3.1975	Geboren in Salta, Argentinien (ARG)
1981-87	Besuch der Primarschule in Buenos Aires (ARG)
1988-92	Besuch der Sekundarschule in Buenos Aires (ARG)
1993-94	Zugeständnisskurs an der Universidad de Buenos Aires (ARG)
1994-2000	Studium an der Universidad de Buenos Aires in Physik (ARG)
davon 1 Jahr Diplomarbeit	Thema "How to find a needle in a haystack using Quantum Mechanics: theory and experiments" unter Prof. J. P. Paz;
2000-2004	Dissertation am Institut für Physik der Universität Basel unter Prof. D. Loss, seit Nov. 2000

An der Ausbildung beteiligte Dozenten: (Universidad de Buenos Aires (ARG)) Profs. L. Sybisz, A. Larotonda, J. Simon, M. Simon, U. Molter, S. Ledesma, R. Ferarro, V. Márquez, H. Kelly, C. Giribet, C. Segovia, F. Povoło, J.P. Paz, D. Gómez, J. Aliaga, M. Ruiz de Azúa, J. Hernando, R. Piegaia, M. Marconi, A. Marzocca, G. Mindlin, S. Hernández, D. Harari.

(Basel:) Profs.

D. Loss, C. Bruder.

## Veröffentlichungen

“*Entanglement transfer from electron spins to photons*”, V. Cerletti, O. Gywat and D. Loss, cond-mat/0411235 (2004)

“*Recipes for spin-based quantum computing*”, V. Cerletti, W. A. Coish, O. Gywat and D. Loss, Nanotechnology **16**, R27-R49 (2005)

“*Molecular spintronics: Coherent spin transfer in coupled quantum dots*”, F. Meier, V. Cerletti, O. Gywat, D. Loss, and D. D. Awschalom Phys. Rev. B **69**, 195315 (2004)